Charles University

Faculty of Science

Study programme: Inorganic Chemistry

Mgr. Jan Bartoň

Novel approaches to chemical modification of diamond surface

Nové přístupy k chemické modifikaci diamantových povrchů

Doctoral thesis

Supervisor: Mgr. Petr Cígler, Ph.D.

Consultant: Doc. RNDr. Jan Kotek, Ph.D.

June, 2020

Prague

The main part of experimental work was done at Institute of Organic Chemistry and Biochemistry of the Czech Academy of Sciences in the laboratory of Synthetic Nanochemistry under supervision of Dr. Petr Cígler.

This document was created in pdfLaTeX using Overleaf.

Prohlášení:

Prohlašuji, že jsem závěrečnou práci zpracoval samostatně, a že jsem uvedl všechny použité informační zdroje a literaturu. Tato práce ani její podstatná část nebyla předložena k získání jiného nebo stejného akademického titulu.

V Praze, dne ..... Podpis .....

Poděkování

Mému školiteli Petrovi, za podporu a vytrvalost v časech dobrých a především těch špatných. Mé rodině za podporu a materiální zajištění při celém studiu, bez kterého by nebylo možné držet tento výtisk v ruce či elektronický dokument.
Všem mým kolegům v laboratoři, především všek Jitce, Jirkovi, Milošovi a Vaškovi za rady a kritické poznámky. Dále pak téměř dvěma desítkám kolegů ve spolupracujících laboratoří v Česku, Německu a Belgii, bez kterých by nebylo možné provést a dokončit zde uvedené projekty. Poděkování též patří ochotným a milým zaměstnancům UOCHB za drobné i větší výpomoci, rady a servisní měření. Všem sekretářkám (Evě, Zuzce, Zuzce a Aleně), Vojtovi a "podpůrným" zaměstnancům za odstínění všemožné a nemožné byrokracie.
Mé nejmilejší Lence za podporu v deštivém počasí, mrazu větru a temných nocích.

"Life is really simple, but we insist on making it complicated."
Confucius

Abstract

Diamond is a unique material for its physical and chemical stability. However, many advance applications rely on surface functionalisation. Here, two types of diamond were modified on the surface - thin layer of chemical vapor deposition (CVD) and nanodiamond particles (NDs) high pressure and high temperature (HPHT).

The aim of CVD surface modification was to prepare photosensitised, conductive, diamond electrodes for dye sensitized solar cells (DSSC). For this purpose, a thin diamond layer doped with boron was deposited on the silicon wafer. Boron doping provided p-type (semi)conductivity to diamonds. The surface of the diamond was hydrogenated with H-plasma, and a short carbon linker with a protected amino group was UV-photografted to the surface. In another study, a photoconverting dye (**P1**) was covalently attached to the amine-linker. Furthermore, a dye designed based on donor-π-acceptor (D-π-A) concepts was attached to the surface. Finally, a systematic study was done for differently conductive diamond layer and the underlying silicon wafer These experiments gradually lead to the highest ever reported photocurrents of 6.6 μA cm^2 for a flat photosensitised boron-doped-diamond (BDD) electrode.

Monomolecular layer surface functionalizations on CVD diamond are difficult to detect or even quantify due to the low surface area and a negligible number of attached molecules. Therefore, we decided to use NDs as a model with similar chemical reactivity and with a number of functional groups available per milligram of diamond material several orders or magniture higher. For this purpose, NDs were modified similarly to the CVD layer, followed by analyses to evaluate conversions of surface reactions.

The modifications of NDs targeted at advance applications of particle tracking and ultrasensitive quantum sensing. The cornerstone for any NDs application is colloidal stability in solution, Without which the available surface is lost altogether with the function, such as targeting, drug delivery or sensing. Equally important is to confirm that the designed surface was modified and that this modification can be reliably reproduced.

In the following study, fNDs with nitrogen vacancy (NV) centres were used for directed motion on a flat graphene surface driven by a pH gradient. For this purpose, polymer-coated fNDs were surface functionalized with aldehyde groups, while the graphene surface was amine terminated. The surface available aldehydes on fNDs were quantified spectrophotometrically by a dye synthesised specifically for this purposed. Reversible formation of imine bond in the direction of the pH gradient resulted in directed motion, as shown by long-time fluorescent tracking of fNDs. Therefore, we developed a new tool based on the surface modification of fNDs for nanoparticle manipulation.

Finally, we developed quantum-based ultrasensitive nanosensor to sense unpaired electrons in close vicinity of fND, which was built on previously gained experiences. The aim was to create a missing tool for monitoring biologically relevant processes in aqueous solution under ambient temperature with a minute resolution. Specifically, we focused on construction of fND

with covalently bound nitroxide radicals to the polymeric coating of fND and their detection using optical relaxometry on NV centers. For that, colloidally stable fNDs were coated with a biocompatible polymer. To the polymer was attached a stable nitroxide radical, which could serve as a redox spin on/off switch. We developed an independent validation method to determine an exact concentration of nitroxide radicals bound per particle using a set of complementary methods (EPR, TGA, NTA, cryo-TEM). Then, using quantum-based sensing, we determined the concentration of nitroxyl radicals by measuring changes of T_1 relaxation times of nitrogen vacancy (NV) centers. We determined the precision of the nitroxide radical readout to be ∼10 single radical spins per one fND. In conclusion, we reached a localised optical readout sensitivity to be approximately 10^{-23} mol of nitroxide radicals in aqueous solution under ambient conditions.

Keywords boron doped diamond (BDD), chemical vapor deposition (CVD), dye-sensitized solar cell (DSSC, DSC), nanosensor, nanodiamond, nitrogen-vacancy center, nitroxide radical, paramagnetic species, L-ascorbate, diamond with NV centres, nanosensors, relaxometry.

Abstrakt

Diamant je výjimečný materiál kvůli své chemické a fyzikální stabilitě. Pokročilé použití materiálů na bázi diamantu jsou založeny na jejich povrchové funkcionalizaci. V této práci byla chemicky modifikována buď tenká vrstva diamantu vzniklého chemickou depozicí z plynné fáze (CVD) nebo nanodiamanty (ND) připravené za vysokého tlaku a teploty (HPHT).

CVD diamanty byly použity pro přípravu fotosenzitizované vodivé diamantové elektrody pro barvivem senzitizované solární články (DSSC). Na křemíkové podložce byla vytvořena tenká vrstva borem dopovaného diamantu (BDD). Přidaný bór vytvořil (polo)vodivostní vlastnosti typu p. Poté byl povrch hydrogenován vodíkovou plasmou a na něj jsme za použití UV záření připojili krátkou uhlíkovou spojku s ochráněným aminem. K aminoskupině jsme kovalentně navázali fotoaktivní barvivo (**P1**), které umožňuje konvertovat fotony na elektrický proud. V dalším projektu jsme k povrchu připojili nové barvivo navržené dle konceptů donor-π-akceptor (DPA). Poslední příspěvek na toto téma systematicky studoval vliv různé vodivosti BDD diamantu a křemíkové podložky na vznikající fotoproudy. Postupně jsme dosáhli zatím nejvyšších zveřejněných fotoproudů 6.6 μA cm^2 pro ploché, fotosensitizované BDD elektrody.

Monomolekulové povrchové úpravy diamantu je díky jeho malému specifickému povrchu obtížné prokázat, natož kvantifikovat. Proto jsme se rozhodli použít jako model ND vykazující podobnou reaktivitu, ale řádově větší množství funkčních skupin přítomných v hmotnostním ekvivalentu materiálu. Nanodiamanty jsme upravili podobným způsobem jako CVD vrstvy. Poté jsme připravené NDs analyzovali a určili míru modifikovaného povrchu diamantu.

Druhá část práce se zabývala pokročilými aplikacemi NDs pro sledování částic a vysoce citlivé kvantové detekce. Základním předpokladem pro úspěšné použití NDs je koloidní stabilita v roztoku. Nestabilní částice ztrácí vlivem asociace dostupný povrch a tedy i funkci sledování, cílení, detekce či transportu léčiv. Neméně důležité je ověřit, že navržené povrchové úpravy provedeny a lze je spolehlivě zopakovat.

Fluorescenční diamanty s centry dusík-vakance (NV) byly použity pro realizaci orientovaného pohybu na grafenovém povrchu ve směru pH gradientu. K tomu byly připraveny fND potažené vrstvou polymeru nesoucím aldehydové funkční skupiny. Povrch grafenu obsahoval amino skupiny. Množství povrchově dostupných aldehydů bylo určeno spektrofotometricky pomocí barviva připraveného k tomuto účelu. Tvorba iminových vazeb ve směru pH gradientu umožnila směrový pohyb fND, který byl sledován fluorescenční mikroskopií. Byl tak vyvinut nový přístup na manipulaci s nanočásticemi, který byl předveden na příkladu povrchově upravených fND. Byl tak vyvinut nový přístup na manipulaci s nanočásticemi, který byl předveden na příkladu povrchově upravených fND.

Na základně zkušeností získaných z předchozích experimentů, byl vyvíjen kvantový ultracitlivý nanosenzor nepárových elektronů v blízkém okolí fND. Cílem bylo připravit chybějící nástroj pro sledování buněčných procesů ve vodných roztocích a pokojové teploty se snímáním v rámci minut. K tomuto účelu bylo vybráno sledování přítomnosti kovalentně navázaných nitroxidových

radikálů na polymerním obalu fND. Nanodiamanty byly pokryty biokompatibilním polymerem, na který byly navázána stabilní nitroxidové radikály. Radikály bylo možné reverzibilně vytvořit a odstranit. Dříve než jsme mohli provést kvantovou detekci, vyvinuli jsme nezávislou metodu ověřující přesnou koncentraci nitroxidových radikálů navázaných na jedné částici. K tomu jsme použili kombinaci metod EPR, TGA, NTA a cryo-TEM. Kvantovým měřením jsme určili koncentraci nitroxidových radikálů, a to měřením T_1 relaxačních časů krystalové poruchy NV centra obsažené v nanodiamantu. Přesnost detekce přítomnosti nitroxidových radikálů jsme určili na ∼10 samostatných radikálových spinů na jeden fND. V této práci jsme dosáhli lokální citlivosti detekce přibližně 10^{-23} mol nitroxidových radikálů ve vodném roztoku za pokojové teploty.

Keywords borem dopovaný diamant (BDD), chemická depozice z plynné fáze (CVD), barvivem senzitizovaný solární článek (DSSC, DSC), nanosenzor, nanodiamant, centrum dusík-vakance, nitroxidový radikál, paramagnetická látka, L-askorbát diamant s NV centry, nanosenzor, relaxometrie.

List of Abbreviations

AFM atomic force microscopy

AIBN azobis(isobutyronitrile)

ATR-FTIR attenuated total reflectance-fourier-transform infrared spectroscopy

ATRP atom transfer radical polymerization

BDD boron-doped-diamond

CuAAC Cu(I)-catalyzed alkyne-azide cycloaddition

CVD chemical vapor deposition

D-π-A donor-π-acceptor

DCC dynamic covalent chemistry

DLS dynamic light scattering

dND detonation nanodiamond

DSSC dye sensitized solar cells

EPR electron paramagnetic resonance

FIB focused ion beam

fND fluorescent ND

HFCVD hot filament chemical vapor deposition

HOMO highest occupied molecular orbital

HPHT high pressure and high temperature

HPMA N-(2-hydroxypropyl)methacrylamide

ICP-MS inductively-coupled plasma mass spectrometry

ICP-OES (inductively coupled plasma optical emission spectrometry

IPCE incident photon to current conversion

IR infrared

LUMO lowest unoccupied molecular orbital

MW-PECV microwave plasma enhanced chemical vapor deposition

MWCVD microwave plasma chemical vapor deposition

ND nanodiamond

NIR near infrared

NMP nitroxide-mediated polymerization

NTA nanoparticle tracking analysis

NV nitrogen vacancy

ODMR optically detected magnetic resonance

PAA poly(acrylic acid)

PAH poly(allylamine hydrochloride)

PBS phosphate buffer saline

PEG poly(ethyleneglycol)

PEI poly(ethyleneimine)

PG poly(glycerol)

PHPMA poly[N-(2-hydroxypropyl)methacrylamide]

PMAA poly(methacrylic acid)

PNIPAM poly(N-isopropylacrylamide)

PPEGMA poly(PEG methyl ether methacrylate)

RAFT reversible addition-fragmentation chain transfer

SEM scanning electron microscopy

SI-CRP surface-initiated controlled radical polymerization

SI-ROP surface-initiated ring-opening polymerization

TEM transmission electron microscopy

TEMPO 2,2,6,6-tetramethylpiperidinyloxy

TGA thermogravimetry

XPS X-ray photoelectron spectroscopy

ZPL zero phonon line

Contents

1 | Introduction

This introduction follows the diamond from material selection through fabrication and surface modification to explaining potential applications of this basic research – for photovoltaics and sensing with nitrogen vacancy (NV) centres.

Diamond is a chemically and physically stable material under ambient conditions and, therefore, suitable for both academic and industrial applications. Novel diamond applications can be developed by modifying its surface. For example, a synthetic diamond can be spiked with numerous elements and lattice defects. However, any capability introduced without directing a selected task provides us with little benefit. Accordingly, we aimed to develop a fictionalised system by modifying a diamond surface, that is, by covering the diamond surface with particular molecules. Here, two modifications were studied: one with a potential application in photovoltaics, and the other in sensing or tracking. In photovoltaics, a diamond can be used as a durable electrode. The intrinsically missing electric conductivity is introduced into a diamond by boron doping, and diamond becomes a p-type conductor. The other modification is nitrogen vacancy (NV) centre – a point defect, which has stable fluorescence in NIR. This is a non-bleachable fluorophore with broad applications in imaging or long-time tracking. Furthermore, measuring the NV in a proper experimental setup shows changes in the electromagnetic surroundings with unprecedented sensitivity.

Within the thesis, a general diamond matter will be called diamond. The chemical vapor deposition (CVD) grown diamond as a thin nanocrystalline layer on a substrate will be referred to as a "thin layer" or "plate", while diamond particles with diameter <1000 nm (usually 30-50 nm) will be called nanodiamond (ND).

The high surface to volume (mass) ratio is crucial for any nanoparticle application. For an illustration, surface to volume ratio increases by 3 orders for 10 times decrease in side length, for the same volume of cubes (Figure 1.1). Thus, two parameters are important – particle size and colloidal stability of particles, for bioapplications it is stability on aqueous buffers. ND used in this work have size ∼50nm. The dimensions can be compared with following biological objects. The thickness of red cell is about 1 μm, HIV virus diameter is 120 nm, ATP synthase 20 x 10 nm, ATP is 1 nm in width and the distance between water molecules is roughly 0.3 nm [1, 2].

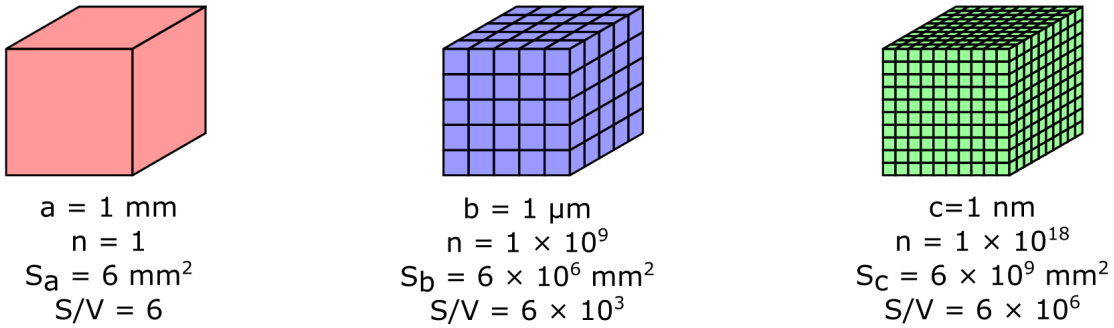

Figure 1.1: Schematic display of increasing surface to volume ratio for cubes with the decrease in edge length where a,c,b is lenght of side, n is number of cubes, S is surface of all cubes and S/V is surface to volume ratio. ND used in the work have irregular shape with ca. 30-50 nm diameter. Created in PGF/TikZ using Overleaf.

1.1 Diamond

Natural diamond is a well-known material due to its hardness, chemical inertness, longevity and optical properties. Synthetic diamonds are fairly new and their availability increased after the development of various manufacturing techniques such as detonation [3], high pressure and high temperature (HPHT) [4] and chemical vapor deposition (CVD) [5, 6]. The size of the material ranges from ultranano-, nano- and microparticles to thin layers, which can be poly- or mono-crystals. Depending on the manufacturing method, high purity sp^3 carbon materials can be prepared (by CVD) with high control of impurities or doping. Conversely, the explosion creates particles with a high content of sp^2 carbon impurities and with residual elements from the explosive itself, mainly nitrogen. Surface chemistry changes significantly, depending on the manufacturing method and on post-processing procedures. Generally, a higher content of a sp^3 C-H surface leads to a hydrophobic surface and, in the case of nanoparticles, to lower colloidal stability in polar solvents (water). Higher sp^2 content and numerous edges on the crystal surface lead to a wide variety of surface chemistry and higher reactivity. However, combining different surface chemistry properties into a single functional group is more challenging. Post-processing methods remove combustible and incombustible surface impurities through sonication, annealing and treatment with acids or hot melted salts to remove unwanted content. Therefore, the selection of the manufacturing and post-procession techniques heavily depends on the target application of diamond.

1.1.1 Fabrication of nanodiamonds (ND)

Diamond synthesis has been of interest of entrepreneurs and businessmen over the last two centuries as much as gold synthesis has been attracting alchemists. James B. Hannay allegedly prepared synthetic diamond in 1880 by explosion in a closed tube, though recent reexamination proved that the diamonds were of natural origin [7]. Nevertheless, a reproducible synthesis of microdiamonds was officially reported in 1955 by the General electric company [4] using technique HPHT. Since then, many techniques have been developed based on the principle of

localised high pressure and temperature, such as detonation [3], CVD [8], ultrasound cavitation [9] and laser ablation [10].

The detonation nanodiamond (dND)s, HPHT and CVD are commercially available in large scale. The dNDs are produced by detonation in a closed vessel, and industrial production is expressed as ton per year [11]. The explosion produces small spherical particles (<5 nm diameter), which aggregate with detonation soot. This soot accounts for 25-70 wt. % depending on detonation conditions [12]. The aggregates holding electrostatically together can be, to some extent, disintegrated by sonication. Development in post-processing (intensive milling) leads to a commercially available colloidal solution of 4-5 nm NDs [13]. dNDs are less suitable for optical tracking than HPHT NDs. That is due to the high content sp^2, amorphous carbon and nitrogen (Section 1.1.4), which results in diamond with less optically activeNV centers [14].

The HPHT are prepared under the following conditions: ∼10 GPa pressure and ∼2300 °C temperature. The resulting micron-size polycrystalline particles are milled to monocrystalline particles (Figure 1.3). Breaking down diamond produces irregular shapes, with available sizes as small as 10-20 nm. Industrial-grade HPHT NDs are nitrogen-rich, which can create a yellow appearance. The nitrogen can be soaked by other elements (Zr, Al, Ti) [15, 16] to remove the colour, albeit slowing down the growth. The nitrogen impurities can also be used to prepare NV centres, see Section 1.1.4.

The CVD method can also be used to prepare nanodiamonds. This is a low-scale approach. When deposition parameters lead to the formation of microcrystalline matter with small grains, prepared layers can be milled. Since CVD enables precise control over purity and doping, B-doped conductive ND can be prepared (Section 1.1.3) [17].

1.1.2 Fabrication of chemical vapor deposition layers (CVD)

Chemical vapor deposition (CVD) is a diamond growth method for single- and poly-crystalline diamonds from a volatile carbon-containing gas (methane, acetone, alcohols) under reduced pressure (∼ 0.1-50 bar) and elevated temperatures (700-1000 °C) [18]. Successful CVD of diamond was first documented by Eversole *et al* [19] in 1958. Using a lower temperature slows diamond growth, with good results in sp^2 non-diamond carbon deposition as well. The thin balance between two allotropes stems from a small a difference between the standard Gibbs free energies of diamond and graphite (2.9 kJ/mol) compared to the standard Gibbs free energy of carbon vapour (671.3 kJ/mol) [20].

However, CVD has been economically impracticable, due to slow growth and high content of sp^2 carbon, until the discovery of atomic hydrogen generation inside the apparatus, which was independently developed by J. Angus (USA) and V. Varnin (USSR) [21]. Atomic hydrogen has several functions. First, radicals are generated in the gas phase by abstracting hydrogen and also on an H-terminated surface. This enables the use of a non-diamond substrate. Secondly, atomic hydrogen etches a non-diamond carbon significantly faster than an sp^3 diamond. Thus,

the diamond layer can be grown continuously, without repetitive etching by hydrogen and with a higher sp^3 carbon content. Nevertheless, atomic hydrogen was only efficiently produced by Japanese scientists a decade later, thereby making CVD of the diamond industrially applicable. The most used activation procedures are hot-filament CVD (HFCVD) [22], microwave plasma CVD (MWCVD) [5], and radiofrequency plasma CVD (RFCVD) [23] among others.

The HFCVD gas is activated by heating a metal wire to 2000 °C near a substrate. This type of activation increases the flexibility of the method to cover a high area or complex-shaped substrates such as cutting tools. The trade-off is the production of a material with lower purity, contaminated with a heating wire [7].

For the MWCVD, the microwave source envelops the deposition reactor with a sample. The stable plasma is formed above the sample by microwave discharge. Absence of wire in the chamber reduces contamination and enables use of various gasses, including aggressive gasses such as oxygen and halogen. Thus, high-purity material is prepared with high control over dopants. Albeit, the geometry of the reactor and substrate affect the microwave discharge, limiting substrate variability. RFCVD is suitable for covering a thin diamond layer over a vast area and for scale-up.

Diamond crystallinity is determined by a substrate and growth conditions. A diamond substrate (wafer) leads to a single crystalline (homoepitaxial) layer, whereas a non-diamond substrate leads to a polycrystalline diamond film. Growth on a non-diamond substrate is often promoted by seeding with NDs for initial nucleation and higher speed [24]. The separated crystallisation nuclei grow until merging into a film, and the grain size gradually increases with film thickness and growth time in hydrogen-rich atmosphere [25]. Based on grain size, the films are sorted as microcrystalline or nanocrystalline diamond [26]. In turn, growth in an argon-rich environment leads to high renucleation rate, suppressing the formation of larger grains [27]. Such polycrystalline films are known as ultrananocrystalline diamond and generally have higher surface roughness and intrinsic conductivity [24, 28].

1.1.3 Impurities and doping

Diamond was traditionally classified using optical properties and subsequently infrared (IR) spectrometry. Modern diamond classification dates back to Robertson *et al*, who sorted "colourless" diamonds by UV and IR absorption spectrometry [29, 30]. Diamond is sorted based on the presence (Type I) and absence (Type II) of nitrogen impurities, see Figure 1.2. Nitrogen impurities can be aggregated (Ia), or isolated (Ib). Most natural diamonds (>95 %) contain high concentrations (up to 3000 ppm) of aggregated nitrogen and are thus type Ia diamonds. Aggregated nitrogen forms pairs (IaA), even-numbered clusters (IaB) or their combination (IaAB). Isolated nitrogen impurities, also known as single substitutional (Type Ib), are found in diamonds with lower nitrogen content. This category includes commercial HPHT diamonds with a nitrogen concentration of approximately 100-300 ppm [31, 32].

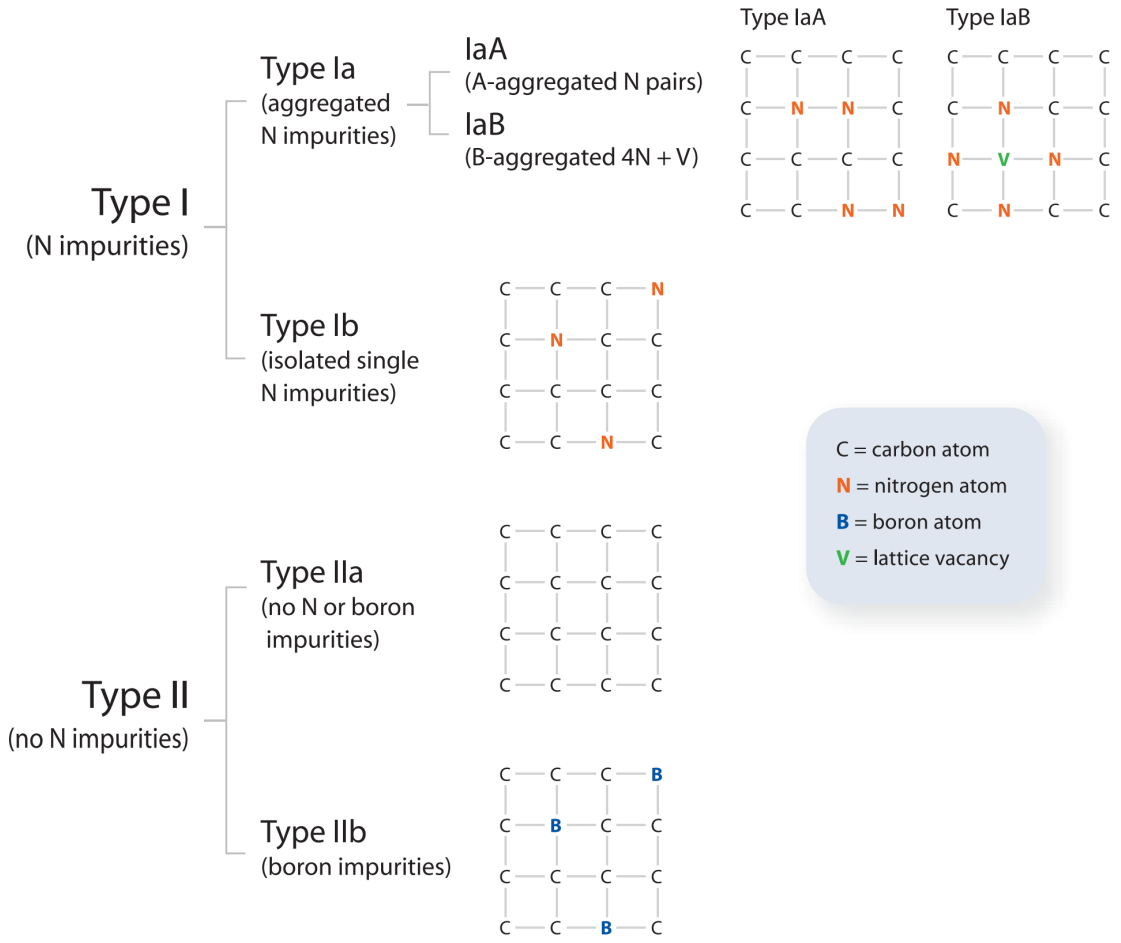

Figure 1.2: Diamond classification based on nitrogen and boron impurities. Simplified 2D crystal lattice demonstrates differences between isolated and aggregated impurities. *Adapted from ref.* [33].

Natural diamonds without nitrogen (Type II) are classified based on the boron presence (Type IIa) or absence (Type IIb). Boron changes the optical properties of diamond to blue and increases diamond conductivity [34]. Typically, CVD leads to nitrogen-free material. It can be doped with boron during deposition by using gaseous diborane or trimethyl borate.

To study changes in properties, scientists doped diamond with various elements and introduced specific lattice errors. Furthermore, various manufacturing and postprocessing contaminations complicate the situation even more, as shown in the table for dNDs Table 1.1. In addition, many foreign elements form optically active defects [35]. Contaminations in HPHT varies with the manufacturer post-processing (e.g., grinding, milling, acid treatments) of micron-sized particles. Since scientific consumption is marginal, purity and quality are batch- and vendor-dependent. Thus, there is no ND standard. Commonly, HPHT contain a higher amount of nitrogen (100-300 ppm) and may contain catalyst metals (e.g. Ni, Co) [36] Higher purity and doping control are achieved by MWCVD; for HFCVD, the heating wire is the main source of metal contamination (Tu, Rh, Ta) [7].

Controlled doping can be performed *in situ* or *ex situ*, which includes diffusion or ion implantation (Section 1.1.4). CVD is an example of *in situ* doping, which is often used to increase conductivity with boron (p-type) or phosphorus and nitrogen (n-type) [37]. Diamonds become semiconductive, depending on the dopant, at lower concentrations ($\leq 10^{19}$ atoms cm^{-3}) and subsequently conductive, with metal-like behaviour ($\geq 10^{20}$ atoms cm^{-3}3) [24]. Due to the small atomic radius of boron, a heavily doped diamond can be prepared by substitutional insertion, with a near-zero activation energy for conductivity [38]. Such material is applicable as an electrochemical electrode [39].

Table 1.1: Overview of elemental impurities for dNDs during production and post-processing. *Adapted from ref.* [40].

Process	Source	Elemental impurities
Detonation synthesis	Explosives	Various
	Construction material of reaction chamber	Fe, Ni, Cr, Mo, W, Si
	Coolant (water, ice)	Ca, Mg, Na
	Detonator/initiator	Pb, Ba, Sb, Al, Cu, Zn, Hg, As
Isolation and purification	Residues of oxidants and washing reagents after wetchemical oxidation of amorphous carbon	Cr, Mn, S from oxidants and various impurities from washing reagents
	Catalysts of oxidation	Ag, Ce
	Inhibitors of oxidation	B
Disaggregation	Sonication with sonotrode	Ti, V, Al, Mo, W
	Milling with microbeads	Zr, Y, Hf, Si, Al, Mg
	Disaggregation media (solid salts, electrolytes, etc.)	Na, K, Mg, Ca, Al, Cl, P, S
Processing and storage	Adsorption of impurities from chemical reagents	Various
	Laboratory glassware	Na, K, B, Si
Targeted doping	Various methods	B, N, Si, Ni, and others

1.1.4 Nitrogen vacancy (NV) centres

The NV centre, first described in 1976 [41], is a crystal lattice point defect comprised of the pair – nitrogen and adjacent vacancy in the diamond lattice. The NV stands out among several hundreds of optical defects in diamond because it is magnetic (non-zero spin), and luminiscence intensity is coupled to the electronic states [42]. Furthermore, the unique properties of the NV centre are photostability, bright single-photon source and sensitivity against optical and magnetic changes. They form the basis for potential applications in the fields of quantum computing, bioimaging, nanoscale quantum sensing, cell tracking and single-spin magnetometry (Section 1.4) [32, 43, 44].

The NV centre shows a [111] crystal orientation (Figure 1.4) and a C_{3v} point group symmetry. The concentration of NV centres is negligible in natural diamond, and therefore they must be prepared artificially. HPHT diamonds are suitable for the production of NV centres since they

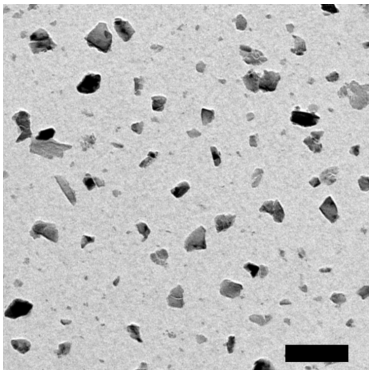

Figure 1.3: TEM image of HPHT NDs, milling creates sharp edges irregular shape. Scale bare represent 100 nm. Image courtesy of Helena Raabova.

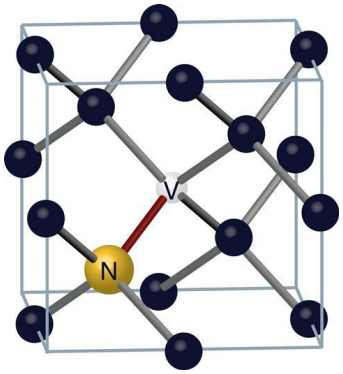

Figure 1.4: Diamond crystal structure with nitrogen-vacancy (NV) centre. *Adapted from ref.* [45].

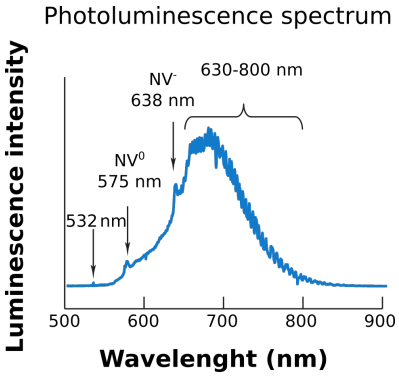

Figure 1.5: Fluorescent emission spetra of NDs with ZPL of NV^- and NV^0 and vibrational side bands. *Adapted from ref.* [42].

already contain nitrogen from manufacturing. The vacancies are then created in the diamond lattice by high-energy irradiation. Afterwards, the material is annealed (600-900 °C) under an inert atmosphere, thereby forming NV by vacancy migration and recombination with nitrogen [46, 47]. The NV can be found in NDs down to the size of 4-5 nm [42]. Due to the small size of dNDs, the concentrations of NV centres are considered low, and controlled formation is challenging [48]. Also, high nitrogen concentration in dND (2000-3000 ppm) can lead to formation of optically inactive complexes [14] Furthermore, NV centres can be found in CVD diamonds [49, 50], annealed after ion implantation in bulk diamond [51] or implanted into CVD layer [52]. In addition, spacing and depth can also be controlled [53].

Created NV centres have two different charged states which differ in one electron – NV^- an NV^0 centres. The neutral NV^0 has a zero phonon line (ZPL) at 575.5 nm (2.156 eV) and NV^- 638 nm (1.945 eV). These electronic states of NV^- can be applied for quantum sensing, as further discussed below. These NV centres also have key properties for biological applications (Section 1.4) such as the position of fluorescence in a NIR optical window [54]. Furthermore, NV^- neither photobleaches nor photoblinks [55, 56] and fluorescence lifetime is significantly longer that cell autofluorescence ($\sim$ 15 ns for NDs, $\sim$1-4 ns for fluorophores used in cell biology [57, 58]). An exception in photoblinking was observed for small dND ($<$ 5nm) with NV^- and this phenomena might be dependent on surface chemistry [56]. However, NV^- fluorescence intensity is lower than that of photobleachable fluorescent dyes, proteins and quantum dots. Excellent reviews explaining spin manipulations and quantum properties of NV^- in detail have been previously published [42, 43, 59].

1.1.5 Electronic states of NV^-

The NV^- consists of six electrons. Two are provided by nitrogen, three from carbon atoms surrounding the vacancy, and the last electron originates from the lattice [42]. The lattice can

lose an electron, thus changing the charge state to NV^0, which is magneto-optically inactive. Shallow NV^- (∼2-5 nm) undergo loss of charge through different mechanisms [56, 60]. The stability of shallow NV^- improves, for example, with surface termination with fluorine or oxygen and decreases with hydrogenation [61]. The stability of deeper NV^- are not significantly affected by surface changes and do not bleach or blink. However, sensitivity to magnetic changes significantly decreases with distance. Therefore, sensing applications require a balance between particle size, number of active NV^- centres, thickness of surface functionalization and particle stability. Figure 1.6 displays an energy diagram of NV^- with two unpaired electrons showed within the diamond energy band gap (E_g = 5.5 eV). The system consists of three main states – a triplet ground state $^3A_2$, from which an electron can be exited by an optical pulse (ZPL = 638 nm or 1.945 eV) to the excited state ^3E. The optical transitions are strongly spin conserving [62, 63]. Lastly, the relaxation pathway to the ground state is either direct or proceeds over a metastable singlet state $^1A_1$ with long relaxation times.

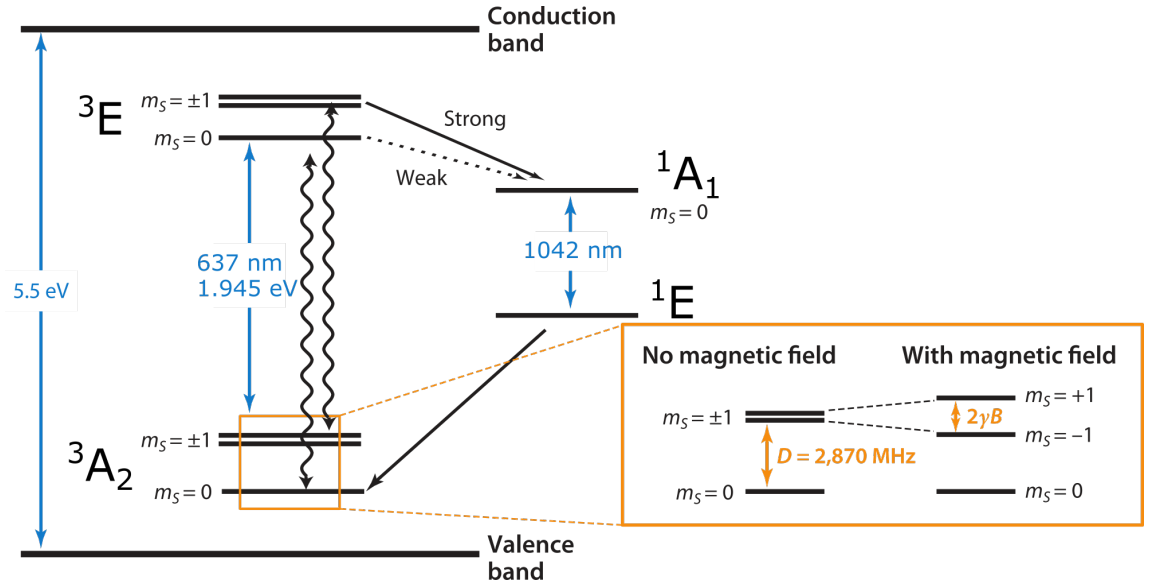

Figure 1.6: Energy levels of single NV^- for two unpaired electrons. Black wiggle lines are radiative transition, black full/dashed denotes strong/weak transition. The main optical transition occurs between triplet ground and exited states ($^3A_2$ and ^3E). The transition from the exited ^3E state to the non-fluorescet pathway $^1A_1$ is allowed. The optical emmision at 1042 nm is negligible. The organge box shows splitting of magnetic sublevels $m_s = \pm 1$ and $m_s = 0$ with and without magnetic field, D is zero-field splitting and $2\gamma B$ is Zeeman splitting, γ is electron gyromagnetic ratio. *Adapted from ref.* [42].

Manipulation of the spin population can result in decrease of the fluorescence intensity. Both the ground and excited states consist of tree sublevels with different magnetic spins $m_s = 0$ and $m_s = \pm 1$, where the second one is double degenerated due to the axial symmetry of the NV centre. Spin states in the absence of external magnetic field are separated by zero-field splitting – D = 2.87 GHz and D = 1.42 GHz for the ground and excited states. In the presence of a magnetic field, the degeneracy is removed, separating the states $m_s = \pm 1$. Furthermore, the transition rate between $m_s = 0$ and $m_s = \pm 1$ depends on the spin-lattice relaxation time T_1, which occurs in the millisecond range at room temperature [64].

A laser excitation (637 nm) from $^3A_2$ ($m_s = 0$) to ^3E ($m_s = 0$) is mainly followed by direct

de-excitation to the ground state. However, excitation from $^3A_2$ ($m_s = \pm 1$) to ^3E ($m_s = \pm 1$) is also followed by intersystem crossing in the non-radiative pathway over $^1A_1$ and ^1E with weak infrared emission (1042 nm). By optical pumping, the $m_s = 0$ ground state is populated, also known as induced spin polarisation [65]. A laser excitation from $m_s = 0$ followed by optical readout results in a higher fluorescence than excitation from $m_s = \pm 1$. Lastly, a resonant microwave field (2.870 MHz) destroys the optically pumped polarisation of $m_s = 0$, which leads to a decrease of fluorescence intensity. This is basis of a optically detected magnetic resonance (ODMR) – resonance between spin sublevels detected by optical transitions [32]. In conclusion, quantum applications of NV^- utilize the transition between spin sublevels and decrease in observed fluorescence.

Optical measurement techniques using NV^-

The luminescence of NV^- depends on the spin, which is used for electron paramagnetic resonance (EPR). The cornerstone experiment is to measure a drop in luminescence in EPR during a microwave sweep over a single NV^-, see Figure 1.7 [55]. During resonance (2.87 MHz), a transition from $m_s = 0$ to $m_s = \pm 1$ occurs, followed by excitation and allowed intersystem crossing to $^1A_1$ with non-fluorescent pathway (Figure 1.6). Repetition of the same measurement in the presence of external magnetic field results in peak split since the degeneracy of spin sublevel $m_s = \pm 1$ is lifted. These experimental setups are termed optically detected magnetic resonance (ODMR).

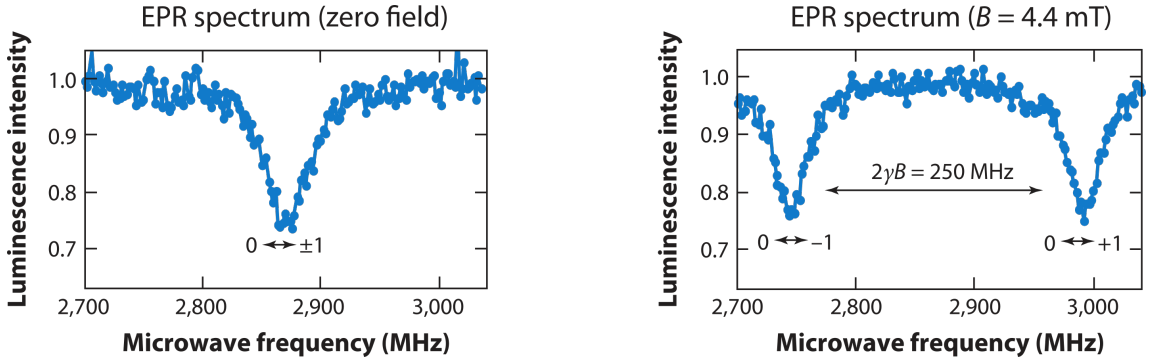

Figure 1.7: Variation of luminescence intensity as a function of EPR during a microwave sweep without (left) and with (right) magnetic field for single NV^-. *Adapted from ref.* [42].

The number of protocols using NV^- has significantly increased over the last decades, see Figure 1.8 for a graphic overview. The protocols can be divided into a static/slowly varying magnetic field (continuous wave and pulsed ODMR and Ramsey, Figure 1.9A,B) and oscillating magnetic field (Hahn echo, dynamical decoupling, Rabi and T_1 relaxometry, Figure 1.9C). The last mentioned, T_1 relaxometry is relevant for sensing ultra-low concentrations of paramagnetic species in the vicinity (< 20nm) of NV^- centre(s) in diamond layers or NDs. A detailed explanation of other techniques can be found in elsewhere [66–69].

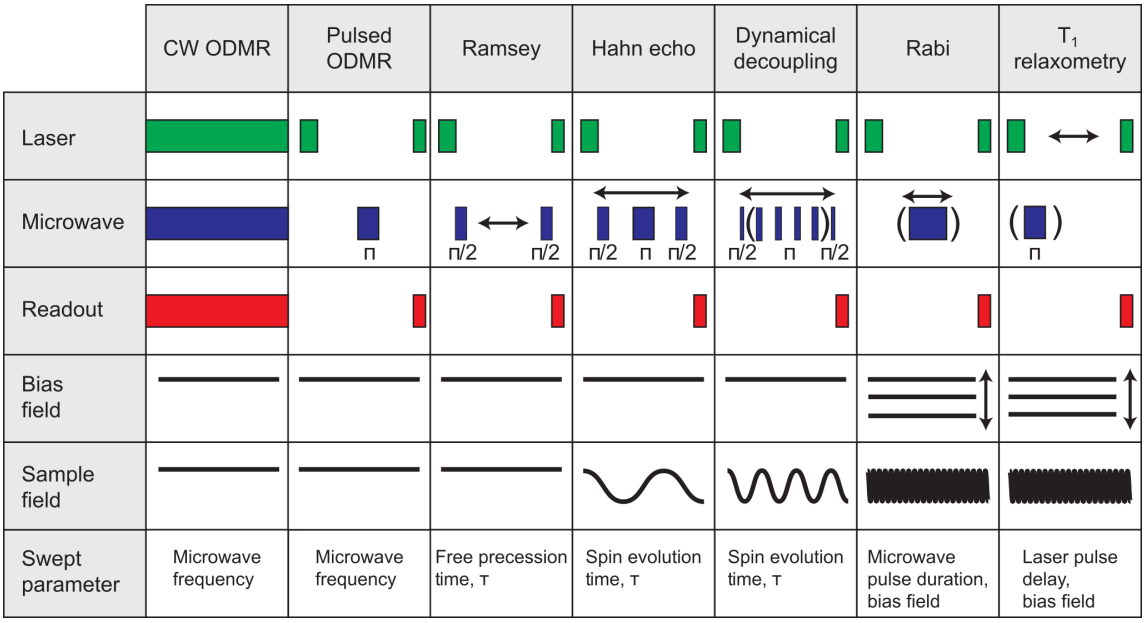

Figure 1.8: Overview of measurement techniques using NV^- based on stable or alternating sample field with increasing frequency. Doublehead arrows indicate varying parameters. Sequences of MW and laser pulses and readout time are represented by filled rectangles. *Adapted from ref.* [67].

T_1 spin-lattice relaxation time

When performing induced spin polarisation to $m_s = 0$, a T_1 time is needed to establish thermal equilibrium between $m_s = 0$ and $m_s = \pm 1$. The time differs for NV^- in bulk diamond or nanoparticles, but an average value can be determined. However, T_1 shortens in the presence of other paramagnetic events (stable radicals, paramagnetic particles Gd^{3+}, Mn^{2+} and Fe^{2+}) as shown in Figure 1.9C. The measurement is based on a changing readout time τ after inducing spin polarisation, and fitting measured τ to determine T_1 time for a given state of the system. Increase in the concentration of paramagnetic species in the vicinity of NV^-shortens T_1, and if properly calibrated, the concentration of paramagnetic species can be quantified [70].

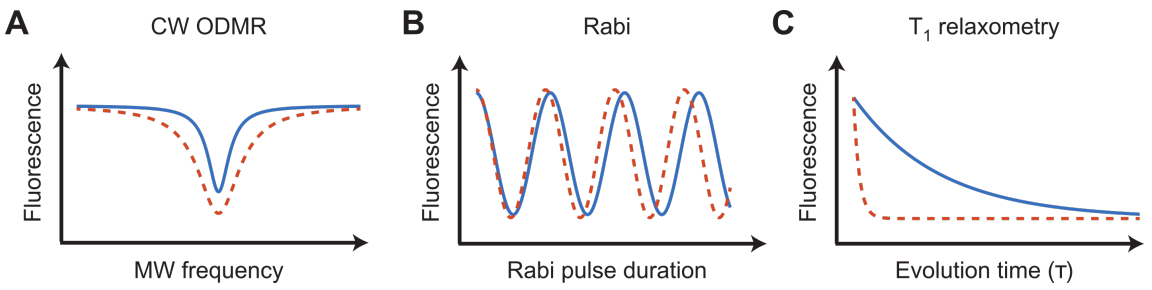

Figure 1.9: Trends in observed curves for magnetometry measurements: A) CW ODMR broadening: microwave power, B) Rabi oscillation: amplitude of microwave frequency, C) T_1 relaxometry: change of τ (T_1 shortening) based on increasing (external) magnetic field. *Adapted from ref.* [67].

1.2 Colloidal properties and particle characterisation

Colloidal stability of NDs is essential for any (bio)applications. Thanks to their high surface and modifiability, nanoparticles are ideal for bioapplications such as targeting and drug delivery. In general, NDs are more stable with decreasing size and higher surface charge. Their colloidal stability depends on their size, mass, shape and concentration, in addition to solvent polarity, ionic strength, particle surface charge and functional groups. Biologically relevant conditions show high concentrations of ions in aqueous solutions. Consequently, unprotected NDs aggregate easily. This aggregation poses the main challenge in surface engineering of NDs: to design chemical interfaces stabilising particles in a physiological environment, which is relevant for targeting applications.

To determine and compare the stability of NDs in solution, researchers commonly use dynamic light scattering (DLS). Using DLS, zeta-potential and hydrodynamic diameter of particles can be measured. Zeta-potential is an indirect measurement of a nanoparticle effective surface charge based on their electrophoretic mobility. In other words, an electrostatic potential is measured at the electrical double layer of ions bound to the charged surface and those freely moving in solution (Figure 1.10). A zeta-potential value close to 0 means that electrostatic repulsive forces between NDs will be low and NDs stabilised solely with charge will aggregate, which is not case for sterically stabilised ND. Conversely, particles with absolute values over 30 mV will be electrostatically stabilised. Furthermore, DLS can be used for determination of particle size, which includes the hydration sphere.

Alternatively, a more accurate particle size distribution is assessed by TEM, followed by image analysis. Such an analysis provides information about the size of bare NDs; HRTEM or cryo-TEM can be used for NDs covered with low-density layers, such as silica-coated NDs (Section 1.3.4). Use of cryo-TEM is advantageous to determine thickness of hydrated polymer, polymer drying leads to polymer contraction. Moreover, DLS can be used for the same NDs under same measurement conditions to compare the relative change in size after polymer coating or heating thermo-responsive polymer [71].

Researchers determine ND concentrations using a combination of indirect methods. DLS can be used to pinpoint the concentration of particles in solution, but the results must be interpreted cautiously, ideally using references under the same conditions (solvent, solvent viscosity, ionic strength, temperature). Elemental analysis of NDs provide more reliable data than DLS, but usually require several milligrams of material. A commonly used thermogravimetry (TGA) monitors thermal decomposition by mass loss. The original weight concentration of both NDs and non-diamond materials (e.g. water, polymer coating)can be calculated from the rate of mass loss and residual mass. ICP-OES or ICP-MS can used for NDs contaminated with other elements of a known concentration to determine the NDs concentration. This is particularly the case for dNDs contaminated with rare earth metals, which are batch- and vendor-dependent [11]. Lastly, nanoparticle tracking analysis (NTA) is a relatively new technique, which analyses the movement of individual particles [74], unlike DLS. The detection principle is based on recording

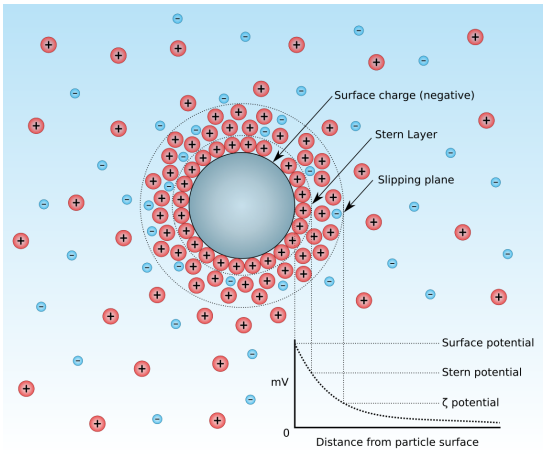

Figure 1.10: Scheme of nanoparticle surface in solvent covered with ions. Zeta-potential is the outer boundary of the charged species in which exchange is slower than in the solution. *Adapted from ref.* [72].

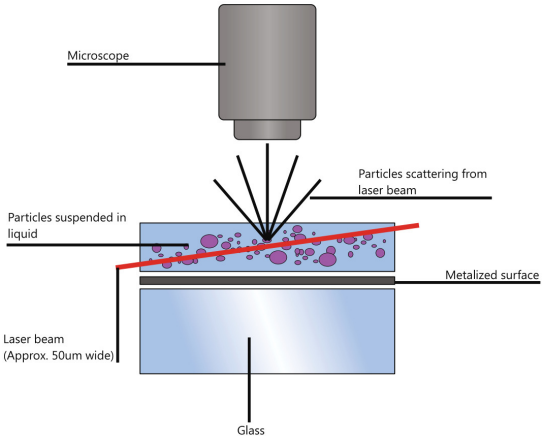

Figure 1.11: Scheme of optical setup for NTA. A laser beam scatters over nanoparticles, and the resulting scattering is recorded by an optical camera and processed by advanced image analysis. *Adapted from ref.* [73].

the light scattering of individual NDs from a laser beam (Figure 1.11). The number of particles of the original solution can be determined, requiring a negligible amount of a diluted sample. Since scattering depends on particle size, the NTA provides reliable data for the narrow particle size distribution. Thus, combining elemental analyses with NTA and DLS is appropriate for determination of ND concentration in solution.

1.3 Surface modifications

The surface composition vary with diamonds synthesis, size and batch. Hence, differences and similarities will be briefly explained. Reactivity decreases from dNDs to HPHT. Comparing the reactivity of CVD layers with ND is complex, and depends on surface roughness and termination. The differences in ND reactivity are attributed to their high surface-to-volume ratio, to the higher surface strain on smaller nanoparticles and to changes in the thermodynamic equilibrium of sp^2/sp^3 in nanoscale [75, 76]. dNDs are the most inexpensive and well-studied NDs with a highly reactive surface. They also contain the highest weight % content of non-diamond carbon and non-carbon impurities from synthesis and post-processing (Table 1.1). HPHT usually contain a higher concentration of nitrogen (hundreds of ppm) and residual impurities from milling, whereas CVD have the highest purity and, depending on the growth conditions, can have a negligible content of sp^2 carbon and other impurities.

ND reactivity will be further evaluated, usually in reference to the diamond type (CVD, HPHT, dND). The transfer of procedures between different diamonds is often complicated, and even common organic reactions can be challenging. Differences between materials are sometimes overlooked in the literature in general and in field-specific reviews. A comparative study would be beneficial, although probably time-consuming. Furthermore, the available surface analyses

are limited and are not sensitive enough for monomolecular layers on diamond films. Thus, caution is needed when planning new diamond functionalisation based on different starting materials.

1.3.1 Differences between diamond types

The chemistry of dNDs is the most different from that of HPHT and CVD diamonds. dNDs are created by "bottom-up" synthesis, growing in the explosion. In contrast, HPHT NDs are synthesised using a "top-down" approach, mechanically milling polycrystalline microdiamonds prepared by slow growth. While HPHT surface is contaminated with only a small amount of sp^2 carbon. The detonation creates aggregates of dNDs, which are covered in soot. The soot is present on both the surface and inside the aggregates, together with a significant amount of a non-diamond carbon and residual metals [77]. The detonation soot is mechanically milled, sonicated and extracted with liquid oxidants and acids (such as HNO_3, H_2SO_4 and HNO_3, $K_2Cr_2O_7$ in H_2SO_4, KOH/KNO_3, Na_2O_2, HNO_3/H_2O_2, $HClO_4$ or HF/KNO_3) to preferentially remove non-diamond carbon and metal impurities [78–80]. Notably, some aggregates resist ultrasonic treatment due to the strength of attractive electrostatic forces [77].

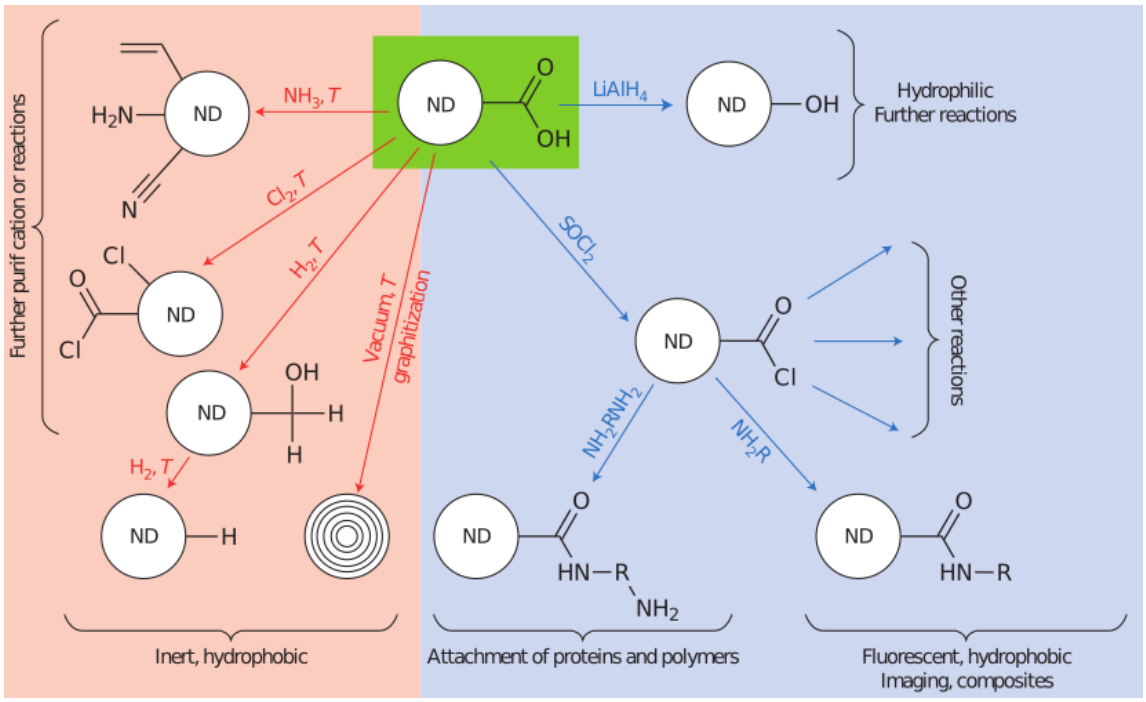

Figure 1.12: Scheme of surface functionalisation starting from the carboxylic acid group (green). Gas and high-temperature treatments are on the left side (red), whereas wet chemistry under room temperature is on the right side (blue). Treatment with NH_3 leads to various surface groups. Use of Cl_2 gas forms acyl chlorides, whereas F_2 leads to C-F [81–83]. Hydrogen treatment or hydrogen plasma reduces even C-H [84], and annealing without oxygen leads to graphitic carbon nanoonions [85]. Furthermore, wet chemistry treatments employ a wide range of functionalisations known from organic syntheses, such as the preparation of reactive acyl chloride intermediates [86, 87]. *Adapted from ref.* [77].

Surface modifications are required for biocompatible and highly selective applications (Section 1.4). Thus, a chemist can combine highly diverse surface chemistry approaches, which can be

divided into non-covalent and covalent or monolayers and multilayers. Generally, non-covalent procedures are easily and swiftly performed and tend to lack long-term stability. Procedures for covalent modification tend to be time-consuming and provide more stable conjugates. Monolayers easily introduce universally reactive functional groups, albeit with only partial surface coverage. Conversely, multilayers hide the nature of the diamond surface while increasing the distance from the surface. The proximity is not important for some applications, such as CVD based biosensors. Surface modification must primarily prevent non-specific protein absorption, whereas the sensitivity range of NV^- centres is limited to tens of nanometres.

The processing methods used by manufacturers commonly lead to a heterogeneous mixture of oxygen-containing groups or hydrogen-terminated surfaces before introducing another modification. The standard procedures include surface oxidation or reduction, graphitisation or non-diamond carbon removal and conversion into one type of functional group, such as -OH, -COOH, -COCl, -H and halogens. Surface oxidation is performed using liquid solutions, air or air with ozone. Air-based methods are cost-effective and environmentally friendlier for mass production [77, 88, 89]. A common feature of those operations is the formation of heterogenous oxygen-containing surface chemistry such as hydroxyl, carboxyl groups, ketones, lactones and anhydrides [90, 91].

Conversely, reaction with hydrogen gas at elevated temperatures or hydrogen plasma treatment leads to hydrogen termination for both CVD and NDs [92]. High-yield of subsequent functionalisation depends on quantitative and reproducible homogenisation of the surface.

1.3.2 Surface modifications with polymer

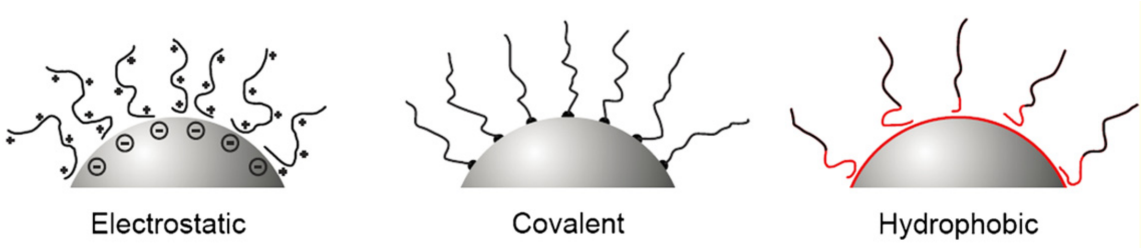

Figure 1.13: Types of surface polymeric modifications used for stabilisation and functionalisation of NDs. Higher surface density of polymer improves stability, loading capacity and reduces non-specific interactions of biomolecules with the ND surface. *Adapted from ref.* [93].

Generally, the ND surface can be modified with three types of interactions – electrostatic, covalent and hydrophobic (Figure 1.13). Charged polymers, such as amine-terminated PEI, can be used for electrostatic modification and removed by aprotic polar solvents (DMSO, DMF). The covalent modification introduces a stable connection with a small molecule, biomolecule or polymer layer. The last modification is hydrophobic interaction, such as interactions between non-polar moieties of lipids and H-terminated diamonds, thereby stabilising the particle in aqueous solutions.

Further examples of mainly electrostatic interactions are NDs surface modifications with

biomolecules, such as peptides [94], enzymes [95], antibodies, nucleic acids and charged polymers [96, 97]. Gene delivery was also demonstrated. First, a polycationic polymer was bound to the negatively charged surface of NDs, followed by a non-covalent attachment of a negatively charged nucleic acid to the polymer [98, 99]. While non-covalent attachments are easy to accomplish, they are limited by their low surface specificity and by exchanges with the solvent or other biomolecules present in biological media. These challenges are addressed by covalent modifications, which are discussed in following sections.

1.3.3 Surface unification and functionalisation

Direct attachment of molecules is a straightforward and simple approach, albeit limited by diamond reactivity and by the heterogeneity of surface functional groups. Scientists commonly use this approach for dNDs due to their high surface reactivity. New molecules should be attached after the unification of the bare diamond surface. Enabling higher reproducibility and yields of subsequent reactions. The functional groups primarily present on the surface of oxidised dNDs and HPHT NDs are carboxylic, carbonyl and hydroxyl groups.

In oxidised diamonds, acidic treatments with $HNO_3/H_2SO_4/HClO_4$ or piranha solution, for example, remove impurities and hydrolyse anhydrides, as well sp^3 carbon [91]. Then, carboxylic groups can be converted into acyl chlorides, amines and hydroxyl groups, as shown in Figure 1.12. Researchers sometimes divide functionalisation into gas, high-temperature treatment or wet chemistry without heating. For example, treatment of ND with lithium aluminium hydride leads to a partial reduction of the surface [100], similarly to borane in THF [101]. Heating NDs in H_2 atmosphere reduces C=O and, over time, C-OH to C-H as well. Such a surface can be similar to the high purity of CVD diamond films. The growth conditions of CVD typically include hydrogen gas, which continuously etches sp^2 carbons faster than sp^3 carbons and thus the CVD surface is by default hydrogenated. However, hydrogenated surface deteriorates over time when exposed to air or other oxidising conditions [87].

Functionalization strategies for hydrogenated surfaces usually rely on C-H bond formation. Reactions on hydrogenated surfaces lead to the formation of hydroxyl groups under UV irradiation with water vapour. Alkenes with variable length and termination or non-UV absorbing functional groups have been UV-grafted [102–104], or diazonium-grafted [92, 105]. These hydrogenated surfaces are commonly present in CVD materials, and specific procedures can be found elsewhere [87].

In addition, a potential approach is to introduce highly reactive (bio)orthogonal groups, known as “click” chemistry [106]. The advantage of this approach is the elimination of side reactions with remaining groups on the surface, thereby enabling further high-yield functionalizations. The introduction of these groups in the surface of NDs was reported for alkyne-azide, *trans*-cyclooctene and indirectly for a polymer shell, as described in the following section [107–110].

1.3.4 Covalent modifications with polymers

For advanced bioapplications, NDs must be colloidally stable, biocompatible and prepared using a reproducible procedure. An important option for surface chemical functionalization is coating of the surface with a polymeric shell. Covering NDs in polymers is a significant approach, among others used for NDs, such as lipid bilayers [111], diamond graphitisation to sp^2 carbon NDs and with gold shell either directly[112] in with intermediate layer of gold[113]. For sharp or irregular-shaped NDs, a thicker polymer softens the edges and reduces a potential mechanical cytotoxicity [114].

The purpose of using organic polymers is to increase colloidal stability in an environment with high ionic strength (physiological conditions, buffers) and to reduce non-specific interactions and immune response. Furthermore, selected groups can be installed for further conjugation of small molecules, fluorophores, proteins and enzymes, for example. Depending on the conditions of polymerisation, a balance is sought between stability, loading capacity, hydrophilicity, synthetic feasibility and reproducibility.

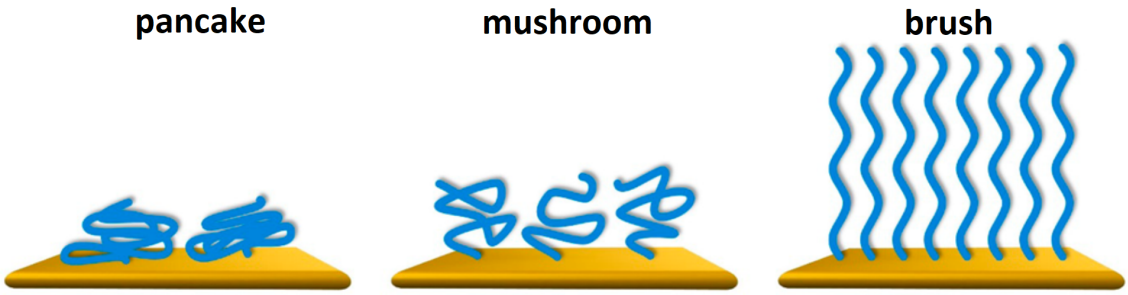

Figure 1.14: Representation of polymer conformations on grafting density-related surfaces, known as pancake, mushroom and brush. *Adapted from ref.* [115].

The polymer layer can form different structures on the surface – ranging from low density coverage, such as pancake or mushroom configurations, to dense brushes (Figure 1.14). These structures will vary as a function of the method of polymer attachment, which is divided into grafting-to and grafting-from approaches, see Figure 1.15. In the former, polymer chains are synthesized separately and then attached to particles. In the latter, the polymer grows from the NDs surface.

Grafting-to is an experimentally straightforward approach, and the polymer chain is easily modified before the attachment. However, it reaches a lower grafting density due to steric hindrance during chain attachment to the surface. In addition, the attachment yield decreases with the increase in molecular weight, which limits the maximal thickness of the polymer. In conclusion, grafting-to provides lower colloidal stabilisation, polymer of known known thickness and can limit the loading capacity for further ligand conjugation [115, 116].

Grafting-from is a bottom-up approach. Polymerisation is initialised on the surface, providing higher control over the process. Therefore, it is referred to as surface-initiated controlled radical

polymerization (SI-CRP) or surface-initiated ring-opening polymerization (SI-ROP) in case of non-radical polymerisation. The selection of the monomer (Figure 1.15) makes it possible to control the polymer architecture, molecular weight, composition and thickness. However, the control over thickness or density is not precise nor straightforwardly determined.

Furthermore, copolymerisation with another monomer can be used for introduction of a specific functional group. It can lead also to polymerisation termination. Due to small molecular dimensions of monomers, grafting-from reaches higher grafting density, but optimisation can be time-consuming. Some examples of polymers used in this approach are shown in right-hand side of Figure 1.15 and a detailed lists of polymerisation strategies can be found in reviews on this topic [115, 116].

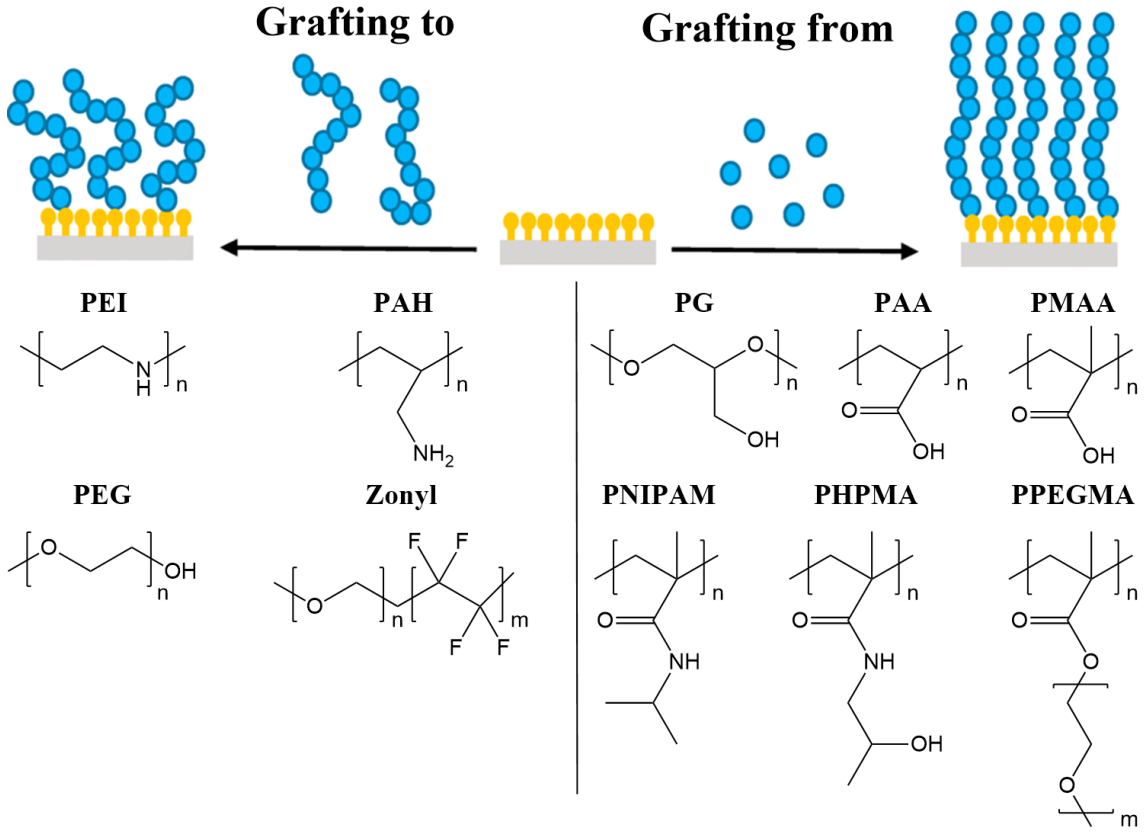

Figure 1.15: Upper: Grafting-to attaches already existing polymer while grafting-from starts polymerisation from the nanoparticle surface. Bottom: Commonly used polymers for grafting-to (left) and grafting-from (right). Polymer names: poly(ethyleneimine) (PEI), poly(allylamine hydrochloride) (PAH), poly(ethyleneglycol) (PEG), Zonyl is commercial polymer of DuPont company, poly(glycerol) (PG), poly(acrylic acid) (PAA), poly(methacrylic acid) (PMAA), poly(N-isopropylacrylamide) (PNIPAM), poly[N-(2-hydroxypropyl)methacrylamide] (PHPMA), poly(PEG methyl ether methacrylate) (PPEGMA). *Adapted from ref.* [93, 115].

Controlled reversible-deactivation radical polymerisation* introduces radicals on the surface. Propagation along the chain is unlikely to be terminated (thus "living") differently then by controlled deactivation. The the other category is called reversible-deactivation radical polymerisation (also denoted as"non-living"). The polymerisation propagation depends on

*Also often denoted as living radical polymerisation, use of this term is not recommended by IUPAC.

initiator presence, since the termination of chain polymerisation is likely to occur. Further, the polymerisations are differentiated by polymerisation mechanism to atom transfer radical polymerization (ATRP) and reversible addition-fragmentation chain transfer (RAFT) methods. ATRP employs halogen-terminated NDs and metal halide catalysts. RAFT is metal-free, uses as a radical source organic compounds such as azobis(isobutyronitrile) (AIBN). The third notable method is nitroxide-mediated polymerization (NMP), which uses radical from nitroxide, such as 2,2,6,6-tetramethylpiperidinyloxy (TEMPO), and has several limitations in controlling the polymerisation speed [116, 117]. In ATRP, the removal of metals can be problematic; thus, the RAFT approach is preferred for metal sensitive applications.

To conclude, the formation of polymer layer is usually an intermediate step before the final functionalisation and application. Specific goals, such as sensing or targeting, are achieved using additional small molecules or biomolecules which are later attached to the polymer. Covering a polymer with small molecules can be advantageous due to their higher loading capacity than that of biomolecules. In turn, for a non-polar molecule, the higher loading can lead to ND destabilisation. Thus, the polymer should stabilise NDs with regard to the further surface functionalisation and a target environment. Further analyses have been discussed in more detailed reviews and book chapters [118, 119].

Polymer coated NDs

Several polymers can be compared to demonstrate the strong link between applications and polymer tailoring. The grafting-from procedure enables further variation by copolymerisation, by changing the polymer composition during growth or by incorporating a monomer terminating the polymerisation. Grafting-to methods often use polymers, which are commercially available with various end-modified groups such as poly(ethyleneimine) (PEI) and poly(ethyleneglycol) (PEG). Usually, amide or ester bonds are used to bind the polymer to NDs, and the other end is used for further conjugation, e.g., for targeting or drug delivery. Cationic polymers (PEI, PAH) are suitable for gene delivery due to electrostatic binding of negatively charged nucleic acids [96, 120, 121]. PNIPAM and PAH are pH- or thermo-responsive, with applications in sensing (Section 1.4.1 [122, 123]. Various polymers have been used, such as modified PEG with CF_2 groups, called Zonyl, was reported by Macron to be ND stable in PBS [124].

The PEG is widely used in biological studies due to its commercial availability (various lengths and end-functionalisation), colloidal stabilisation and small non-specific binding. There are several issues referred to as the "PEG dilemma", such as enzymatic oxidation of terminal hydroxyl groups to aldehydes, followed by reactions with biomolecules and immune response to PEG-coated nanoparticles. Oxidation can be addressed by using methoxy derivatives of PEG [125].

Alternatively, a layer of silica is used as a spacer between NDs and a polymer or a biomolecule [101, 126, 127]. There are several reasons for this additional step before polymerisation. The surface of NDs is normalised regardless of the synthetic origin of the diamond. It simplifies

method transfer for different surfaces with different reactivity. Furthermore, a well-established toolbox of silane chemistry is available, leaving free silanol groups on the surface [101, 118, 128]. Colloidally stable silica coated NDs have been created, subsequently covered with PHPMA copolymerised with monomer containing an alkyne or azide groups. Thus, further bioorthogonal reactions became available using Cu(I)-catalyzed alkyne-azide cycloaddition (CuAAC). These particles showed minimal non-specific interactions and were stable in 1M NaCl [129]. However, the silica layer can be completely hydrolysed in 0.1 M HCl [101].

Glycidol polymerisation is a non-radical ring-opening reaction (SI-ROP). Growth begins from the oxygen-containing groups on the surface of NDs. Due to the branched structure of monomer, it creates a hyperbranched, dense poly(glycerol) (PG) layer [130, 131]. The NDs are colloidally stable and compatible with CuAAC functionalisation, showing very low non-specific interactions. Such polymer has a high potential when equipped with an additional targeting moiety, as shown for targeting, gene delivery and magnetic resonance [99, 131, 132].

1.4 Nanodiamonds applications

Nanodiamonds (NDs) in general are used in industry and research. Many NDs applications are mechanical (lubricants, abrasives, tribology and seeding for CVD) and utilize dNDs because of their high availability, low price and insensitivity of these applications toward size distribution and impurities [77]. Conversely, bioapplications, fluorescence and quantum-based applications require high purity fNDs with NV^- with a narrow size distribution and with reproducible and well-defined properties. fND is used as non-bleachable, biocompatible, stable fluorophore emitting within a NIR imaging optical window (650 - 1350 nm). In this range, light penetration peaks [54], with minimal background autofluorescence of the cell. In addition, the fluorescence lifetime is longer than for the cells, which can be further filtered out [57]. Therefore, fND is suitable for long-term particle tracking, unlike organic dyes [57, 133]. Instead of listing similar optical applications, the following overview focuses on the use of the unique properties of NV^- centres.

1.4.1 ND with NV^-centres

Applications for ND with NV^- are emerging in fields of biology, medicine, physics, quantum computing and nanoscale magnetometry. For optical detection, many of them are using standard or modified optical microscopy setup. Sensing can be divided into single NV^- detection, ensemble measurements (ND with multiple NV^-) and bulk diamonds.

Optical diffraction resolution is limited to approximately half the wavelength of light, although super-resolution microscopy has partly overcome this limitation. The spatial resolution of an NV^- centre is limited by the magnetic field sensitivity and could reach levels bellow the optical diffraction limit [134]. FNDs with NV^- can be used in nanoscale quantum sensing due to the

unique magneto-optical properties of NV^- centres [135]. This includes nanoscale temperature, orientation sensing; spin detection (Section 3.3.2), magnetic field sensing, scanning magnetometry [42, 136] and quantum diamond microscopy for imaging electric, magnetic, stress areas and even nanoscale NMR and ESR spectrometry [67, 137, 138].

Bioapplications

Applications for a biological environment, cellular research or medicinal uses require biocompatibility (non-toxicity, no non-specific adsorption) and colloidal stability under physiological conditions [93]. Torelli used fND to imagine tumour-targeted with functionalised fNDs [110]. DNA transfection with imaging and tracking was demonstrated by Petrakova when using non-covalently attached DNA payload [139]. Chow demonstrated the delivery and therapeutic effects of doxorubicin equipped NDs [140]. Further biomedical and *in vivo* applications are described in reviews on this topic [32, 141–145].

A key goal, which remained only a fantasy for several decades, is to acquire detailed information from living cells with high spatiotemporal resolution, that is, detecting some quantity (pH, temperature, pressure or specific molecule) at room temperature in a specific part of the cell. McGuinness demonstrated detection of single ND by tracking orientations and movements of an unmodified ND inside living cells [146]. Furthermore, a proof-of-concept study has shown nanoscale temperature sensing at first [147, 148], with microsecond time resolution subsequently [149]. Balasubramanian showed nanoscale magnetometry at room temperature [150].

Considerable research efforts have been made to detect paramagnetic species (radicals, Mn^{2+} or Fe^{2+} ions) inside the cell, potentially more sensitive than EPR and with a spatial resolution unavailable by EPR or indirect fluorescent detection [151–153]. The limiting factor is the functionalisation of fNDs which should selectively interact with their surrounding environment and are stable inside cells. Grotz showed the feasibility of detecting a single spin (radical) localised on the surface of ND [70]. Furthermore, sensitivity limits have been explored from ultra-low concentrations of paramagnetic ions – to the tens of Gd^{3+} ions [154] and also to 175 Mn^{2+} ions or 10 ferritin proteins in water [155, 156]. Moreover, Sadzak has detected iron oxide nanoparticles (10 nm diameter) [157]. More recently, polymer-coated fNDs equipped with Gd^{3+} were used to monitor changes in pH or redox potential [158] and Fujisaku developed a T_1 pH-sensing procedure based on changes in the surface charge of fNDs [159]. Recently, Gorrini reported fast detection (μs) of Gd^{3+} mixed with ND in diluted deoxygenated blood sample [160].

In conclusion, selective sensing of processes inside living cells, such as radical sensing to explain the free radical processes related to cellular ageing, seems to be reachable [161]. Further improvements in selectivity and stability of fNDs are needed to obtain such valuable data for research in life sciences.

1.5 CVD diamond applications

The unique properties of diamond materials drive the development of their applications – hardness, physical and chemical stability and low absorption in several spectral regions. The CVD technique with seeding makes it possible to grow diamond with diverse surface and shapes. Furthermore, the high versatility of material properties (thickness, doping, substrate) broadens the range of applications. Diamond layers are used not only as components of DSSC, which will be further discussed below, but also in high-end applications such as surface acoustic wave (SAW) devices, biosensors [162], electrochemical electrodes [163], radiation detectors, X-ray or IR transmission windows [7, 164], tribology [27], conductive AFM tips [165, 166] and inject for corrosive liquids [167]. The general limitation of CVD diamond technique is the limited speed of growth, thickness and scalability to larger uneven surfaces.

1.5.1 Light conversion to energy

Energy production is crucial to support human life on Earth. The use of non-renewable energy sources is no longer sustainable, and harvesting light is one of the renewable sources with potential. The overall contribution of renewable sources to electricity production is 22 %, and photovoltaics account for less than 1 % [168], despite the widening use and improved efficiency of commercial solar cells.

Current mass-produced photovoltaic devices are based mainly on silicon, and high-efficiency cells often contain environmental toxic metals (Ga, As, Cd, Te [169]). Silicon-based devices are energy, resources and costly (high- thickness, high-purity silicon) and must be sealed under vacuum to work, which lowers the device lifetime. In turn, a thin semiconductor layer is cheaper to manufacture and less mechanically sensitive. One approach is to manufacture only a thin silicon layer, albeit with significantly lower conversion.

The operation principle is based on light absorption and charge separation in silicon by an internal electric field (p-n junction) [170]. The alternative approach is use of dye sensitized solar cells (DSSC). The sensitisation concept was developed by O'Regan and Grätzel, who prepared dye-sensitised TiO_2 photoanode (n-type [171]). It employs a thin, transparent electrode layer, which is covered with absorbing dye. Thus, this type of device can generate a photocurrent without affecting the ability to reuse the photo-converting layer multiple times. The theoretical efficiency of a single junction device is described by the Shockley-Queisser limit to 33 % at AM 1.5 solar spectrum* [172]. This limit can be surpassed by multi-junction or tandem cells (two p-n junctions), with a theoretical limit of 68 % and 43 % [173], respectively.

The diamond-based electrode doped with boron is suitable for electrode development thanks to high optical transparency, stability and conductivity as a photocathode (p-type) or as a part of tandem solar cells (n, p-type).

*The AM (air mass) is the sunlight spectrum after passing the Earth's atmosphere. The coefficient 1.5 represents lower light intensity relevant for significant human habitats in temperature latitudes.

1.5.2 DCCS solar cells

The DSSCs is an attractive alternative to silicon photovoltaics due to a less demanding manufacturing process and potentially lower production costs. Furthermore, the different operation mechanism enables the use of transparent materials and good performance under low-light conditions. Thus, it is possible to integrate such devices into other existing materials such as the windows or walls of a building [174]

Unlike silicon photovoltaics, in DSSC, charge separation and light absorption are performed by different parts – electrode/electrolyte and dye sensitiser. They can be separately tuned or, due to transparency, arranged in several layers [175, 176].

Harvesting photons on both electrodes (n,p-junction) in one device should ideally lead to the sum of photocurrent generation. Currently, the photoanodes (n-junction) are well optimised and achieve significantly higher photocurrents (13.0 % and 14.7 % power conversion efficiency [175, 177]) compared to p-type photocathodes [169]. Thus, there is a gap in p-type cathodes before tandem cell will overcome the efficiency of single-junction n-type DSSC.

1.5.3 Comparison of n- and p-type devices

The field of n-DSSC solar cells was popularised by work of O'Regan and Grätzel based on the TiO_2 anode [171]. The basic operation of the n-type device is the following: the photon excites sensitiser (dye), and the electron transfers from the dye to the conduction band of the anode. In p-type devices, the exited dye transfers the electron to the electrolyte, and a separate hole is injected into the cathode valence band, see Figure 1.16.

The first p-DSSC was remade as an n-type cell [179]. The TiO_2 anode sensitised with ruthenium complex was exchanged for a NiO cathode with erythrosine B, observing and smaller photocurrent than that of the n-type cell. Although the device functions similarly, the p-type must overcome several challenges. The energy level cascade for electron/hole transfer must be changed. The levels of valence, a conductive band of the electrode, must be tuned and matched to a dye and electrolyte solution. Furthermore, the p-type efficiency is lowered by fast charge recombination of an electron-hole pair.

1.5.4 P-type devices

The electrode for the p-type device should be a stable, transparent p-type semiconductor with a wide bandgap [180]. The BDD is a suitable candidate due to high chemical stability and transparency. To design photoconverting device, following components need to be consider: surface porosity, optically or electrochemically active impurities, electrolyte selection, dye selection its attachment to the surface.

The higher the electrode porosity is, the higher dye loading and thus efficiency will be. The

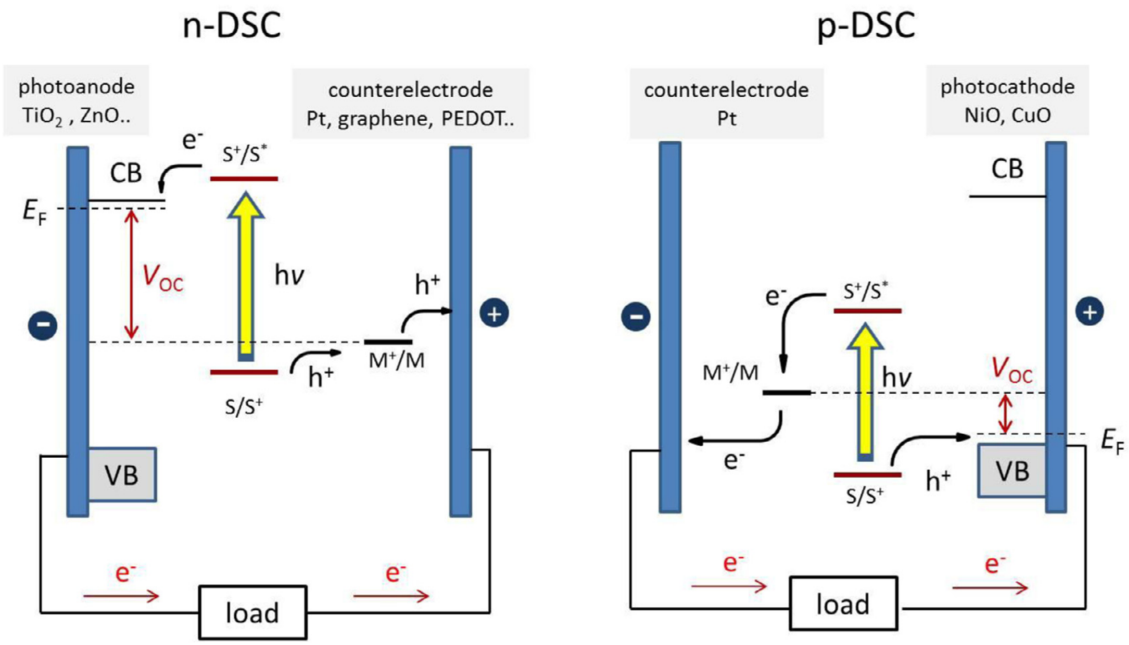

Figure 1.16: Scheme of dye sensitised solar cells of n-type (left) and p-type (right). The operation of cells is the same, based on photoexication of dye (sensitiser), followed by electron injection into the photoanode or electrolyte solution (mediator) *Adapted from ref.* [178].

surface-to-volume ratio can be generally increased using top-down or bottom-up approaches. A typical top-down approach is the CVD technique, which can precisely control surface thickness and crystallinity. Unsurprisingly, the surface area is significantly lower than the deposition of nanoparticles such as NiO or TiO_2. Furthermore, the amount of sp^2 impurities needs to be controlled during CVD deposition. This pose an issue since a non-diamond carbon is often light-absorbing and electrochemically active. The effect of these impurities can be mitigated by selective annealing or etching, as performed for NDs. Such an approach often requires time-consuming experimental optimisation of conditions. Higher precision is achieved by inductively coupled plasma etching [181] or focused ion beam (FIB). ICP etching removes a significant portion of the material using oxygen or hydrogen plasma. FIB is time-consuming, suitable for precise surface patterning, but not for scale-up of surface alterations.

A bottom-up approach suitable for DSSC applications is growing diamond on highly porous substrate. A surface was covered with multiple layers of SiO_2 spheres, and spheres are seeded with NDs. Spheres are used as a template, growing by MWCVD and controlling thickness by deposition time, similar procedure can be done with SiO_2 fibers [182]. Lastly, the SiO_2 template is removed by HF acid etching and high surface is available for dye sensitisation [183, 184].

An electrolyte is responsible for dye regeneration to the ground state and electron transport to the anode. Although the triiodide/iodide (I_3^- / I^-) redox couple is often used, an intrinsic drawback is strong light absorption. Moreover, open-circuit voltage is limited in combination with NiO cathode. Many alternatives are pursued, most commonly based on inorganic redox couples (Co, Fe, Cu) or organic redox couples based on thiolates or quaternary ammonium

compound [180, 185]. Since optimisation is performed for each p-type device, the comparison of the most promising materials is not straightforward.

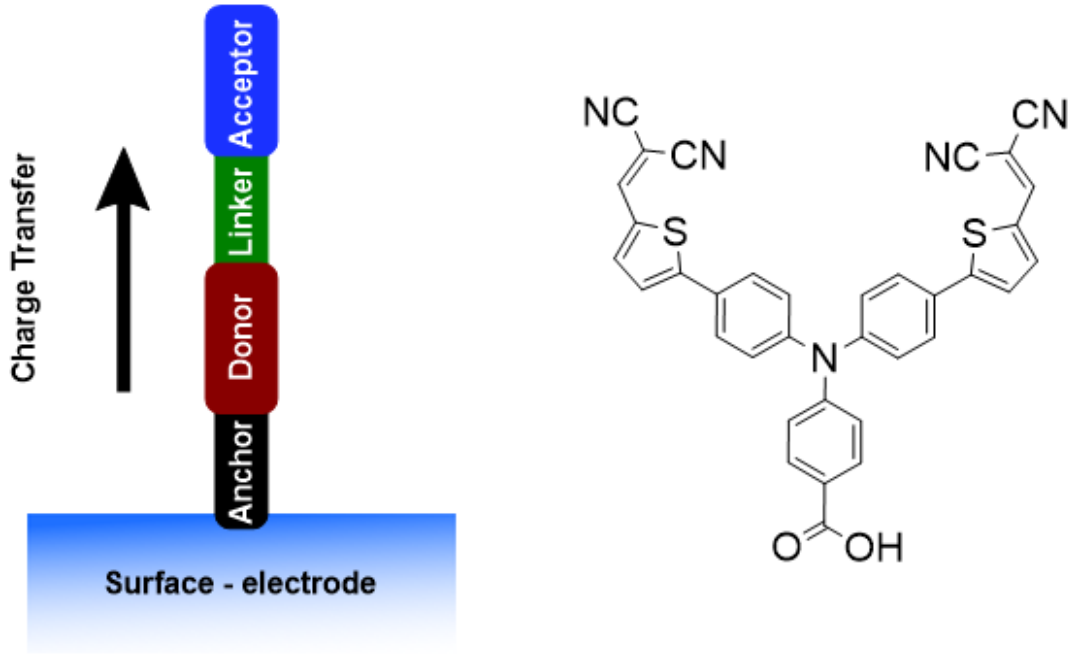

Figure 1.17: Scheme of push-pull design demonstrated on **P1** dye. Carboxylic group is used as an anchor, triphenylamine as a donor and two dicyanovinyl as electron acceptors. *Adapted from ref.* [180].

Selection and design of an organic dye for dye sensitized solar cells (DSSC) depends on the type of solar cell (p- or n-type), electrode material and electrolyte. General requirements for dye are photon absorption in visible-NIR region, high absorption coefficient, anchor to the surface, suitable position of HOMO and LUMO levels, photo- and electrochemical stability.

For p-DSSC, the dye HOMO needs to be more positive than valence band of cathode and LUMO needs to be more negative than the electrolyte redox potential, see Figure 1.16 [186]. Further, dye should delay charge recombination of an electron-hole pair. This is often done by donor-π-acceptor (D-π-A), where the charge separation is promoted on the far-end of dye – away from the surface, Figure 1.17 [180]. An excellent results were obtained for p-DSSC for **P1** dye on NiO by Qin in 2008 [187]. Based on this design, many modifications were tried to improve efficiency of p-DSSC with various surface and electrolytes [180, 188] Strategies for design and selection of dyes for p-type devices can found in elsewhere [174, 189, 190].

In conclusion, improving the efficiency of the solar cell is an essential part of efforts for sustainable energy production. The DSSC is in a perspective approach for cheaper and energy less demanding manufacturing process. Efficiency and lifetime challenges for DSSC, where a BDD is an excellent candidate for extending the stability of devices.

2 | Scope of the thesis

The objective of this thesis was to develop new chemical interfaces on diamond surfaces and to demonstrate the use of diamonds for applications such as photovoltaics, sensing and ultrasensitive detectors.

For such purposes, we selected two diamond forms differing in surface-to-volume ratio. The first form was a microcrystalline diamond films. The second material consisted of nanodiamond particles (NDs) with a high surface-to-volume ratio. NDs are particularly challenging in terms of balancing chemical functionalization with colloidal stability.

The aims of this thesis were, therefore, divided into two parts:

Microcrystalline diamond films

1. To develop a reactive interface on the surface of boron-doped-diamond (BDD) and to attach a photocurrent-generating dye to the surface.
2. To prepare and characterise a semi-conductive BDD surface with a dye tailored to improve stability, photon absorption and photoconversion.
3. To facilitate systematic study of changes in photocurrent based on differences in conductivity for a BDD and a silicon substrate.

Nanodiamond particles

4. To assess and quantify the chemical processes on BDD surface by use of NDs with similar chemical properties.
5. To develop a small molecule for quantification of available functional groups on the surface of biocompatible polymer coated NDs.
6. To create a ND based system for ultrasensitive detection of paramagnetic species based on previous findings and practical know-how.

This proposed system must meet the following criteria:

- To attach a small molecule capable of reversibly forming stable radicals to the NDs surface.
- To prepare NDs with nitrogen vacancy (NV) centres and stable radicals within tens of nanometers from NV centres.
- To validate the system using an independent method for detecting and quantifying paramagnetic species in the system.
- To prepare colloidally stable particles in water and aqueous buffers to meet basic requirements for bioapplications.
- To verify presence and number of stable radicals in the system after radical deactivation.

3 | Results & discussion

3.1 Microcrystalline diamond films

This section explores the possibilities and limitations of diamond-based photocathodes for sustainable energy production. Currently, dye-sensitized solar cells (DSSC, DSC or Grätzel cell) are mostly based on n-type photoanodes, which provide higher photocurrents than p-type photocathodes. The aim was to improve generated photocurrents for BDD cathodes sensitised with a dye. The following section focuses on surface modifications on silicon substrates 5×10 mm with a 0.5 μm layer of a microcrystalline diamond.

Thin diamond layers are promising materials considering their high stability, photo- and electrochemical properties and high optical transparency. In addition, boron doping introduces electric conductivity and enables their use as p-type cathodes. Optically transparent electrodes are essential for tandem devices (p,n-DSSC) to harvest more light. In turn, multi-junction devices can surpass the thermodynamic limitations of single-junction devices, Section 1.5.1 [180]. Currently, low photocurrents were reported for diamond based cathodes. Main reason are challenging chemical modification and tuning the energy band levels between the individual components of the solar cell. Therefore, we focused on developing and improving the following parameters: stably attaching the photosensitizer (dye), increasing dye loading, preparing a custom-made dye, and alternating the conductivity properties of the substrates.

3.1.1 Surface modification of boron-doped-diamond electrodes by covalent bonding P1 dye* (A)

We set out to develop a procedure for covalently modifying microcrystalline boron-doped-diamond (BDD) with **P1** dye (Figure 3.1, Figure 1.17) to generate a photocurrent. Diamond was selected because of its high electrochemical stability towards reactive electrolytes. High-purify microdiamond is an insulator, but boron-doping makes possible to control p-type (semi)conductivity. A photocurrent is generated by an additionally attached chromophore. BDD itself absorbs a little in visible-NIR region, yet residual sp^2 carbon impurities create unintended absorption

*__Published as__: Krysova, H.; **Barton, J.**; Petrak, V.; Jurok, R.; Kuchar, M.; Cigler, P.; Kavan, L.; *Efficiency and stability of spectral sensitization of boron-doped-diamond electrodes through covalent anchoring of a donor-π-acceptor organic chromophore (P1).*

without generating photocurrent. Thus, we used a commercially available dye **P1** to facilitate direct comparisons and to enhance the reproducibility of our work.

Energy is transferred between dye and cathode based on proximity. To ensure short and reproducible distances, we covalently attached the dye to the surface. We have previously tried non-covalent attachment of poly(ethyleneimine) (PEI) with **P1** dye to BDD. Although that procedure bypassed more complex multi-step surface modification, dye loading was low, and the dye desorbed over time [183].

The following premises were used for developing the described procedure: The reactivity is low for the CVD diamond surface, and conversion should be as quantitative and clean as possible. Further, degradation of reagent or surface was not preferred. The requirement was met by forming C-C bonds under UV-light in which the resulting adduct is chemically stable during and after UV-photografting [103]. This excluded direct attachment of dye and non-UV degradable linker was selected. Furthermore, the length of the linker was also considered because we suspected that the larger distance contributed to the lower photocurrents in a non-covalent attachment [183]. In addition, the efficiency of hole-injection depends on the distance between dye and surface; thus, we selected a short four carbon linker.

The commercial dye **P1** from Dyenamo AB(Figure 3.1) was selected as a photon absorbing material [191]. **P1** has a high extinction coefficient (58 000 $M^{-1}cm^{-1}$) and it is used for a p-DSSC. Its function has been demonstrated on NiO cathode [187, 192]. The **P1** dye consists of three parts: an electron acceptor (malononitrile), a conjugated chain (malononitrile) and an electron-donating triphenylamine part terminated with a carboxylic group, Figure 1.17. The amino-terminated linker dye was used to the anchor a dye at a defined distance from the surface.

Photosensitised plates were prepared in the following sequence. First, the silicon wafer (9×9 cm) was nucleated with dNDs. From then, a 0.5-µm-thick microcrystalline diamond film doped with 4000 ppm of boron was grown by microwave plasma enhanced chemical vapor deposition (MW-PECV). The resulting surface of BDD can contain various functional groups (Section 1.3.1). Modifying only one type of functional group would decrease dye loading, and loading capacity is limited by the sterical hindrance of the dye itself. Thus, the microdiamond surface was treated using hydrogen plasma to terminate the diamond surface with hydrogen. The modified silicon wafer was cut to smaller plates of 0.5×1 cm for linker and dye attachment.

Two types of protected allylamine were UV-photografted to the hydrogen-terminated surface (Figure 3.1). The protecting group was cleaved from allylamine. Then, the amine-terminated surface was covered overnight with the freshly prepared **P1**-Cl in dark, dry inert atmosphere and thoroughly washed with solvent mixtures for several days. The washing and sonication procedure varied on the degree of dye adsorption to the surface of a particular plate.

The low sensitivity of analytical methods precluded any accurate comparison of yield of photografting, deprotection or dye attachment. Thus, only the final photocurrents could be

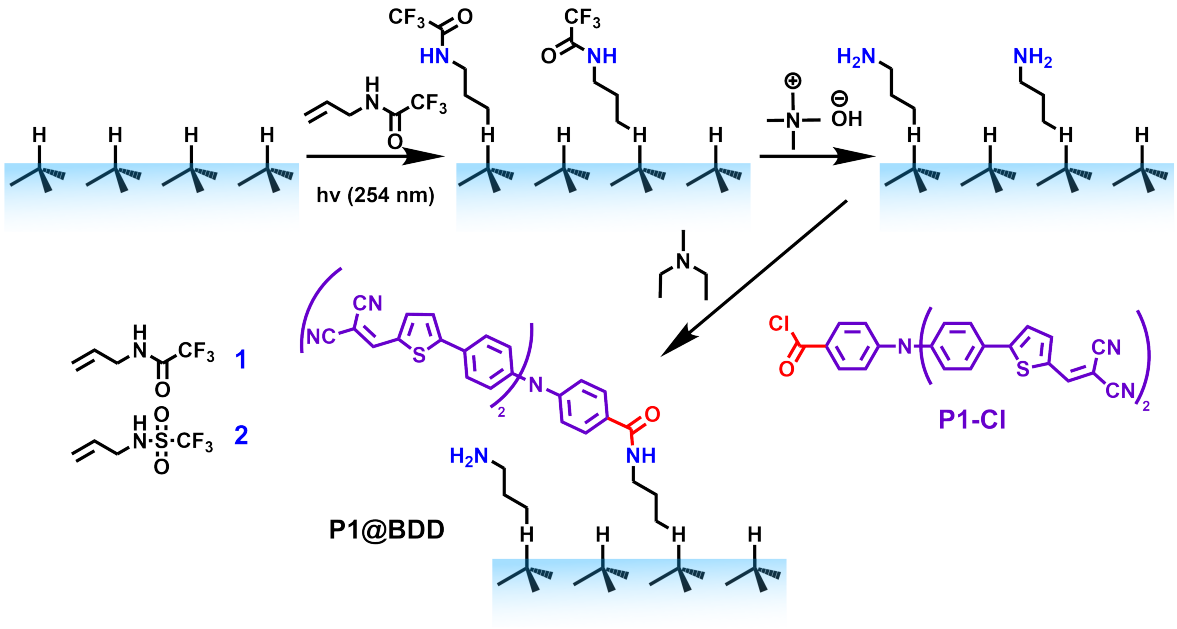

Figure 3.1: Scheme of surface modifications on BDD. A short protected allylamines were photografted to the surface, differing in the protecting group. 1 – *N*-allyltrifluoroacetamide and 2 – *N*-allyltrifluoromethanesulfonamide. The allylamines were deprotected and the **P1**-Cl was attached to amine for 3 days, and an excess of dye was washed out. *Adapted from Appendix* A.

compared by adding all reaction yields and other variables. Thus, multiple approaches were used to compare and indirectly evaluate the best approach.

The dye sensitised plates were characterised by XPS and Raman spectroscopies. The Raman spectra together with XPS supported each chemical modification step. However, we were unable to quantify reaction yields in detail due to the low signal-to-noise ratio of XPS data, Figure 3.2.

We compared resulting photocurrents on plates photografted with linker **1** (*N*-allyltrifluoroacetamide) and **2** (*N*-allyltrifluoromethanesulfonamide). We anticipated that the trifluoromethylsulfonamide protecting group as an electron acceptor would improve the grafting yield, which was not the case. We reason that harsher deprotection conditions (overnight at 105 °C with sodium bis(2-methoxyethoxy)aluminium hydride) did not lead to quantitative deprotection or changed properties of the surface, compared to the a methanolic solution of tetramethylammonium hydroxide.

We characterised the electrochemical properties, long-term stability under and determined IPCE. The unmodified BDD electrode showed a negligible response of ca. 20 nA cm^2 of dark current, which was attributed to sp^2 impurities or states related to boron in diamond lattice [193]. Modified **P1** sensitised BDD electrode showed a response of approximately 0.9 µA cm^2. Over a period of 45 h, the response ranged from 1 µA cm^2 to 1.5 µA cm^2, which afterwards dropped to ca. 0.6 µA cm^2. We assigned an increase followed by a decrease to changes followed by partical decomposition of the dye attached to the surface.

To conclude, we measured a maximum of 1.5 µA cm^2 (simulated illumination AM 1.5 solar

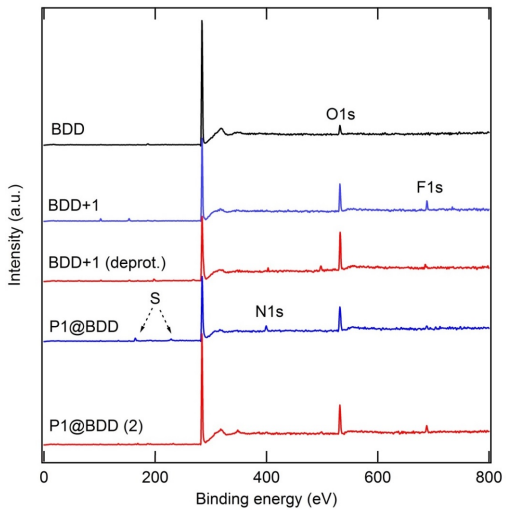

Figure 3.2: XPS spectra, from top: BDD, BDD with linker **1**, BDD with deprotected linker **1**, **P1** sensitised BDD with linker **1**, or **2**. Curves are offset for clarity, the intensity scale is the same for all spectra. *Adapted from Appendix* A.

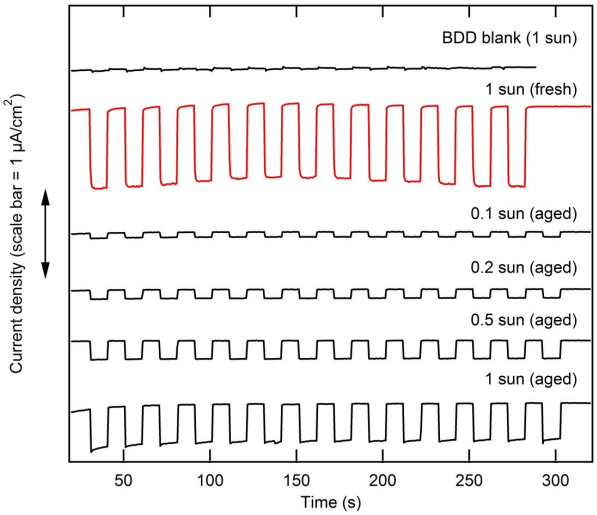

Figure 3.3: Electrochemical characterisation: BDD electrode (top) and **P1** on BDD after 5 min (fresh) and 45 h (aged). Bare BDD showed negligible photocurrent response, while **P1** sensitised BDD (red) showed 0.9 μA cm^2 which decreased over 45 h. *Adapted from Appendix* A.

light), which is *ca.* 4-times larger than the previously reported best result with non-covalent anchoring the **P1** to BDD. The reported value was similar to or better than other results on BDD electrodes [194–196]. Although the measured values of photocurrent were smaller than those of sensitized p-NiO, which are reported in order of mA cm^2, the covalent attachment significantly improved the photocurrents. We thus decided to design new dye and focus on optimisation of the substrate in our next studies.

3.1.2 Diamond photocathodes sensitised with a bis(perylenemonoimide-dithiophene) donor-acceptor dye* (B)

The second study aimed at designing a new donor-π-acceptor dye to tune the dye energy levels for BDD electrode. Furthermore, we intended to avoid metal based dyes due to their environmental toxicity and lower observed photocurrents for p-type cathodes [180]. The proposed dye was based on the electron push-pull concept (Section 1.5.4). Secondary aims were to improve dye attachment to the surface and to reach stronger photoconversion in the visible-NIR spectral region.

The dye **DpA** was designed for a p-type cathode (Figure 3.4), reflecting the donor-π-acceptor (D-π-A) concepts from **P1** dye (Section 1.5.4) [187]. Two carboxylic groups at the triphenylamine moiety were introduced to the structure for improving the anchoring to the amine-terminated surface of BDD. The triphenylamine moiety serves as an electron donor. The main absorption band of **DpA** is red-shifted by bithiophene which is conjugated to ensure electron flow to an electron acceptor part. Lastly, the perylenemonoimide units can accept the electrons and

*__Manuscript in preparation:__ Bartova, K.; Jurok, R.; **Barton, J.**; Krysova, H.; Kuchar, M.; Mortet, V.; Taylor, A.; Cigler, P.; Kavan, L.; *Diamond photocathodes sensitised with a bis(perylenemonoimide-dithiophene) donor-acceptor dye.*

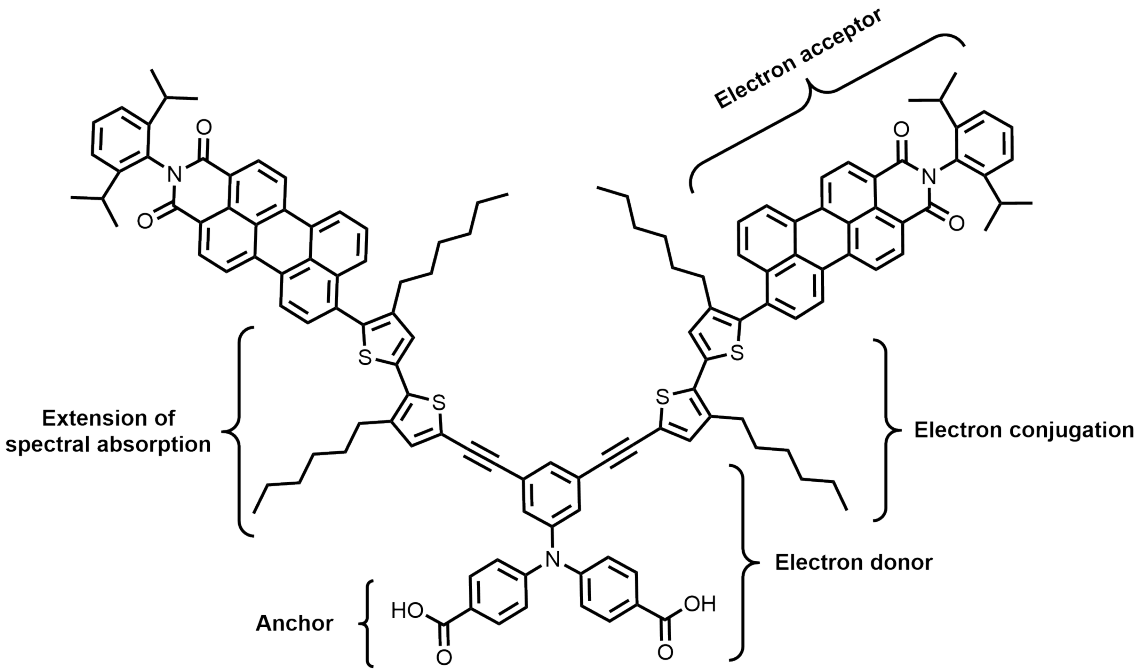

Figure 3.4: Structure and particular functions of donor-π-acceptor (D-π-A) dye **DpA** designed for attachment to BDD surface for preparation of p-DSSC. *Adapted from Appendix* B.

facilitate the formation of an electron-hole pair. The electron flow continues to the electrolyte solution (dimethylviologen) and hole can jumps to the valence band of BDD.

The complex synthesis of D-π-A dye **DpA** yielded 12 mg over 17 reactions steps in a convergent synthesis which was performed in the laboratory of Dr. Martin Kuchař. **DpA** dye has two absorption maxima, and we determined its molar absorption coefficient in dichloromethane at $\lambda_{max} = 347$ nm to be $\epsilon = 21500$ M^{-1} cm^{-1}. However, the value of the molar absorption coefficient might be slightly underestimated due to residual impurities contained in the final product. The product was low soluble in most of solvents. Despite the repeated chromatography purifications, some impurities thus might not be removed, see bellow.

The plates were covered with dye **DpA** using an improved procedure of previously described (Section 3.1.1), and the substrate B-doping was lowered to 250 ppm boron (Section 3.2.1). To anchor the dye in close proximity to microdiamond surface, we used linker **1** (Figure 3.1). The dye was converted into acyl chloride and deposited on a BDD plate for 4 days under strictly dark and inert conditions. Compared to **P1**-Cl dye, we extended the reaction time to maximise the anchoring yield due to the higher molecular weight of the dye **DpA**. We did not observe any unintended polymerisation of the dye on the sample surface, as was the case for the **P1** dye. The finalised sensitised plates were characterised by XPS (Figure 3.6). In comparison with **P1** dye, the surface coverage **DpA** of dye was lower, which can be attributed to slower reaction kinetics. In detailed XPS measurements of a blank BDD plate, we found no elements on the surface other than C (97.2 %) and O (2.7 %), which was expected. On the surface of dye sensitised plate, we found a higher content of N, S and O, and in addition signals of B, Cl, Zn and Si (Tab. bellow Figure 3.6). The elements found by XPS clearly originate in reagents used

in dye synthesis, which we attribute to poor dye solubility and uneasy purification.

Based on measured photocurrents and on XPS analysis, we deduced that a monomolecular layer of dye was attached to surface. However, we were unable to precisely determine the surface coverage, and further analyses were limited by the finite amount of the newly prepared dye. Notwithstanding, we performed an electrochemical characterisation of dye sensitised microdiamond thin film and the measured photocurrent was approximately 0.5 μA cm^2 under the illumination of 0.2 Sun. The response was improved in comparison to the non-covalent attachment of **P1** dye, albeit without outperforming the covalently bound **P1** on the same BDD microdiamond cathode.

In conclusion, a complex, multi-step synthetic approach was used to prepare a custom-designed donor-π-acceptor dye, which was successfully attached to a diamond surface and characterised. Electrochemical characterisation showed photocurrents slightly improved compared to the results from non-covalent attachment, yet only comparable to the previous covalent attachment of **P1**. We assume that the photocurrent response was hindered by the presence of unwanted elements on the surface of the diamond. Based on the limited amount of dye and on the roughly similar photocurrents, we decided to proceed on a systematic study investigating variation in conductivity of BDD layer and the underlying silicon wafer.

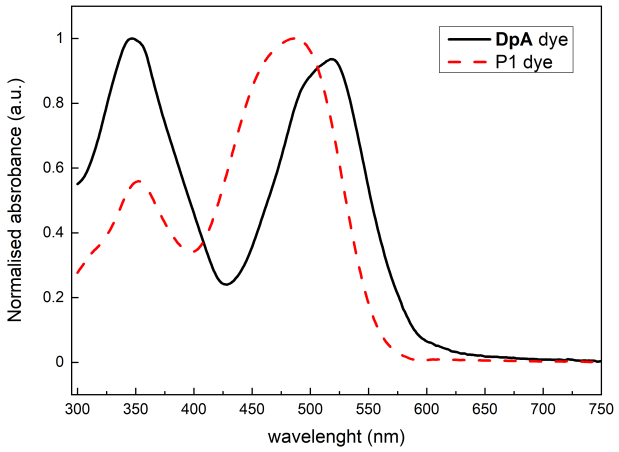

Figure 3.5: Comparison between the absorption spectra of a commercially available **P1** dye and **DpA** dye. *Adapted from Appendix* B.

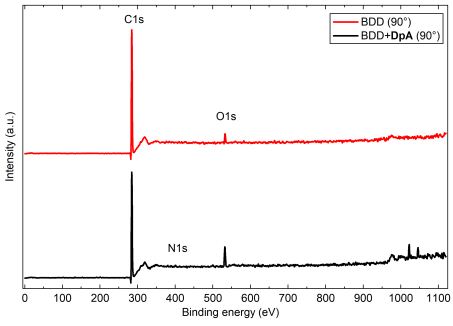

Elemental concentrations in atom %

Sample / Element	C 1s	O 1s	Si 2s	N 1s	S 2p	Zn	Cl 2p	P 2p
BDD (90°)	97.2	2.7	0.1	0.0	0.0	0.0	0.0	0.0
BDD+**DpA** (90°)	91.8	6.2	0.4	0.3	0.1	0.4	0.3	0.6
BDD (5°)	96.2	3.7	0.1	0.0	0.0	0.0	0.0	0.0
BDD+**DpA** (5°)	86.3	9.6	0.7	0.6	0.2	0.6	0.6	1.5

Figure 3.6: XPS spectra of BDD and BDD with **P1** dye. In detailed measurements, we observed weak signals other residual elements from synthesis (N, S, Zn, B, Cl, Si). *Adapted from Appendix* B.

3.2 Transition from a microcrystalline diamond film to nanodiamond particles

3.2.1 Systematic study of diamond surface properties and substrate conductivity* (C)

The third study on BDD diamond surface modifications assessed the effect of substrate conductivity on photocurrents. More specifically, this study aimed to determine which combination of BDD doping and silicon substrate conductivity would decrease the recombination rate of the electron-hole pair, and improve thus the photocurrents. The second objective was to use ND for quantification of reaction yields on the surface. Reasons for this were low sensitivity of techniques available for analysis of monoatomic layers and the long experimental cycle, which generally took 3-4 months.

To enable a straightforward comparison, the basic modification method of BDD plates was similar to previously described one (Section 3.1.1). The BDD layers were deposited on low- or high-conductive silicon. The B/C ratio of the newly prepared BDD was 250, 500, 1000, 2000 and 4000 ppm. Furthermore, we improved the photochemical irradiation setup for the attachment of the *N*-allyltrifluoroacetamide linker. We used three UV lamps positioned in a close proximity to a quartz tube in a polished hexagonal steel tube reflector. Thus, more light reached the sample, and the use of an efficient UV source prevented overheating of the sample and the volatile reagent. The **P1** dye was attached to the sample, and the samples were characterised by available surface analyses, Figure 3.7 - 2D surfaces.

3.2.2 Hydrogenated NDs: a model material mimicking the reactivity of BDD

We used NDs to understand processes occurring on the BDD surfaces. Reaction progress on NDs was determined for protected linker and for the deprotected amine. Furthermore, we analysed the number of reactive amino groups available on the surface of the NDs and correlated these data with zeta-potential analysis, as shown in Table 3.1.

To evaluate the reaction conversion, we mimicked the chemical modifications using high pressure and high temperature (HPHT) NDs. The oxidised NDs were treated with hydrogen plasma. All reaction times were extended, since ND with a 50 nm diameter have a significantly higher surface-to-volume ratio and the surface is less available for reaction, especially UV-irradiation. Then, the linker was photografted in the same apparatus described for BDD; only the quartz tube was rotated slowly to irradiate the whole volume of the sample. The samples were washed and deprotected. Then, we analysed each reaction step using relevant analytical methods, as shown in Figure 3.7 and Table 3.1.

*__Published as: Barton, J.__; Krysova, H.; Janda, P.; Tarabkova, H.; Ashcheulov, P.; Mortet, V.; Taylor, A.; Vavra, J.; Cigler, P.; Kavan, L.; *Chemical modification of diamond surface by a donor-acceptor organic chromophore (P1): Optimization of diamond surface chemistry and electronic properties.*

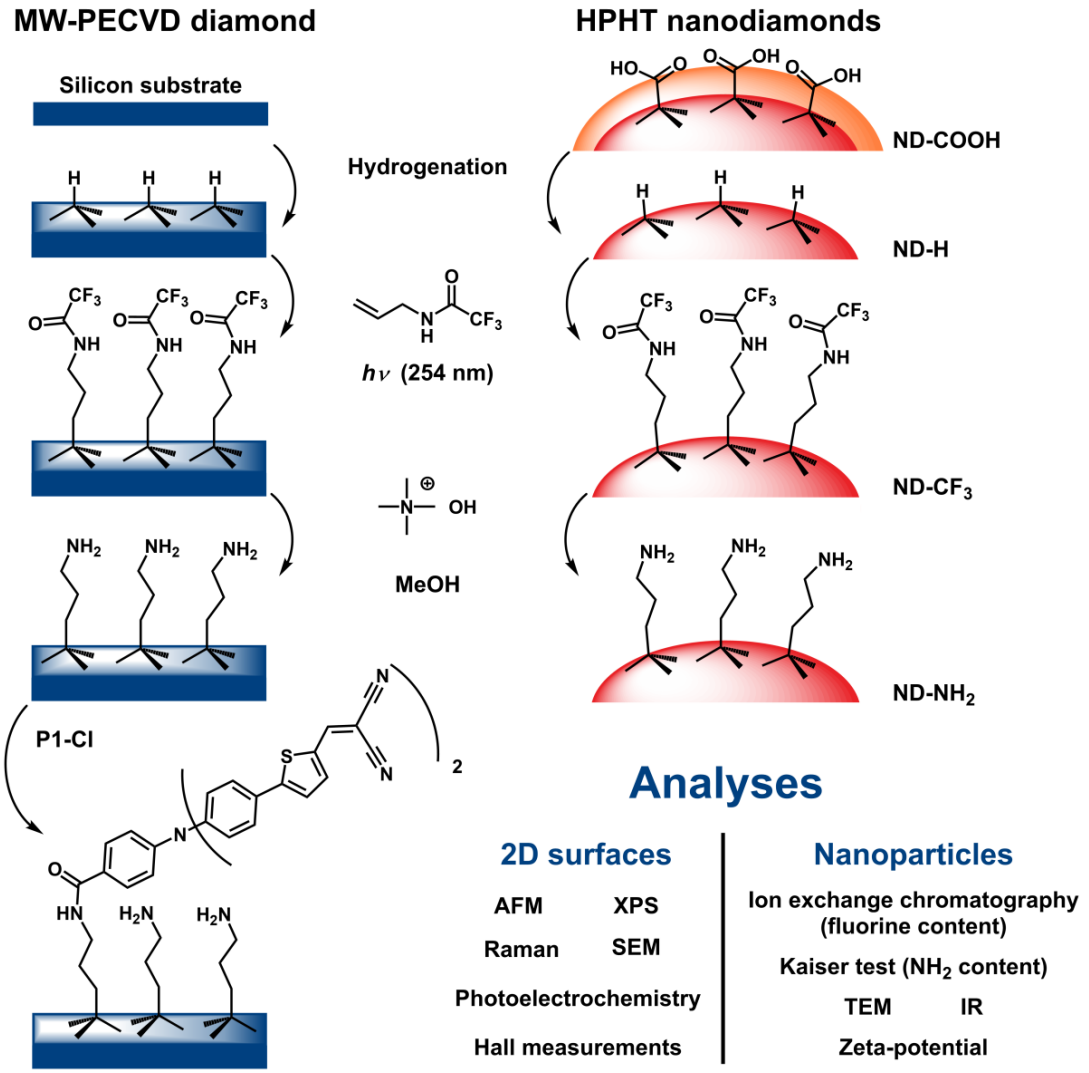

Figure 3.7: Scheme of modifications and analysis of diamond layer and NDs. *Adapted from Appendix* C.

The fluorine context was determined by burning the NDin oxygen followed by ion-exchange chromatography. Analysis confirmed a reasonable photografting conversion (surface coverage ca. 10-15 %) and almost quantitative deprotection. In a quantitative Kaiser test, we estimated a surface coverage of amino groups of approximately 26 %, while samples with the protective group were below the detection limit of the method. We attributed the discrepancy to the fluorine analysis, which likely underestimated fluorine content. In turn, the Kaiser test reports only reactive and sterically accessible amino groups. The zeta-potential corresponds to the surface charge of particles; hence, samples without charge or with deprotonated amino groups showed slightly negative to negative values. The samples with protonated amino groups shifted to positive values with the pH increase, which is in line with other analyses.

3.2.3 Analyses of thin diamond layers

For flat diamond samples, the B/C doping ratio was verified by Raman spectroscopy and Hall measurements. The attachment of the **P1** dye was confirmed by XPS analysis. Furthermore,

Table 3.1: Newly prepared NDs were characterised by overall fluorine content after combustion of NDs, content of accessible amino groups on surface (Kaiser test), and variation of zeta-potential as a function of pH.

ND type	CF_3 content		NH_2 content (Kaiser test)		Zeta-potential		
	[mmol/g]	surface coverage [%]	[mmol/g]	surface coverage [%]	pH 3.6	pH 5.6	pH 10.2
ND-H	0.01	0.61	–	–	–	–	–
ND-CF_3	0.20	13.4	–	–	-7	-17	-41
ND-NH_2	0.04	2.7	0.38 ± 0.07	25.7 ± 4.8	21	4	-45

when measuring the surface morphology with AFM, we observed a change from a smooth surface to nanograin-covered surface after the attachment of the **P1** dye, as shown in Figure 3.8. No observable differences in surface morphology were found by SEM analysis on the surface modified by **P1** or in diamond surfaces with various doping levels. The ATR-FTIR analysis of modified BDD samples showed identical results, confirming the low sensitivity of the technique for a monomolecular layer.

TEM analysis of NDs showed no changes in the morphology of the particles. IR measurements confirmed each step of the chemical modification. The combination of indirect analyses on both flat diamond surfaces and NDs was in agreement with the proposed chemistry modifications designed for the diamond surface.

The photo- and electrochemical behaviour was similar to that of our previous observations (Section 3.1.1). With the decrease in boron doping, the photocurrents improved. The high conductive Si-substrate showed doubled photocurrents compared to those of the low-conductive substrate for 250 ppm B-doping. This difference decreased with the increase in B-doping. The observed behaviour can be explained by electron-hole recombination in which the holes are trapped in BDD layer. This is supported by the lowest photocurrents that are observed for the low-conductive substrate with low-conductive BDD. Increasing the conductivity of either substrate or BDD layer reduced the difference. However, we did not observe the highest photocurrents for the highest B-doping on the conductive substrate.

In conclusion, we performed a systematic study of conductivity variation of sensitised BDD cathode and Si-substrate. The improvements in photografting procedure combined with conductivity optimisation, led to increase of photocurrents to 6.6 μA cm^2. Obtained value was three times higher than the photocurrent recorded in our previous study. Furthermore, to our knowledge, this was also the best value ever reported for a flat BDD electrode.

3.3 Nanodiamond particles

In the second part of thesis, I will describe two different applications of ca. 50 nm nanodiamond (ND)s. The first shows directed motion of ND in pH gradient. The second uses ND with NV^- centres to detect and quantify tens of nitroxide radicals present on the surface of polymer

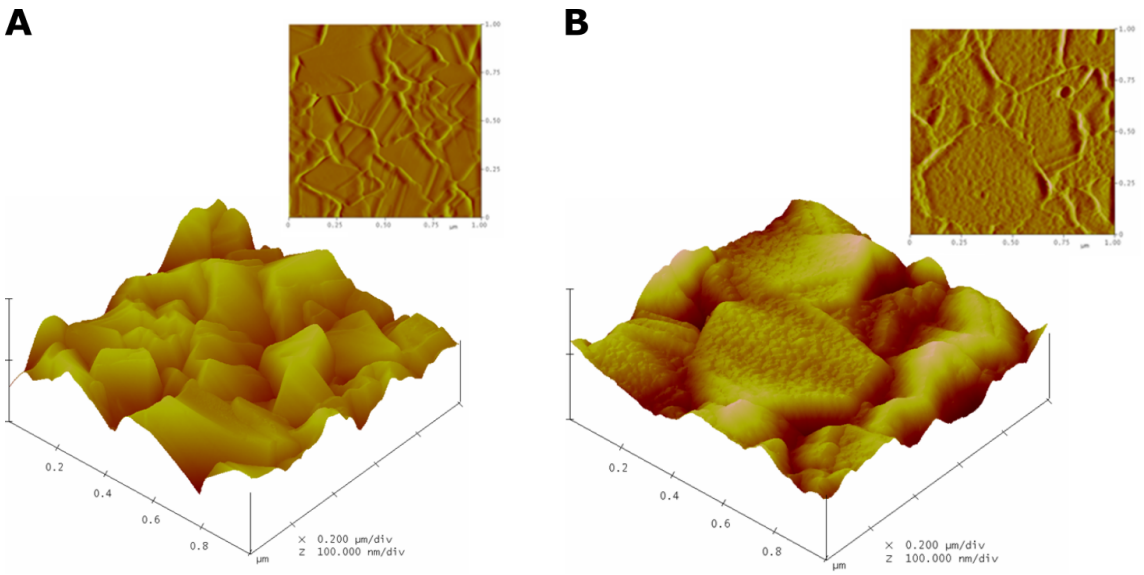

Figure 3.8: AFM images of BDD surface **A**) as deposited, **B**) modified with **P1**. Topography/height displayed as 2D view (top) and 3D (bottom). *Adapted from Appendix* C.

coated ND particle in aqueous solutions.

3.3.1 Proton-gradient-driven oriented motion of nanodiamonds grafted to graphene by dynamic covalent bonds* (D)

Moving nano-objects in a specific direction by external activation is one of the fundamental skills for nanoscience. For instance, particle can be attached to the surface and achieve a rolling motion by formation-termination of bonds to the underlying surface. However, designing, preparing, and verifying such nanosystems is quite challenging. Furthermore, monitoring such movements in real-time with sufficient resolution under ambient conditions is a demanding task. Here, surface-functionalized NDs were prepared, its surface functionalisation was verified and pH directed motion was observed.

For such purposes, the following concepts have been combined – dynamic covalent chemistry (DCC), surface modification of graphene and ND and real-time tracking of nanoparticles by epifluorescence. DCC is based on reversible bond formation. A stable link between nanoparticle and surface is kept to prevent particle detachment from the surface [197, 198]. Here, an imine formation from primary amine and aldehyde was selected. It proceeds under mild conditions which are compatible with functionalized ND and with the biological environment. Further, it is synthetically available and chemically stable. The movement mechanism is driven by imine formation on the high end of the pH gradient, while imine hydrolysis accelerates in lower pH.

We used HPHT fND with NV^- centres, which were processed in our laboratory [83]. To stabilise them in water but also in a buffered solution, we coated particles with PHPMA.

*__Published as:__ Kovaricek, P.; Cebecauer, M.; Neburkova, J.; **Barton, J.**; Fridrichova, M.; Drogowska, K. A.; Cigler, P.; Lehn, J.-M.; Kalbac, M. *Proton-gradient-driven oriented motion of nanodiamonds grafted to graphene by dynamic covalent bonds.* ACS Nano 2018, 12 (7), 7141-7147.

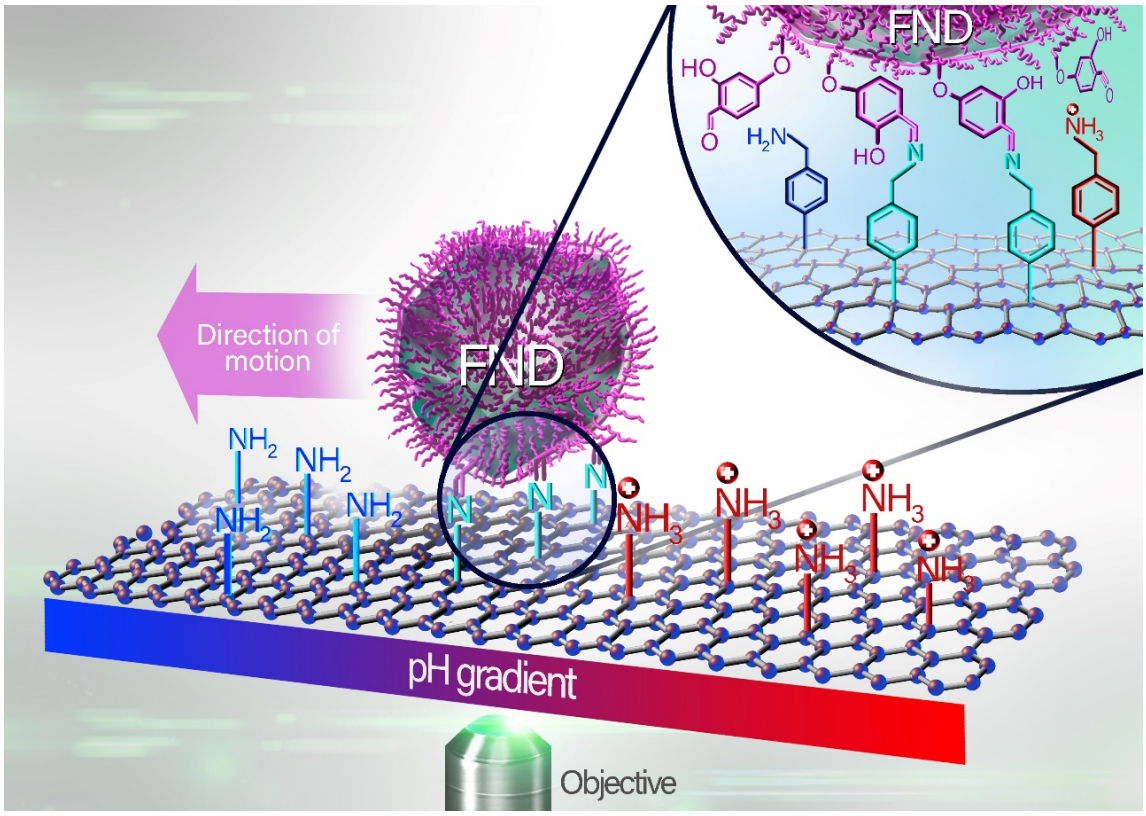

Figure 3.9: Scheme of rolling motion of modified NDs attached to graphene surface in a pH gradient. *Adapted from Appendix* D.

The optimisation of polymerisation increased the stability of NDs in a buffered solution and minimised non-specific absorption to graphene surface and aggregation. NDs were functionalized with HPMA copolymerised to contain azide groups. 2-hydroxy-4-propargyloxybenzaldehyde was conjugated to the azido groups using the CuAAC reaction, Figure 3.10. The polymer surface contained aldehyde groups, although part of them was sterically unavailable. Also, the sequence of steps needed to be verified.

Before proceeding, we verified the functionalisation of the surface. We assessed spectrophotometrically the number of available aldehyde groups on the surface to be ca. 2500 per particle. For this purpose, we synthesised a water-soluble fluorescent BODIPY dye containing aminooxy groups for detection and sulfonate groups for solubility (Figure 3.10).

A graphene monolayer was selected as a supporting surface for the reaction. The graphene can be used as a thin transparent layer suitable for fluorescence spectroscopy and can be chemically functionalized. In this study, amine functionalisation was introduced to the surface using two different approaches. The functionalization was confirmed by Raman spectroscopy, XPS and surface-enhanced Raman spectroscopy.

ND with NV^- centres provide stable fluorescence under laser illumination for hours [199], thus making possible to track fluorescence for longer time periods, unlike organic fluorescent dyes which rapidly photobleach. In addition, epifluorescence microscopy allows real-time detection of

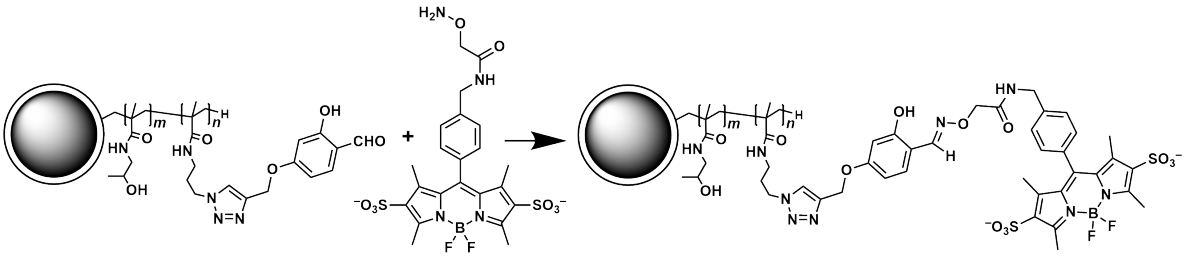

Figure 3.10: Scheme of modifications of polymer coated NDs. *Adapted from Appendix* D.

nano-sized fluorescent objects with high spatio-temporal resolution. This was used to observe pH directed motion of NDs on the functionalized graphene surface.

In conclusion, our results showed directed motion of aldehyde equipped fNDs in the pH gradient on the amine-terminated graphene surface. The functionalized, polymer-coated fND created a stable interface necessary for the application of NDs and independent verification method was developed. Fluorescent spectroscopy made possible to observe particle motion in real-time, thus demonstrating the proposed mechanism of motion control for NDs. In pKa of amine-aldehyde system a Brownian motion of particles was observed. The pH cycle was repeated several times until the gradually increasing ionic strength caused particle adsorption on the graphene surface. A promising tool for the manipulation of nanosized objects in 2D space was developed in this study.

3.3.2 Nanoscale dynamic readout of a chemical redox process using radicals coupled with NV^-centers in nanodiamonds* (F)

Cellular communication, oxidative stress and immune response are facilitated by free radicals and paramagnetic ions [200]. Yet, the extent or dynamics of those processes are difficult to study due to lack of suitable methods. The analysis of cellular processes requires using methods with high sensitivity, selectivity and spatiotemporal resolution. The ND with NV centres are suitable candidates for such a task since their fluorescence behaviour of NV centre is highly dependent on the magnetic field around the ND. The aim of this project was to determine the sensitivity of fND to the presence of stabilised organic radicals and to utilise this interaction to detect biologically relevant ascorbate anion. The development of a biocompatible, functionalized nanosensor is described in the following paragraphs and summarised in Figure 3.11.

The preparation of fND itself was developed in our lab, among others, by Havlik [47]. HPHT NDs of approximately 50 nm in diameter were irradiated in a cyclotron, annealed to form NV centres and oxidised. Then, we covered the diamond surface with a thin, biocompatible layer, which could be further chemically functionalized without affecting the colloidal stability. For this purpose, several different types of polymer were grown on the fND surface, notably PHPMA

*__Manuscript under revision as: Barton, J.__; Gulka, M.; Tarabek, J.; Mindarava, Y.; Wang, Z.; Schimer, J.; Raabova, H.; Bednar, J.; Plenio, M.; Jelezko, F.; Nesladek, M.; Cigler, P.; *Nanoscale dynamic readout of a chemical redox process using radicals coupled with NV^- centers in nanodiamonds.*

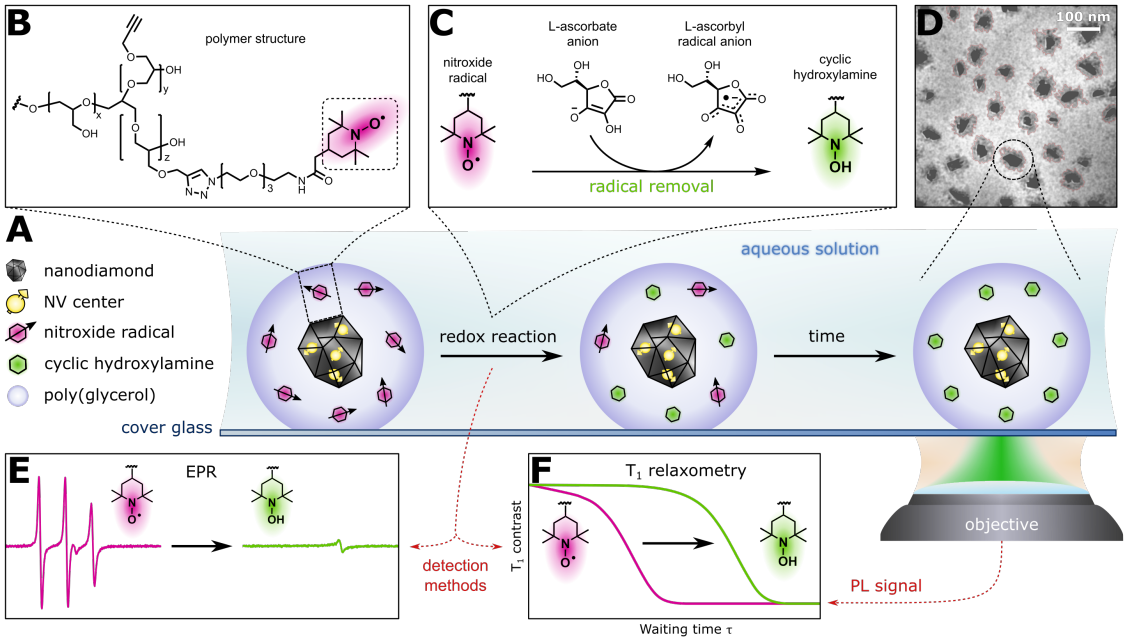

Figure 3.11: Scheme of ND nanosensor and its use for optical relaxometric sensing: **A**) NDs with NV^- centres coated with polymer containing nitroxide radicals, which can be turned on/off. **B**) Schematic structure of poly(glycerol) (PG) with attached TEMPO-based nitroxide spin probe. The PG has a dendritic structure with many branching points. **C**) Radical deactivation by reaction with L-ascorbate provided a diamagnetic cyclic hydroxylamine. **D**) Cryo-TEM of polymer coated NDs – irregular dark shapes are NDs, surrounded by a grey polymer shell. **E**) Change in EPR signal after removing the nitroxide radicals. **F**) Quantifiable increase in T_1 of NV^- after removal of stable radicals from the polymer layer.

and PG. From the start or during growth, an additional copolymer was added, which contained alkyne group. This group was further used to attach a small molecule **3** (Figure 3.12) through a CuAAC reaction. This spin probe is capable of repeated formation of stable nitroxide radicals. The used small molecule is a derivative of the stable radical molecule known as TEMPO or (2,2,6,6-tetramethylpiperidin-1-yl)oxyl.

The fND were reacted with different concentrations of the small molecule. We optimised the ratio between stability and loading of the radical trapping molecule for both polymers. However, the small molecule attached to the PHPMA did not respond to radical activation and was thus dismissed. In contrast, PG on fNDs responded to activation by sonication. Furthermore, we observed a five-fold increase in radical generation during sonication with air in comparison to an argon-secured solution. This provided a robust and reliable method for repeatedly activating the whole system without its destruction since the final fNDs would be damaged under the commonly used harsh activation conditions. Lastly, the conjugated nitroxide radical responded to sodium ascorbate addition with complete reduction to cyclic hydroxylamine.

To independently verify the total number of paramagnetic species in fND, we used a combination of EPR, TGA, NTA, DLS and cryo-TEM spectroscopy. EPR spectra contain a triplet corresponding to the nitroxide radical and a smaller signal of paramagnetic impurities present in fNDs (Figure 3.11E). We determined a polymer thickness of 17.0 ± 8.8 nm from information

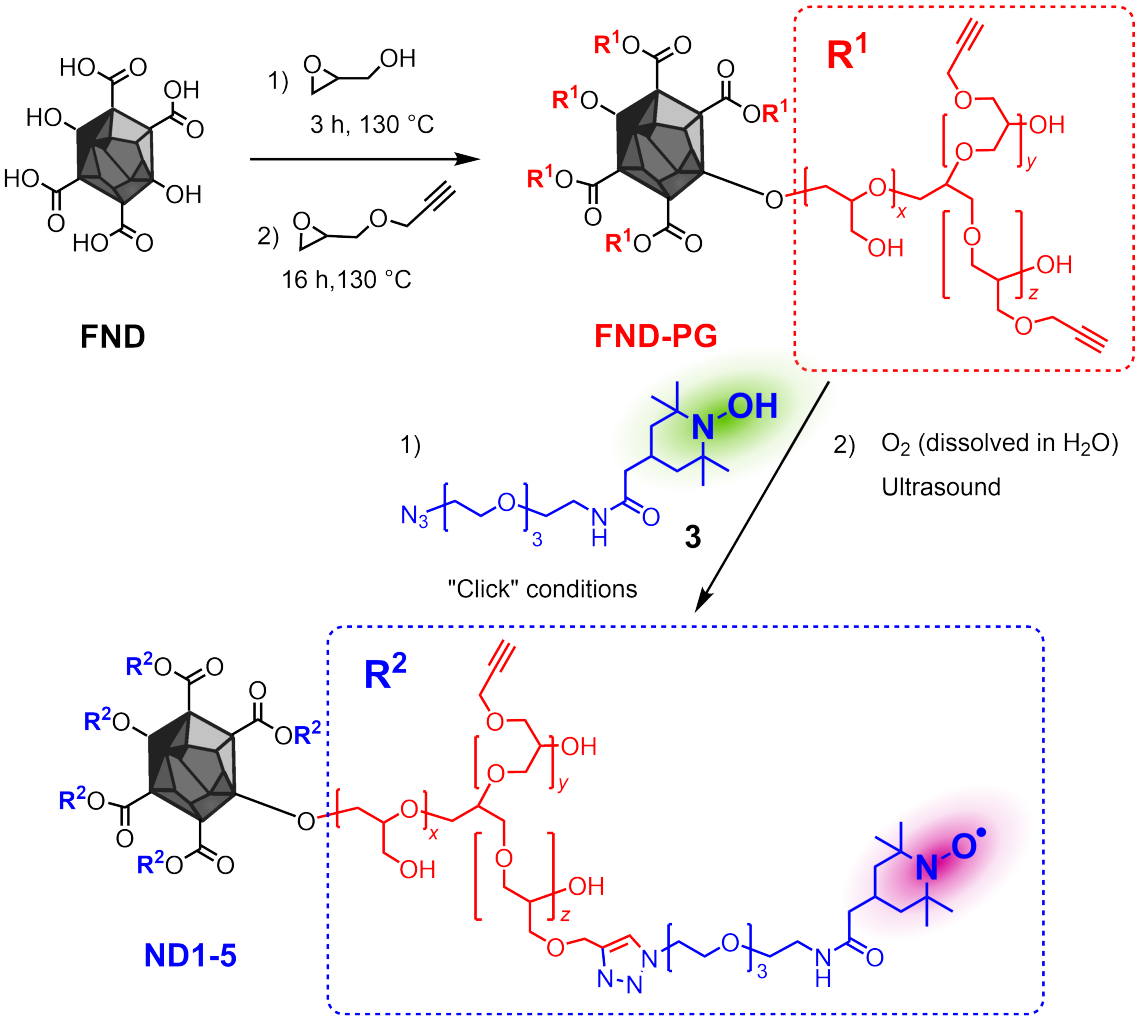

Figure 3.12: Scheme of surface modification of fNDs. Dendritic PG was grown on fND surface. The polymerisation was terminated by addition of glycidyl propargyl ether. The radical trapping molecule was attached to the alkyne using a CuAAC ("click") reaction. The attached cyclic hydroxylamine was repeatedly activated to nitroxide radical by ultrasound treatment (with/without O_2 and deactivated by sodium ascorbate addition). *Adapted from Appendix* E.

on the fNDs and polymer mass from (TGA) and hydrated polymer thickness from cryo-TEM). Furthermore, we combined measurements of particle concentration from NTA and from concentrations of nitroxide radical and fND paramagnetic impurities from EPR, and corrected them with the size distribution of bare particles from TEM. From those measurements, we calculated and independently verified the presence and concentration of radicals in the polymeric shell for the aqueous colloidal solution of the sample. This was the cornerstone for determining the validity and sensitivity of the proposed method for quantum sensing.

This quantum sensing method is based on the change of T_1 which increases with the decrease in paramagnetic concentration in the effective sensing radius of the NV^- centre (<20nm), Figure 3.11F. Average T_1 is calculated from the fluorescence readout collected from single particle measurements in aqueous solution at room temperature. Thus, a controlled increase in the concentration of nitroxide radical covalently bound to the polymer should shorten the T_1 and

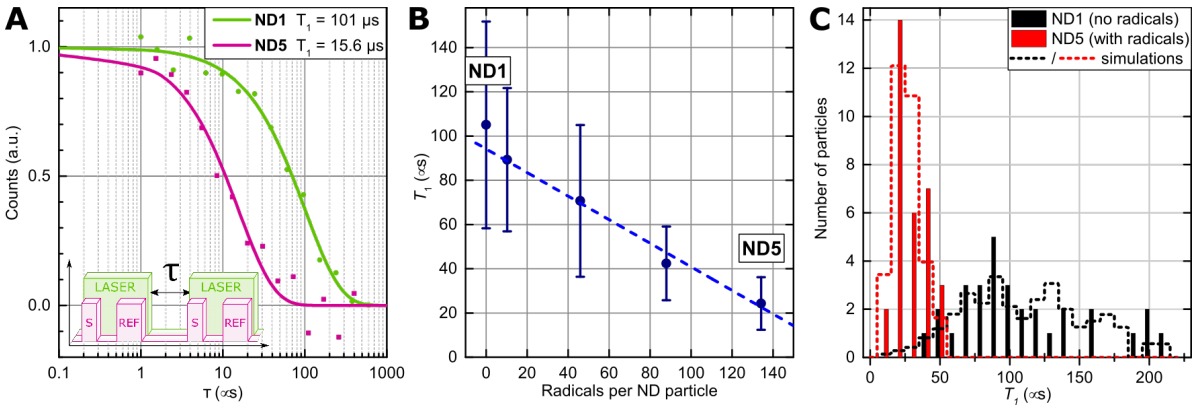

Figure 3.13: **A**) Two representative determinations of T_1 of single **ND1** and **ND5** particles. The used pulse sequence is shown in the inset. Consecutive laser pulses are used for spin-initialisation and readout, while increasing the waiting time τ. The spin-contrast signal is detected optically at the beginning of the laser pulses (S) and is referenced to the polarised state signal (REF) at the end of the laser pulses. **B**) The graph shows the variation of the average T_1 relaxation time as a function of the concentration of stable nitroxide radicals in the polymer. **C**) The histogram shows the variation of T_1 as a function of nitroxyl radical concentration. The sample **ND1** is without nitroxyl radicals, and the **ND5** contained 134 radicals per particle on average. The bars represent the T_1 measured for a single particle, and the dashed lines represent theoretical simulations. *Adapted from Appendix* E.

other way round. To further prove the feasibility of the proposed technique, we performed the experiment in aqueous solution at room temperature.

After verifying the radical concentration, we performed the T_1 time measurements. We observed that the T_1 time decreased with the increase in the concentration of nitroxide radical, Figure 3.13C. Theoretical simulations agree with the measured T_1 time distribution of fND with (**ND5**) and without (**ND1**) radicals (Figure 3.13C). Furthermore, addition of sodium ascorbate led to the conversion of nitroxide radicals into diamagnetic hydroxylamine. Conversion progress was observed by lengthening of T_1 time, which fully recovered (Figure 3.13 B).

In conclusion, we demonstrated that the sensitivity of the method was ∼10 nitroxide radical covalently bound to the fND particle, which corresponds to a localised readout of $\sim 10^{-23}$ mol radicals. Such a nanosensor could be utilised to determine, for example, the intracellular concentrations of ascorbate stable under physiological conditions.

4 | Conclusion

The research presented here aimed to develop interfaces for diamond applications, either for CVD layer or for NDs particles. In the introduction, we identified major challenges to overcome when designing surface modifications for novel diamond applications. Such applications include modifications of BDD thin layers as electrodes for photoconversion and NDs as biocompatible, colloidally stable nanosensors.

The modification of the CVD layer was presented in three studies (**A-C**). The third study also employed nanodiamond particles. The photosensitisation of BDD surfaces was developed in the author's previous work (**F**) with non-covalent attachment of a **P1** dye close to the diamond surface. Since then, we have developed a procedure for covalent surface photosensitisation. A short linker was photografted, followed by a covalent attachment of a **P1** dye. This surface photosensitisation led to a four-fold improvement in photocurrents (**A**) compared to previous non-covalent modifications.

Encouraged by these results, we developed a specifically tailored donor-π-acceptor (D-π-A) dye **DpA**. The structure was derived from the **P1** dye, while strengthening the spectral absorption, electron-accepting and donating part of the molecule. The multi-step synthesis yielded the designed dye, which was covalently attached to a BDD surface. However, the photocurrents of the newly designed dye were similar to those reached in our previous efforts. We suspect that residual impurities remaining after complex dye purification negatively affected electrochemical properties of the resulting system (**B**).

Based on previous results, we conducted a thorough analysis of surface reactions and conductivity of the BDD diamond and underlying silicon wafer in the third study (**C**). The sensitivity of applicable surface analyses was too low to analyse individual reactions for monolayer functionalization on microcrystalline diamond films. Therefore, we decided to use hydrogenated NDs as a model with similar chemical properties, albeit with a significantly higher surface-to-volume ratio. The nanoparticle model made it possible to evaluate the reaction conversion by subsequent analyses of residual fluorine or by reaction with surface available amines and therefore to improve the experimental procedures. Furthermore, the systematic study of different conductivities of a silicon wafer and boron doping resulted in yet another improvement in photocurrents for the sensitised BDD cathode. In conclusion, we reached the best ever reported value, to our knowledge, of 6.6 μA cm^2 for a flat surface sensitised BDD electrode.

In the second part of my doctoral work, biocompatible polymer-coated NDs were prepared.

The fourth study (**D**) focused on the hypothesis that fNDs could be rolled in the direction of a pH gradient. Colloidally stable fNDs were prepared, and surface functionalisation with aldehydes was verified using a tailored fluorescent dye. Furthermore, an amine-functionalized graphene layer was prepared so that fluorescent microscopy could track the movement of non-bleachable fNDs in real time and for extended periods of time. The rolling motion of fNDs in the pH gradient was observed and could be repeated until the ionic strength destabilised fNDs in the solution. In summary, we prepared a colloidally stable system of fNDs and observed their directed motion in the pH gradient. Thus, bond formation on a molecular level enables us to move larger objects, such as 50 nm nanodiamonds in a given direction.

In the fifth, main work (**E**), we developed a quantum-based ultrasensitive nanosensor for dynamic readout of redox processes in aqueous solution at room temperature. We prepared colloidally stable, polymer-coated fNDs and equipped them with switchable, nitroxyl radical molecules. Furthermore, we independently assessed the quantum sensing of fND with NV^- centres. To determine the absolute concentration of nitroxyl radicals on the polymer coating for a single fND particle, we developed an independent method for combining all feasible analytical methods to validate the proposed quantum sensing experiment.

Then, we measured the T_1 time, which is highly dependent on changes in the magnetic field in an effective sensing radius of NV^- centres (<20nm). From these measurements, we were able not only to quantify the number of stable radicals present on single fND but also to determine the precision of the sensing method, which was ∼10 single radical spins per one fND particle. This value corresponds to the localised readout of approximately 10^{-23} mol of radicals (**E**). On the example of nitroxide radical reduction by sodium L-ascorbate, we demonstrated the possibility of monitoring redox reactions in real-time and on a minute-scale in aqueous solution with a spatial resolution of confocal microscopy.

Future perspectives

Based on the current state of the art, sensing using NV^- in fNDs holds very promising applications. The detection or tracking of specific paramagnetic species inside living cells may be achieved during this decade. An additional study based on the same detection principle but applied to different paramagnetic species is currently in progress. Our understanding of the free radical theory of cellular ageing and oxidative stress will most likely advance in the coming years thanks to the development of these tools.

5 | List of publications

The contents of this thesis are based on the following publications:

A) Krysova, H.; **Barton, J.**; Petrak, V.; Jurok, R.; Kuchar, M.; Cigler, P.; Kavan, L. *Efficiency and Stability of Spectral Sensitization of Boron-Doped-Diamond Electrodes through Covalent Anchoring of a Donor-Acceptor Organic Chromophore (P1).* Physical Chemistry Chemical Physics 2016, 18 (24), 16444-16450. https://doi.org/10.1039/C6CP02209J. IF = 3.6

B) Bartova, K.; Jurok, R.; **Barton, J.**; Krysova, H.; Kuchar, M.; Mortet, V.; Taylor, A.; Cigler, P.; Kavan, L.; *Diamond photocathodes sensitised with a bis(perylenemonoimide-dithiophene) donor-acceptor dye.* **Manuscript in preparation.**

C) **Bartoň, J.**; Krýsová, H.; Janda, P.; Tarábková, H.; Ashcheulov, P.; Mortet, V.; Taylor, A.; Vávra, J.; Cígler, P.; Kavan, L. *Chemical Modification of Diamond Surface by a Donor-Acceptor Organic Chromophore (P1): Optimization of Surface Chemistry and Electronic Properties of Diamond.* Applied Materials Today 2018, 12, 153-162. https://doi.org/10.1016/j.apmt.2018.04.005. IF = 8.0

D) Kovaříček, P.; Cebecauer, M.; Neburková, J.; **Bartoň, J.**; Fridrichová, M.; Drogowska, K. A.; Cigler, P.; Lehn, J.-M.; Kalbac, M. *Proton-Gradient-Driven Oriented Motion of Nanodiamonds Grafted to Graphene by Dynamic Covalent Bonds.* ACS Nano 2018, 12 (7), 7141-7147. https://doi.org/10.1021/acsnano.8b03015. IF = 13.9

E) **Barton, J.**; Gulka, M.; Tarabek, J.; Mindarava, Y.; Wang, Z.; Schimer, J.; Raabova, H.; Bednar, J.; Plenio, M.; Jelezko, F.; Nesladek, M.; Cigler, P.; *Nanoscale dynamic readout of a chemical redox process using radicals coupled with NV^- centers in nanodiamonds.* **Manuscript under revision.**

Other related publication

F) Krysova, H.; Vlckova-Zivcova, Z.; **Barton, J.**; Petrak, V.; Nesladek, M.; Cigler, P.; Kavan, L. *Visible-Light Sensitization of Boron-Doped Nanocrystalline Diamond through Non-Covalent Surface Modification.* Phys. Chem. Chem. Phys. 2015, 17 (2), 1165-1172. https://doi.org/10.1039/C4CP04148H. IF = 3.6

6 | The author's contributions to the publications

The projects presented by the author are result of a team effort of several co-authors and collaboration between different fields of science – physics, mathematics and various spectroscopies. The author primarily contributed to the chemistry, materials characterisation, communication, coordination of experiments in this study and writing of the manuscripts. His particular contributions to individual projects are summarised below.

A) Jan Bartoň developed and performed all procedures for surface modification of BDD plates and modification of **P1** dye, including HPLC characterisation.

B) Jan Bartoň modified all BDD plates, developed a new UV irradiation setup and coordinated experiments between three collaborating workplaces.

C) Jan Bartoň performed chemical synthesis, all sample modifications and surface characterisation by SEM. The author was responsible for the coordination between laboratories (samples and time schedules) and was involved in writing the manuscripts.

D) Jan Bartoň developed and performed the synthesis of a small fluorescent molecule for aldehyde quantification on the NDs surface.

E) Jan Bartoň performed all chemical syntheses and polymer modifications of NDs, contributed to preparation of different polymers, handled complex preparation of ND samples in an inert atmosphere, conducted chemical and sample characterisation experiments (NMR, HPLC, NTA, DLS, zeta potential) and was involved in writing the manuscript.

.....

Mgr. Petr Cígler, Ph.D.

Bibliography

1. Philips, R. M. R̃. *» How Big Are Biochemical Nuts and Bolts?* http://book.bionumbers.org/how-big-are-biochemical-nuts-and-bolts/ (2020).
2. Börsch, M. *et al. Fluorescent Nanodiamonds for FRET-Based Monitoring of a Single Biological Nanomotor F o F 1 -ATP Synthase* in. SPIE BiOS: Biomedical Optics (eds Periasamy, A. & So, P. T. C.) (San Jose, CA, Feb. 12, 2009), 71832N. doi:10.1117/12.812720.
3. Volkov, K., Danilenko, V. & Elin, V. Synthesis of Diamond from the Carbon in the Detonation Products of Explosives. *Combust. Explos.* **26,** 366–368. ISSN: 0010-5082. doi:10.1007/BF00751383 (May 1990).
4. Bundy, F. P. *et al.* Man-Made Diamonds. *Nature* **176,** 51–55. ISSN: 1476-4687. doi:10.1038/176051a0 (July 1955).
5. Kamo, M. *et al.* Diamond Synthesis from Gas Phase in Microwave Plasma. *Journal of Crystal Growth* **62,** 642–644. ISSN: 0022-0248. doi:10.1016/0022-0248(83)90411-6 (Aug. 1, 1983).
6. Matsumoto, S. *et al.* Growth of Diamond Particles from Methane-Hydrogen Gas. *J Mater Sci* **17,** 3106–3112. ISSN: 1573-4803. doi:10.1007/BF01203472 (Nov. 1, 1982).
7. Werner, M. & Locher, R. Growth and Application of Undoped and Doped Diamond Films. *Rep. Prog. Phys.* **61,** 1665–1710. ISSN: 0034-4885, 1361-6633. doi:10.1088/0034-4885/61/12/002 (Dec. 1, 1998).
8. Frenklach, M. *et al.* Induced Nucleation of Diamond Powder. *Appl. Phys. Lett.* **59,** 546–548. ISSN: 0003-6951. doi:10.1063/1.105434 (July 29, 1991).
9. Galimov, É. M. *et al.* Experimental Corroboration of the Synthesis of Diamond in the Cavitation Process. *Dokl. Phys.* **49,** 150–153. ISSN: 1562-6903. doi:10.1134/1.1710678 (Mar. 1, 2004).
10. Yang, G.-W., Wang, J.-B. & Liu, Q.-X. Preparation of Nano-Crystalline Diamonds Using Pulsed Laser Induced Reactive Quenching. *J. Phys. Condens. Matter* **10,** 7923. http://iopscience.iop.org/0953-8984/10/35/024 (2013) (1998).
11. Shenderova, O. & Nunn, N. in *Nanodiamonds* (ed Arnault, J.-C.) 25–56 (Elsevier, 2017). ISBN: 978-0-323-43029-6. http://www.sciencedirect.com/science/article/pii/B9780323430296000027.
12. Shenderova, O. A. & McGuire, G. E. Science and Engineering of Nanodiamond Particle Surfaces for Biological Applications (Review). *Biointerphases* **10,** 030802. ISSN: 1934-8630, 1559-4106. doi:10.1116/1.4927679 (Sept. 2015).

13. Ōsawa, E. Recent Progress and Perspectives in Single-Digit Nanodiamond. *Diam. Relat. Mater.* **16,** 2018–2022. ISSN: 09259635. doi:10.1016/j.diamond.2007.08.008 (Dec. 2007).

14. Shenderova, O. A. *et al.* Nitrogen Control in Nanodiamond Produced by Detonation Shock-Wave-Assisted Synthesis. *J. Phys. Chem. C* **115,** 14014–14024. ISSN: 1932-7447. doi:10.1021/jp202057q (July 28, 2011).

15. Wentorf Jr, R. H. Diamond Growth Rates. *J. Phys. Chem.* **75,** 1833–1837. http://pubs.acs.org/doi/abs/10.1021/j100681a013 (2017) (1971).

16. Burns, R. C. *et al.* Growth-Sector Dependence of Optical Features in Large Synthetic Diamonds. *J. Cryst. Growth* **104,** 257–279. http://www.sciencedirect.com/science/article/pii/0022024890901266 (2017) (1990).

17. Heyer, S. *et al.* Toward Deep Blue Nano Hope Diamonds: Heavily Boron-Doped Diamond Nanoparticles. *ACS Nano* **8,** 5757–5764. ISSN: 1936-0851. doi:10.1021/nn500573x (June 24, 2014).

18. Gracio, J. J., Fan, Q. H. & Madaleno, J. C. Diamond Growth by Chemical Vapour Deposition. *J. Phys. Appl. Phys.* **43,** 374017. ISSN: 0022-3727, 1361-6463. doi:10.1088/0022-3727/43/37/374017 (Sept. 22, 2010).

19. Eversole, W. G. *US Patent* 3030188A. https://patents.google.com/patent/US3030188/en (2020)(1962).

20. *CRC Handbook of Chemistry and Physics: A Ready-Reference Book of Chemical and Physical Data* (eds Company, C. R. & Lide, D. R.) 85. ed (CRC Press, Boca Raton, 2004). ISBN: 978-0-8493-0485-9.

21. Popovici, G., Bigelow, L. K. & Prelas, M. A. *Handbook of Industrial Diamonds and Diamond Films* ISBN: 978-0-367-40084-2. https://www.routledge.com/Handbook-of-Industrial-Diamonds-and-Diamond-Films/Prelas-Popovici-Bigelow/p/book/9780367400842 (2020) (Routledge, Boca Raton, 2018).

22. Matsumoto, S. *et al.* Vapor Deposition of Diamond Particles from Methane. *Jpn. J. Appl. Phys.* **21,** L183. ISSN: 1347-4065. doi:10.1143/JJAP.21.L183 (4A Apr. 1982).

23. Meyer, D. E., Dillon, R. O. & Woollam, J. A. Radio-frequency Plasma Chemical Vapor Deposition Growth of Diamond. *Journal of Vacuum Science & Technology A* **7,** 2325–2327. ISSN: 0734-2101. doi:10.1116/1.575936 (May 1, 1989).

24. Yang, N. *et al.* Conductive Diamond: Synthesis, Properties, and Electrochemical Applications. *Chem. Soc. Rev.* **48,** 157–204. ISSN: 1460-4744. doi:10.1039/C7CS00757D (Jan. 2, 2019).

25. Van der Drift, A. Evolutionary Selection, a Principle Governing Growth Orientation in Vapour-Deposited Layers. *Philips Res. Rep.* **22,** 267–288. http://projects.iq.harvard.edu/files/taolab/files/evolutionary_selection_ref.pdf (1967).

26. Wang, S. *et al.* The Structural and Electrochemical Properties of Boron-Doped Nanocrystalline Diamond Thin-Film Electrodes Grown from Ar-Rich and H2-Rich Source Gases. *Diamond and Related Materials* **18,** 669–677. ISSN: 0925-9635. doi:10.1016/j.diamond.2008.11.033 (Apr. 1, 2009).

27. Gruen, D. M. Nanocrystalline Diamond Films. *Annual Review of Materials Science* **29,** 211. ISSN: 00846600. doi:10.1146/annurev.matsci.29.1.211 (Aug. 1999).

28. Correa, E. J. *et al.* Electrical Conduction in Undoped Ultrananocrystalline Diamond Thin Films and Its Dependence on Chemical Composition and Crystalline Structure. *Journal of Applied Physics* **102,** 113706. ISSN: 0021-8979. doi:10.1063/1.2816214 (Dec. 1, 2007).

29. Robertson, R., Fox, J. J. & Martin, A. E. Two Types of Diamond. *Philosophical Transactions of the Royal Society of London. Series A, Containing Papers of a Mathematical or Physical Character* **232,** 463–535. doi:10.1098/rsta.1934.0013 (May 17, 1933).

30. Robertson, R., Fox, J. J. & Martin, A. E. Further Work on Two Types of Diamond. *Proceedings of the Royal Society of London. Series A - Mathematical and Physical Sciences* **157,** 579–593. doi:10.1098/rspa.1936.0217 (Dec. 2, 1936).

31. Su, L.-J. *et al.* Creation of High Density Ensembles of Nitrogen-Vacancy Centers in Nitrogen-Rich Type Ib Nanodiamonds. *Nanotechnology* **24,** 315702. ISSN: 0957-4484. doi:10.1088/0957-4484/24/31/315702 (Aug. 9, 2013).

32. Chang, H.-C., Hsiao, W. W.-W. & Su, M.-C. *Fluorescent Nanodiamonds* ISBN: 978-1-119-47709-9. http://doi.wiley.com/10.1002/9781119477099 (2020) (John Wiley & Sons, Ltd, Chichester, UK, Oct. 10, 2018).

33. Breeding, C. M. & Shigley, J. E. The "Type" Classification System of Diamonds and Its Importance in Gemology. *Gems Gemol.* **45,** 96–111. ISSN: 0016-626X. doi:10.5741/GEMS.45.2.96 (July 1, 2009).

34. Custers, J. F. H. Semiconductivity of a Type II b Diamond. *Nature* **176,** 173–174. ISSN: 1476-4687. doi:10.1038/176173a0 (July 1955).

35. *Optical Engineering of Diamond* (eds Mildren, R. P. & Rabeau, J. R.) (Wiley-VCH, Weinheim, 2013). 520 pp. ISBN: 978-3-527-41102-3.

36. Chevillard, S. *et al.* in *Nanodiamonds* (ed Arnault, J.-C.) 323–338 (Elsevier, 2017). ISBN: 978-0-323-43029-6. doi:10.1016/B978-0-32-343029-6.00013-1.

37. Gheeraert, E. *et al.* Electronic States of Boron and Phosphorus in Diamond. *Phys. Status Solidi A* **174,** 39–51. ISSN: 1521-396X. doi:10.1002/(SICI)1521-396X(199907)174:1<39::AID-PSSA39>3.0.CO;2-E (1999).

38. Lagrange, J. .-.-P., Deneuville, A. & Gheeraert, E. Activation Energy in Low Compensated Homoepitaxial Boron-Doped Diamond films1Paper Presented at the Diamond 1997 Conference.1. *Diamond and Related Materials* **7,** 1390–1393. ISSN: 0925-9635. doi:10.1016/S0925-9635(98)00225-8 (Sept. 9, 1998).

39. Kraft, A. Doped Diamond: A Compact Review on a New, Versatile Electrode Material. *Int J Electrochem Sci* **2,** 355–385 (2007).

40. Treussart, F. & Vlasov, I. I. in *Nanodiamonds* (ed Arnault, J.-C.) 155–181 (Elsevier, 2017). ISBN: 978-0-323-43029-6. doi:10.1016/B978-0-32-343029-6.00007-6.

41. Davies, G. & Hamer, M. F. Optical Studies of the 1.945 eV Vibronic Band in Diamond. *Proc. R. Soc. Lond. Math. Phys. Eng. Sci.* **348,** 285–298. ISSN: 1364-5021, 1471-2946. doi:10.1098/rspa.1976.0039 (Feb. 24, 1976).

42. Schirhagl, R. *et al.* Nitrogen-Vacancy Centers in Diamond: Nanoscale Sensors for Physics and Biology. *Annu. Rev. Phys. Chem.* **65,** 83–105. ISSN: 0066-426X, 1545-1593. doi:10.1146/annurev-physchem-040513-103659 (Apr. 2014).

43. Jelezko, F. & Wrachtrup, J. Single Defect Centres in Diamond: A Review. *phys. stat. sol. (a)* **203,** 3207–3225. ISSN: 1862-6319. doi:10.1002/pssa.200671403 (Oct. 1, 2006).

44. Zaitsev, A. M. Vibronic Spectra of Impurity-Related Optical Centers in Diamond. *Phys. Rev. B* **61,** 12909–12922. doi:10.1103/PhysRevB.61.12909 (May 15, 2000).

45. September 2017, T. W. *Putting a New Spin on Things* https://www.chemistryworld.com/news/putting-a-new-spin-on-things/3007939.article (2020).

46. Stursa, J. *et al.* Mass Production of Fluorescent Nanodiamonds with a Narrow Emission Intensity Distribution. *Carbon* **96,** 812–818. ISSN: 0008-6223. doi:10.1016/j.carbon.2015.09.111 (Jan. 2016).

47. Havlik, J. *et al.* Boosting Nanodiamond Fluorescence: Towards Development of Brighter Probes. *Nanoscale* **5,** 3208–3211. ISSN: 2040-3372. doi:10.1039/C2NR32778C (Mar. 28, 2013).

48. Chang, S. L. Y. *et al.* Counting Vacancies and Nitrogen-Vacancy Centers in Detonation Nanodiamond. *Nanoscale* **8,** 10548–10552. ISSN: 2040-3372. doi:10.1039/C6NR01888B (May 19, 2016).

49. Du Preez, L. *Electron Paramagnetic Resonance and Optical Investigations of Defect Centres in Diamond* Thesis (University of the Witwatersrand, Johannesburg, Sept. 1, 1965). http://wiredspace.wits.ac.za/handle/10539/20866 (2020).

50. Ohno, K. *et al.* Engineering Shallow Spins in Diamond with Nitrogen Delta-Doping. *Appl. Phys. Lett.* **101,** 082413. ISSN: 0003-6951, 1077-3118. doi:10.1063/1.4748280 (Aug. 20, 2012).

51. Meijer, J. *et al.* Generation of Single Color Centers by Focused Nitrogen Implantation. *Appl. Phys. Lett.* **87,** 261909. ISSN: 0003-6951, 1077-3118. doi:10.1063/1.2103389 (Dec. 26, 2005).

52. Chakraborty, T. *et al.* CVD Growth of Ultrapure Diamond, Generation of NV Centers by Ion Implantation, and Their Spectroscopic Characterization for Quantum Technological Applications. *Phys. Rev. Materials* **3,** 065205. doi:10.1103/PhysRevMaterials.3.065205 (June 26, 2019).

53. Haruyama, M. *et al.* Triple Nitrogen-Vacancy Centre Fabrication by C 5 N 4 H n Ion Implantation. *Nat. Commun.* **10,** 1–9. ISSN: 2041-1723. doi:10.1038/s41467-019-10529-x (June 13, 2019).

54. Weissleder, R. & Ntziachristos, V. Shedding Light onto Live Molecular Targets. *Nat. Med.* **9,** 123–128. ISSN: 1546-170X. doi:10.1038/nm0103-123 (Jan. 2003).

55. Gruber, A. *et al.* Scanning Confocal Optical Microscopy and Magnetic Resonance on Single Defect Centers. *Science* **276,** 2012–2014. ISSN: 0036-8075, 1095-9203. doi:10.1126/science.276.5321.2012 (June 27, 1997).

56. Bradac, C. *et al.* Observation and Control of Blinking Nitrogen-Vacancy Centres in Discrete Nanodiamonds. *Nat. Nanotechnol.* **5,** 345–349. ISSN: 1748-3395. doi:10.1038/nnano.2010.56 (May 2010).

57. Wu, T.-J. *et al.* Tracking the Engraftment and Regenerative Capabilities of Transplanted Lung Stem Cells Using Fluorescent Nanodiamonds. *Nat Nano* **8,** 682–689. ISSN: 1748-3387. doi:10.1038/nnano.2013.147 (Sept. 2013).

58. Billinton, N. & Knight, A. W. Seeing the Wood through the Trees: A Review of Techniques for Distinguishing Green Fluorescent Protein from Endogenous Autofluorescence. *Anal. Biochem.* **291,** 175–197. ISSN: 00032697. doi:10.1006/abio.2000.5006 (Apr. 2001).

59. Doherty, M. W. *et al.* The Nitrogen-Vacancy Colour Centre in Diamond. *Phys. Rep.* **528,** 1–45. ISSN: 03701573. doi:10.1016/j.physrep.2013.02.001 (July 2013).

60. Hauf, M. V. *et al.* Chemical Control of the Charge State of Nitrogen-Vacancy Centers in Diamond. *Phys. Rev. B* **83,** 081304. ISSN: 1098-0121. doi:10.1103/PhysRevB.83.081304 (Feb. 14, 2011).

61. Petrakova, V. *et al.* Luminescence of Nanodiamond Driven by Atomic Functionalization: Towards Novel Detection Principles. *Adv. Funct. Mater.* **22,** 812–819. ISSN: 1616-3028. doi:10.1002/adfm.201101936 (Feb. 22, 2012).

62. Rogers, L. J. *et al.* Singlet Levels of the NV $^-$ Centre in Diamond. *New J. Phys.* **17,** 013048. ISSN: 1367-2630. doi:10.1088/1367-2630/17/1/013048 (Jan. 27, 2015).

63. Zvyagin, A. V. & Manson, N. B. in *Ultananocrystalline Diamond* 327–354 (Elsevier, 2012). ISBN: 978-1-4377-3465-2. doi:10.1016/B978-1-4377-3465-2.00010-4.

64. Jarmola, A. *et al.* Temperature-and Magnetic-Field-Dependent Longitudinal Spin Relaxation in Nitrogen-Vacancy Ensembles in Diamond. *Phys. Rev. Lett.* **108,** 197601. doi:10.1103/PhysRevLett.108.197601 (2012).

65. Tetienne, J.-P. *et al.* Magnetic-Field-Dependent Photodynamics of Single NV Defects in Diamond: An Application to Qualitative All-Optical Magnetic Imaging. *New J. Phys.* **14,** 103033. ISSN: 1367-2630. doi:10.1088/1367-2630/14/10/103033 (Oct. 2012).

66. Degen, C. L., Reinhard, F. & Cappellaro, P. Quantum Sensing. *Rev. Mod. Phys.* **89.** ISSN: 0034-6861, 1539-0756. doi:10.1103/RevModPhys.89.035002 (July 25, 2017).

67. Levine, E. V. *et al.* Principles and Techniques of the Quantum Diamond Microscope. arXiv: 1910.00061 [cond-mat, physics:physics, physics:quant-ph]. http://arxiv.org/abs/1910.00061 (2020) (Sept. 30, 2019).

68. Neu, E. in *Nanodiamonds* (ed Arnault, J.-C.) 419–438 (Elsevier, 2017). ISBN: 978-0-323-43029-6. doi:10.1016/B978-0-32-343029-6.00018-0.

69. Rondin, L. *et al.* Magnetometry with Nitrogen-Vacancy Defects in Diamond. *Rep. Prog. Phys.* **77,** 056503. ISSN: 0034-4885. doi:10.1088/0034-4885/77/5/056503 (May 2014).

70. Grotz, B. *et al.* Sensing External Spins with Nitrogen-Vacancy Diamond. *New J. Phys.* **13,** 055004. ISSN: 1367-2630. doi:10.1088/1367-2630/13/5/055004 (May 2011).

71. Gicquel, E. *et al.* Adsorption versus Grafting of Poly(N-Isopropylacrylamide) in Aqueous Conditions on the Surface of Cellulose Nanocrystals. *Carbohydrate Polymers* **210,** 100–109. ISSN: 0144-8617. doi:10.1016/j.carbpol.2019.01.022 (Apr. 15, 2019).

72. in. *Wikipedia* (Jan. 31, 2020). https://en.wikipedia.org/w/index.php?title=Zeta_potential&oldid=938423397 (2020).

73. *Exosomes and Microvesicles: An Introduction Nanoparticle Tracking Analysis (NTA) Overview* https://www.malvernpanalytical.com/en/learn/knowledge-center/whitepapers/WP140820-Exosomes-Microvesicles-Introduction.html.

74. Filipe, V., Hawe, A. & Jiskoot, W. Critical Evaluation of Nanoparticle Tracking Analysis (NTA) by NanoSight for the Measurement of Nanoparticles and Protein Aggregates. *Pharm Res* **27,** 796–810. ISSN: 0724-8741, 1573-904X. doi:10.1007/s11095-010-0073-2 (May 2010).

75. Williams, O. A. *et al.* Size-Dependent Reactivity of Diamond Nanoparticles. *ACS Nano* **4,** 4824–4830. ISSN: 1936-0851. doi:10.1021/nn100748k (Aug. 24, 2010).

76. Wang, C. *et al.* Thermodynamic Stability and Ultrasmall-Size Effect of Nanodiamonds. *Angew. Chem. Int. Ed.* **44,** 7414–7418. ISSN: 1433-7851, 1521-3773. doi:10.1002/anie.200501495 (Nov. 18, 2005).

77. Mochalin, V. N. *et al.* The Properties and Applications of Nanodiamonds. *Nat Nano* **7,** 11–23. ISSN: 1748-3387. doi:10.1038/nnano.2011.209 (Jan. 2012).

78. Dolmatov, V. Y. Detonation Synthesis Ultradispersed Diamonds: Properties and Applications. *Russ. Chem. Rev.* **70,** 607–626. doi:10.1070/RC2001v070n07ABEH000665 (Jan. 1, 2001).

79. Pichot, V. *et al.* An Efficient Purification Method for Detonation Nanodiamonds. *Diamond and Related Materials* **17,** 13–22. ISSN: 0925-9635. doi:10.1016/j.diamond.2007.09.011 (Jan. 2008).

80. Shenderova, O. A. & Gruen, D. M. *Ultrananocrystalline Diamond: Syntheses, Properties, and Applications* ISBN: 978-1-4377-3465-2 (William Andrew, Norwich, N.Y., 2012).

81. Lisichkin, G. V. *et al.* Halogenation of Detonation-Synthesised Nanodiamond Surfaces. *Mendeleev Communications* **19,** 309–310. ISSN: 0959-9436. doi:10.1016/j.mencom.2009.11.004 (Nov. 1, 2009).

82. Liu, Y., Khabashesku, V. N. & Halas, N. J. Fluorinated Nanodiamond as a Wet Chemistry Precursor for Diamond Coatings Covalently Bonded to Glass Surface. *J. Am. Chem. Soc.* **127,** 3712–3713. ISSN: 0002-7863. doi:10.1021/ja042389m (Mar. 1, 2005).

83. Havlik, J. *et al.* Benchtop Fluorination of Fluorescent Nanodiamonds on a Preparative Scale: Toward Unusually Hydrophilic Bright Particles. *Adv. Funct. Mater.* **26,** 4134–4142. ISSN: 1616-3028. doi:10.1002/adfm.201504857 (June 1, 2016).

84. Arnault, J.-C. *et al.* Surface Chemical Modifications and Surface Reactivity of Nanodiamonds Hydrogenated by CVD Plasma. *Phys. Chem. Chem. Phys.* **13,** 11481–11487. ISSN: 1463-9084. doi:10.1039/C1CP20109C (June 7, 2011).

85. Portet, C., Yushin, G. & Gogotsi, Y. Electrochemical Performance of Carbon Onions, Nanodiamonds, Carbon Black and Multiwalled Nanotubes in Electrical Double Layer Capacitors. *Carbon* **45,** 2511–2518. ISSN: 0008-6223. doi:10.1016/j.carbon.2007.08.024 (Nov. 1, 2007).

86. Mochalin, V. N. & Gogotsi, Y. Wet Chemistry Route to Hydrophobic Blue Fluorescent Nanodiamond. *J. Am. Chem. Soc.* **131,** 4594–4595. ISSN: 0002-7863. doi:10.1021/ja9004514 (Apr. 8, 2009).

87. Raymakers, J., Haenen, K. & Maes, W. Diamond Surface Functionalization: From Gemstone to Photoelectrochemical Applications. *J. Mater. Chem. C* **7,** 10134–10165. ISSN: 2050-7534. doi:10.1039/C9TC03381E (Aug. 22, 2019).

88. Petrov, I. *et al.* Detonation Nanodiamonds Simultaneously Purified and Modified by Gas Treatment. *Diamond and Related Materials* **16,** 2098–2103. ISSN: 0925-9635. doi:10.1016/j.diamond.2007.05.013 (Dec. 2007).

89. Ackermann, J. & Krueger, A. Efficient Surface Functionalization of Detonation Nanodiamond Using Ozone under Ambient Conditions. *Nanoscale* **11,** 8012–8019. ISSN: 2040-3372. doi:10.1039/C9NR01716J (Apr. 23, 2019).

90. Osswald, S. *et al.* Control of Sp2/Sp3 Carbon Ratio and Surface Chemistry of Nanodiamond Powders by Selective Oxidation in Air. *J. Am. Chem. Soc.* **128,** 11635–11642. ISSN: 0002-7863. doi:10.1021/ja063303n (Sept. 1, 2006).

91. Krueger, A. & Lang, D. Functionality Is Key: Recent Progress in the Surface Modification of Nanodiamond. *Adv. Funct. Mater.* **22,** 890–906. ISSN: 1616-3028. doi:10.1002/adfm.201102670 (Mar. 7, 2012).

92. Girard, H. A. *et al.* Surface Properties of Hydrogenated Nanodiamonds: A Chemical Investigation. *Phys. Chem. Chem. Phys.* **13,** 11517–11523. ISSN: 1463-9084. doi:10.1039/C1CP20424F (June 7, 2011).

93. Neburkova, J., Vavra, J. & Cigler, P. Coating Nanodiamonds with Biocompatible Shells for Applications in Biology and Medicine. *Current Opinion in Solid State and Materials Science* **21,** 43–53. ISSN: 1359-0286. doi:10.1016/j.cossms.2016.05.008 (2017).

94. Vial, S. *et al.* Peptide-Grafted Nanodiamonds: Preparation, Cytotoxicity and Uptake in Cells. *ChemBioChem* **9,** 2113–2119. ISSN: 1439-7633. doi:10.1002/cbic.200800247 (Sept. 1, 2008).

95. Nicolau, E. *et al.* Bioelectrochemistry of Non-Covalent Immobilized Alcohol Dehydrogenase on Oxidized Diamond Nanoparticles. *Bioelectrochemistry* **85,** 1–6. ISSN: 15675394. doi:10.1016/j.bioelechem.2011.11.002 (June 2012).

96. Zhang, X.-Q. *et al.* Polymer-Functionalized Nanodiamond Platforms as Vehicles for Gene Delivery. *Acs Nano* **3,** 2609–2616. doi:10.1021/nn900865g (Sept. 2009).

97. Man, H. B. *et al.* Nanodiamond-Therapeutic Complexes Embedded within Poly(Ethylene Glycol) Diacrylate Hydrogels Mediating Sequential Drug Elution. *Phys. Status Solidi A* **209,** 1811–1818. ISSN: 18626300. doi:10.1002/pssa.201200073 (Sept. 2012).

98. Turcheniuk, K. & Mochalin, V. N. Biomedical Applications of Nanodiamond (Review). *Nanotechnology* **28,** 252001. ISSN: 0957-4484, 1361-6528. doi:10.1088/1361-6528/aa6ae4 (June 23, 2017).

99. Zhao, L. *et al.* Polyglycerol-Functionalized Nanodiamond as a Platform for Gene Delivery: Derivatization, Characterization, and Hybridization with DNA. *Beilstein J. Org. Chem.* **10,** 707–713. ISSN: 1860-5397. doi:10.3762/bjoc.10.64 (Mar. 24, 2014).

100. Zheng, W.-W. *et al.* Organic Functionalization of Ultradispersed Nanodiamond: Synthesis and Applications. *J. Mater. Chem.* **19,** 8432. ISSN: 0959-9428, 1364-5501. doi:10.1039/b904302k (2009).

101. Krüger, A. *et al.* Surface Functionalisation of Detonation Diamond Suitable for Biological Applications. *J. Mater. Chem.* **16,** 2322–2328. ISSN: 1364-5501. doi:10.1039/B601325B (June 13, 2006).

102. Strother, T. *et al.* Photochemical Functionalization of Diamond Films. *Langmuir* **18,** 968–971. ISSN: 0743-7463. doi:10.1021/la0112561 (Feb. 1, 2002).

103. Yang, W. *et al.* DNA-Modified Nanocrystalline Diamond Thin-Films as Stable, Biologically Active Substrates. *Nat. Mater.* **1,** 253–257. ISSN: 14761122, 14764660. doi:10.1038/nmat779 (Dec. 2002).

104. Zhuang, H. *et al.* Elucidation of Different Steps Involved in Allylamine Functionalization of the Diamond Surface and Its Polymerization by Time-of-Flight Secondary Ion Mass Spectrometry. *Chem. Mater.* **22,** 4414–4418. ISSN: 0897-4756. doi:10.1021/cm1009674 (Aug. 10, 2010).

105. Raymakers, J. *et al.* Functionalization of Boron-Doped Diamond with a Push–Pull Chromophore *via* Sonogashira and CuAAC Chemistry. *RSC Adv.* **8,** 33276–33290. ISSN: 2046-2069. doi:10.1039/C8RA07545J (2018).

106. Escorihuela, J., Marcelis, A. T. M. & Zuilhof, H. Metal-Free Click Chemistry Reactions on Surfaces. *Adv. Mater. Interfaces* **2,** 1500135. ISSN: 2196-7350. doi:10.1002/admi.201500135 (2015).

107. Barras, A. *et al.* Functionalization of Diamond Nanoparticles Using "Click" Chemistry. *Langmuir* **26,** 13168–13172. ISSN: 0743-7463. doi:10.1021/la101709q (Aug. 17, 2010).

108. Meinhardt, T. *et al.* Pushing the Functionality of Diamond Nanoparticles to New Horizons: Orthogonally Functionalized Nanodiamond Using Click Chemistry. *Adv. Funct. Mater.* **21,** 494–500. ISSN: 1616-3028. doi:10.1002/adfm.201001219 (Feb. 8, 2011).

109. Kennedy, Z. C., Barrett, C. A. & Warner, M. G. Direct Functionalization of an Acid-Terminated Nanodiamond with Azide: Enabling Access to 4-Substituted-1,2,3-Triazole-Functionalized Particles. *Langmuir* **33,** 2790–2798. ISSN: 0743-7463, 1520-5827. doi:10.1021/acs.langmuir.6b04477 (Mar. 21, 2017).

110. Torelli, M. D. *et al.* Targeting Fluorescent Nanodiamonds to Vascular Endothelial Growth Factor Receptors in Tumor. *Bioconjugate Chem.* **30,** 604–613. ISSN: 1043-1802. doi:10.1021/acs.bioconjchem.8b00803 (Mar. 20, 2019).

111. Vavra, J. *et al.* Supported Lipid Bilayers on Fluorescent Nanodiamonds: A Structurally Defined and Versatile Coating for Bioapplications. *Adv. Funct. Mater.* **28,** 1803406. ISSN: 1616301X. doi:10.1002/adfm.201803406 (Nov. 2018).

112. Minati, L. *et al.* Synthesis of Novel Nanodiamonds–Gold Core Shell Nanoparticles. *Diamond and Related Materials* **53,** 23–28. ISSN: 0925-9635. doi:10.1016/j.diamond.2015.01.004 (Mar. 2015).

113. Rehor, I. *et al.* Plasmonic Nanodiamonds: Targeted Core-Shell Type Nanoparticles for Cancer Cell Thermoablation. *Adv. Healthc. Mater.* **4,** 460–468. ISSN: 21922640. doi:10.1002/adhm.201400421 (Feb. 2015).

114. Chu, Z. *et al.* Unambiguous Observation of Shape Effects on Cellular Fate of Nanoparticles. *Sci. Rep.* **4,** 4495. doi:10.1038/srep04495 (2014).

115. Zoppe, J. O. *et al.* Surface-Initiated Controlled Radical Polymerization: State-of-the-Art, Opportunities, and Challenges in Surface and Interface Engineering with Polymer Brushes. *Chem. Rev.* **117,** 1105–1318. ISSN: 0009-2665. doi:10.1021/acs.chemrev.6b00314 (Feb. 8, 2017).

116. Wu, L., Glebe, U. & Böker, A. Surface-Initiated Controlled Radical Polymerizations from Silica Nanoparticles, Gold Nanocrystals, and Bionanoparticles. *Polym. Chem.* **6,** 5143–5184. ISSN: 1759-9954, 1759-9962. doi:10.1039/C5PY00525F (2015).

117. Hawker, C. J., Bosman, A. W. & Harth, E. New Polymer Synthesis by Nitroxide Mediated Living Radical Polymerizations. *Chem. Rev.* **101,** 3661–3688. ISSN: 0009-2665, 1520-6890. doi:10.1021/cr990119u (Dec. 2001).

118. Neburkova, J. *et al.* in *Nanodiamonds* (ed Arnault, J.-C.) 339–363 (Elsevier, 2017). ISBN: 978-0-323-43029-6. doi:10.1016/B978-0-32-343029-6.00014-3.

119. Řehoř, I. *et al.* in *Carbon Nanomaterials for Biomedical Applications* (eds Zhang, M., Naik, R. R. & Dai, L.) 319–361 (Springer International Publishing, Cham, 2016). ISBN: 978-3-319-22861-7. doi:10.1007/978-3-319-22861-7_11.

120. Chen, M. *et al.* Nanodiamond Vectors Functionalized with Polyethylenimine for siRNA Delivery. *J. Phys. Chem. Lett.* **1,** 3167–3171. ISSN: 1948-7185, 1948-7185. doi:10.1021/jz1013278 (Nov. 4, 2010).

121. Alhaddad, A. *et al.* Influence of the Internalization Pathway on the Efficacy of siRNA Delivery by Cationic Fluorescent Nanodiamonds in the Ewing Sarcoma Cell Model. *PLoS One* **7,** e52207. ISSN: 1932-6203. doi:10.1371/journal.pone.0052207 (Dec. 20, 2012).

122. Petrakova, V. *et al.* Charge-Sensitive Fluorescent Nanosensors Created from Nanodiamonds. *Nanoscale* **7,** 12307–12311. ISSN: 2040-3372. doi:10.1039/C5NR00712G (July 16, 2015).

123. Su, S. *et al.* Thermo- and pH-Responsive Fluorescence Behaviors of Sulfur-Functionalized Detonation Nanodiamond-Poly(N-Isopropylacrylamide). *Colloid Polym. Sci.* **293,** 1299–1305. ISSN: 0303-402X, 1435-1536. doi:10.1007/s00396-015-3531-x (Apr. 2015).

124. Marcon, L. *et al.* Preparation and Characterization of Zonyl-Coated Nanodiamonds with Antifouling Properties. *Chem. Commun.* **47,** 5178. ISSN: 1359-7345, 1364-548X. doi:10.1039/c1cc10338e (2011).

125. Amoozgar, Z. & Yeo, Y. Recent Advances in Stealth Coating of Nanoparticle Drug Delivery Systems. *Wiley Interdiscip. Rev. Nanomed. Nanobiotechnol.* **4,** 219–233. ISSN: 19395116. doi:10.1002/wnan.1157 (Mar. 2012).

126. Rehor, I. *et al.* Fluorescent Nanodiamonds with Bioorthogonally Reactive Protein-Resistant Polymeric Coatings. *ChemPlusChem* **79,** 21–24. ISSN: 2192-6506. doi:10.1002/cplu.201300339 (Jan. 1, 2014).

127. Rehor, I. *et al.* Fluorescent Nanodiamonds Embedded in Biocompatible Translucent Shells. *Small* **10,** 1106–1115. ISSN: 1613-6829. doi:10.1002/smll.201302336 (2014).

128. Stöber, W., Fink, A. & Bohn, E. Controlled Growth of Monodisperse Silica Spheres in the Micron Size Range. *Journal of Colloid and Interface Science* **26,** 62–69. ISSN: 0021-9797. doi:10.1016/0021-9797(68)90272-5 (Jan. 1968).

129. Slegerova, J. *et al.* Designing the Nanobiointerface of Fluorescent Nanodiamonds: Highly Selective Targeting of Glioma Cancer Cells. *Nanoscale* **7,** 415–420. ISSN: 2040-3364, 2040-3372. doi:10.1039/C4NR02776K (2015).

130. Zhao, L. *et al.* Chromatographic Separation of Highly Soluble Diamond Nanoparticles Prepared by Polyglycerol Grafting. *Angew. Chem. Int. Ed.* **50,** 1388–1392. ISSN: 14337851. doi:10.1002/anie.201006310 (Feb. 7, 2011).

131. Zhao, L. *et al.* Platinum on Nanodiamond: A Promising Prodrug Conjugated with Stealth Polyglycerol, Targeting Peptide and Acid-Responsive Antitumor Drug. *Adv. Funct. Mater.* **24,** 5348–5357. ISSN: 1616-3028. doi:10.1002/adfm.201304298 (Sept. 1, 2014).

132. Zhao, L. *et al.* Polyglycerol-Coated Nanodiamond as a Macrophage-Evading Platform for Selective Drug Delivery in Cancer Cells. *Biomaterials* **35,** 5393–5406. ISSN: 0142-9612. doi:10.1016/j.biomaterials.2014.03.041 (July 2014).

133. Faklaris, O. *et al.* Detection of Single Photoluminescent Diamond Nanoparticles in Cells and Study of the Internalization Pathway. *Small* **4,** 2236–2239. ISSN: 1613-6829. doi:10.1002/smll.200800655 (Dec. 1, 2008).

134. Balasubramanian, G. *et al.* Nanoscale Imaging Magnetometry with Diamond Spins under Ambient Conditions. *Nature* **455,** 648–651. ISSN: 0028-0836, 1476-4687. doi:10.1038/nature07278 (Oct. 2, 2008).

135. Wu, Y. *et al.* Diamond Quantum Devices in Biology. *Angew. Chem. Int. Ed.* **55,** 6586–6598. ISSN: 14337851. doi:10.1002/anie.201506556 (June 1, 2016).

136. in. Chang, H.-C., Hsiao, W. W.-W. & Su, M.-C. *Fluorescent Nanodiamonds* 195–213 (John Wiley & Sons, Ltd, Chichester, UK, Sept. 14, 2018). ISBN: 978-1-119-47704-4. doi:10.1002/9781119477099.ch11.

137. Aslam, N. *et al.* Nanoscale Nuclear Magnetic Resonance with Chemical Resolution. *Science* **357,** 67–71. ISSN: 0036-8075, 1095-9203. doi:10.1126/science.aam8697 (July 7, 2017).

138. Bucher, D. B. *et al.* Quantum Diamond Spectrometer for Nanoscale NMR and ESR Spectroscopy. *Nat. Protoc.* **14,** 2707–2747. ISSN: 1750-2799. doi:10.1038/s41596-019-0201-3 (Sept. 2019).

139. Petrakova, V. *et al.* Imaging of Transfection and Intracellular Release of Intact, Non-Labeled DNA Using Fluorescent Nanodiamonds. **8,** 12002–12012. ISSN: 2040-3372. doi:10.1039/C6NR00610H (June 9, 2016).

140. Chow, E. K. *et al.* Nanodiamond Therapeutic Delivery Agents Mediate Enhanced Chemoresistant Tumor Treatment. *Sci Transl Med* **3,** 73ra21. http://bravus.jp/pdf/15-02.pdf (2013) (2011).

141. Van der Laan, K. *et al.* Nanodiamonds for In Vivo Applications. *Small* **14,** 1703838. ISSN: 1613-6829. doi:10.1002/smll.201703838 (2018).

142. Passeri, D. *et al.* Biomedical Applications of Nanodiamonds: An Overview. *J. Nanosci. Nanotechnol.* **15,** 972–988. ISSN: 15334880, 15334899. doi:10.1166/jnn.2015.9734 (Feb. 1, 2015).

143. Ho, D., Wang, C.-H. K. & Chow, E. K.-H. *Nanodiamonds: The Intersection of Nanotechnology, Drug Development, and Personalized Medicine* in *Science Advances* (2015). doi:10.1126/sciadv.1500439.

144. Rosenholm, J. M. *et al.* Nanodiamond-Based Composite Structures for Biomedical Imaging and Drug Delivery. *J. Nanosci. Nanotechnol.* **15,** 959–971. ISSN: 15334880, 15334899. doi:10.1166/jnn.2015.9742 (Feb. 1, 2015).

145. Chipaux, M. *et al.* Nanodiamonds and Their Applications in Cells. *Small* **14,** 1704263. ISSN: 1613-6829. doi:10.1002/smll.201704263 (2018).

146. McGuinness, L. P. *et al.* Quantum Measurement and Orientation Tracking of Fluorescent Nanodiamonds inside Living Cells. *Nat. Nanotechnol.* **6,** 358–363. ISSN: 1748-3387. doi:10.1038/nnano.2011.64 (2011).

147. Neumann, P. *et al.* High-Precision Nanoscale Temperature Sensing Using Single Defects in Diamond. *Nano Lett.* **13,** 2738–2742. ISSN: 1530-6984, 1530-6992. doi:10.1021/nl401216y (June 12, 2013).

148. Kucsko, G. *et al.* Nanometre-Scale Thermometry in a Living Cell. *Nature* **500,** 54–58. ISSN: 0028-0836. doi:10.1038/nature12373 (Aug. 1, 2013).

149. Tzeng, Y.-K. *et al.* Time-Resolved Luminescence Nanothermometry with Nitrogen-Vacancy Centers in Nanodiamonds. *Nano Lett.* **15,** 3945–3952. ISSN: 1530-6984, 1530-6992. doi:10.1021/acs.nanolett.5b00836 (June 10, 2015).

150. Balasubramanian, G. *et al.* Nitrogen-Vacancy Color Center in Diamond — Emerging Nanoscale Applications in Bioimaging and Biosensing. *Current Opinion in Chemical Biology. Molecular Imaging* **20,** 69–77. ISSN: 1367-5931. doi:10.1016/j.cbpa.2014.04.014 (June 2014).

151. Zhang, Y., Dai, M. & Yuan, Z. Methods for the Detection of Reactive Oxygen Species. *Anal. Methods* **10,** 4625–4638. ISSN: 1759-9679. doi:10.1039/C8AY01339J (Oct. 4, 2018).

152. Wardman, P. Fluorescent and Luminescent Probes for Measurement of Oxidative and Nitrosative Species in Cells and Tissues: Progress, Pitfalls, and Prospects. *Free Radical Biology and Medicine* **43,** 995–1022. ISSN: 0891-5849. doi:10.1016/j.freeradbiomed.2007.06.026 (Oct. 1, 2007).

153. Dikalov, S. I. *et al.* EPR Detection of Cellular and Mitochondrial Superoxide Using Cyclic Hydroxylamines. *Free Radic. Res.* **45,** 417–430. ISSN: 1071-5762. doi:10.3109/10715762.2010.540242 (Apr. 1, 2011).

154. Steinert, S. *et al.* Magnetic Spin Imaging under Ambient Conditions with Sub-Cellular Resolution. *Nat Commun* **4,** 1–6. ISSN: 2041-1723. doi:10.1038/ncomms2588 (Mar. 19, 2013).

155. Ziem, F. C. *et al.* Highly Sensitive Detection of Physiological Spins in a Microfluidic Device. *Nano Lett.* **13,** 4093–4098. ISSN: 1530-6984. doi:10.1021/nl401522a (Sept. 11, 2013).

156. Ermakova, A. *et al.* Detection of a Few Metallo-Protein Molecules Using Color Centers in Nanodiamonds. *Nano Lett.* **13,** 3305–3309. ISSN: 1530-6984. doi:10.1021/nl4015233 (July 10, 2013).

157. Sadzak, N., Héritier, M. & Benson, O. Coupling a Single Nitrogen-Vacancy Center in Nanodiamond to Superparamagnetic Nanoparticles. *Sci Rep* **8,** 1–8. ISSN: 2045-2322. doi:10.1038/s41598-018-26633-9 (May 30, 2018).

158. Rendler, T. *et al.* Optical Imaging of Localized Chemical Events Using Programmable Diamond Quantum Nanosensors. *Nat. Commun.* **8,** ncomms14701. ISSN: 2041-1723. doi:10.1038/ncomms14701 (Mar. 20, 2017).

159. Fujisaku, T. *et al.* pH Nanosensor Using Electronic Spins in Diamond. *ACS Nano* **13,** 11726–11732. ISSN: 1936-0851. doi:10.1021/acsnano.9b05342 (Oct. 22, 2019).

160. Gorrini, F. *et al.* Fast and Sensitive Detection of Paramagnetic Species Using Coupled Charge and Spin Dynamics in Strongly Fluorescent Nanodiamonds. *ACS Appl. Mater. Interfaces* **11,** 24412–24422. ISSN: 1944-8244, 1944-8252. doi:10.1021/acsami.9b05779 (July 10, 2019).

161. Van der Laan, K. J. *et al.* Toward Using Fluorescent Nanodiamonds To Study Chronological Aging in Saccharomyces Cerevisiae. *Anal. Chem.* **90,** 13506–13513. ISSN: 0003-2700. doi:10.1021/acs.analchem.8b03431 (Nov. 20, 2018).

162. Butler, J. E. & Sumant, A. V. The CVD of Nanodiamond Materials. *Chem. Vap. Depos.* **14,** 145–160. ISSN: 1521-3862. doi:10.1002/cvde.200700037 (2008).

163. Muzyka, K. *et al.* Boron-Doped Diamond: Current Progress and Challenges in View of Electroanalytical Applications. *Anal. Methods* **11,** 397–414. doi:10.1039/C8AY02197J (2019).

164. Brooks, C. J. *et al.* Characteristics of Chemical Vapor Deposition Diamond Films for X-Ray Mask Substrates. *Journal of Vacuum Science & Technology B: Microelectronics and Nanometer Structures Processing, Measurement, and Phenomena* **17,** 3144–3148. ISSN: 1071-1023. doi:10.1116/1.590969 (Nov. 1, 1999).

165. Tsigkourakos, M. *et al.* Diamond Nano-Particle Seeding for Tip Moulding Application. *Diamond and Related Materials* **35,** 14–18. ISSN: 0925-9635. doi:10.1016/j.diamond.2013.03.008 (May 1, 2013).

166. Smirnov, W. *et al.* Diamond-Modified AFM Probes: From Diamond Nanowires to Atomic Force Microscopy-Integrated Boron-Doped Diamond Electrodes. *Anal. Chem.* **83,** 4936–4941. ISSN: 0003-2700. doi:10.1021/ac200659e (June 15, 2011).

167. Müller, R. *et al.* An "All-Diamond" Inkjet Realized in Sacrificial Layer Technology. *Diamond and Related Materials. Proceedings of Diamond 2004, the 15th European Conference on Diamond, Diamond-Like Materials, Carbon Nanotubes, Nitrides and Silicon Carbide* **14,** 504–508. ISSN: 0925-9635. doi:10.1016/j.diamond.2005.01.005 (Mar. 1, 2005).

168. Lewis, N. S. *et al. Basic Research Needs for Solar Energy Utilization. Report of the Basic Energy Sciences Workshop on Solar Energy Utilization, April 18-21, 2005* 899136 (Apr. 21, 2005). doi:10.2172/899136.

169. Green, M. A. *et al.* Solar Cell Efficiency Tables (Version 54). *Prog. Photovolt. Res. Appl.* **27,** 565–575. ISSN: 10627995. doi:10.1002/pip.3171 (July 2019).

170. Yoshikawa, K. *et al.* Silicon Heterojunction Solar Cell with Interdigitated Back Contacts for a Photoconversion Efficiency over 26%. *Nat. Energy Lond.* **2,** 17032. doi:http://dx.doi.org.ezproxy.uochb.cas.cz:2048/10.1038/nenergy.2017.32 (Mar. 2017).

171. O'Regan, B. & Grätzel, M. A Low-Cost, High-Efficiency Solar Cell Based on Dye-Sensitized Colloidal TiO 2 Films. *Nature* **353,** 737–740. ISSN: 1476-4687. doi:10.1038/353737a0 (Oct. 1991).

172. Rühle, S. Tabulated Values of the Shockley–Queisser Limit for Single Junction Solar Cells. *Sol. Energy* **130,** 139–147. ISSN: 0038092X. doi:10.1016/j.solener.2016.02.015 (June 2016).

173. Vos, A. D. Detailed Balance Limit of the Efficiency of Tandem Solar Cells. *J. Phys. D: Appl. Phys.* **13,** 839–846. ISSN: 0022-3727. doi:10.1088/0022-3727/13/5/018 (May 1980).

174. Boschloo, G. Improving the Performance of Dye-Sensitized Solar Cells. *Front. Chem.* **7.** ISSN: 2296-2646. doi:10.3389/fchem.2019.00077 (Feb. 14, 2019).

175. Kakiage, K. *et al.* Highly-Efficient Dye-Sensitized Solar Cells with Collaborative Sensitization by Silyl-Anchor and Carboxy-Anchor Dyes. *Chem. Commun.* **51,** 15894–15897. ISSN: 1364-548X. doi:10.1039/C5CC06759F (Oct. 22, 2015).

176. Freitag, M. *et al.* Dye-Sensitized Solar Cells for Efficient Power Generation under Ambient Lighting. *Nat. Photonics* **11,** 372–378. ISSN: 1749-4893. doi:10.1038/nphoton.2017.60 (June 2017).

177. Mathew, S. *et al.* Dye-Sensitized Solar Cells with 13% Efficiency Achieved through the Molecular Engineering of Porphyrin Sensitizers. *Nat. Chem.* **6,** 242–247. ISSN: 1755-4349. doi:10.1038/nchem.1861 (Mar. 2014).

178. Kavan, L. Electrochemistry and Dye-Sensitized Solar Cells. *Curr. Opin. Electrochem.* **2,** 88–96. ISSN: 24519103. doi:10.1016/j.coelec.2017.03.008 (Apr. 2017).

179. He, J. *et al.* Dye-Sensitized Nanostructured p-Type Nickel Oxide Film as a Photocathode for a Solar Cell. *J. Phys. Chem. B* **103,** 8940–8943. ISSN: 1520-6106, 1520-5207. doi:10.1021/jp991681r (Oct. 1999).

180. Benazzi, E. *et al.* Developing Photocathode Materials for P-Type Dye-Sensitized Solar Cells. *J. Mater. Chem. C* **7,** 10409–10445. ISSN: 2050-7526, 2050-7534. doi:10.1039/C9TC01822K (2019).

181. Yang, N. *et al.* Vertically Aligned Nanowires from Boron-Doped Diamond. *Nano Lett.* **8,** 3572–3576. ISSN: 1530-6984. doi:10.1021/nl801136h (Nov. 12, 2008).

182. Petrák, V. *et al.* Fabrication of Porous Boron-Doped Diamond on SiO2 Fiber Templates. *Carbon* **114,** 457–464. ISSN: 00086223. doi:10.1016/j.carbon.2016.12.012 (Apr. 2017).

183. Krysova, H. *et al.* Dye-Sensitization of Boron-Doped Diamond Foam: Champion Photoelectrochemical Performance of Diamond Electrodes under Solar Light Illumination. *RSC Adv.* **5,** 81069–81077. ISSN: 2046-2069. doi:10.1039/C5RA12413A (Sept. 23, 2015).

184. Gao, F., Wolfer, M. T. & Nebel, C. E. Highly Porous Diamond Foam as a Thin-Film Micro-Supercapacitor Material. *Carbon* **80,** 833–840. ISSN: 00086223. doi:10.1016/j.carbon.2014.09.007 (Dec. 2014).

185. Amano, F., Ebina, T. & Ohtani, B. Enhancement of Photocathodic Stability of P-Type Copper(I) Oxide Electrodes by Surface Etching Treatment. *Thin Solid Films* **550,** 340–346. ISSN: 0040-6090. doi:10.1016/j.tsf.2013.10.122 (Jan. 1, 2014).

186. Gibson, E. A. *et al.* Role of the Triiodide/Iodide Redox Couple in Dye Regeneration in p-Type Dye-Sensitized Solar Cells. *Langmuir* **28,** 6485–6493. ISSN: 0743-7463. doi:10.1021/la300215q (Apr. 17, 2012).

187. Qin, P. *et al.* Design of an Organic Chromophore for P-Type Dye-Sensitized Solar Cells. *J. Am. Chem. Soc.* **130,** 8570–8571. http://pubs.acs.org/doi/abs/10.1021/ja8001474 (2014) (2008).

188. Farré, Y. *et al.* Synthesis and Properties of New Benzothiadiazole-Based Push-Pull Dyes for p-Type Dye Sensitized Solar Cells. *Dyes and Pigments* **148,** 154–166. ISSN: 0143-7208. doi:10.1016/j.dyepig.2017.08.055 (Jan. 1, 2018).

189. Agarwala, P. & Kabra, D. A Review on Triphenylamine (TPA) Based Organic Hole Transport Materials (HTMs) for Dye Sensitized Solar Cells (DSSCs) and Perovskite Solar Cells (PSCs): Evolution and Molecular Engineering. *J. Mater. Chem. A* **5,** 1348–1373. ISSN: 2050-7488, 2050-7496. doi:10.1039/C6TA08449D (2017).

190. Bártová, K. *Synthesis of dyes for diamond-based dye-sensitized solar cells* (VSCHT, Prague, 2016). 63 pp. https://repozitar.vscht.cz/theses/22374/.

191. *Organic DSSC Dyes | Dyenamo* https://dyenamo.se/dyenamo_dyes.php#dnfp01 (2020).

192. Li, L. *et al.* Double-Layered NiO Photocathodes for p-Type DSSCs with Record IPCE. *Adv. Mater.* **22,** 1759–1762. ISSN: 09359648, 15214095. doi:10.1002/adma.200903151 (Apr. 18, 2010).

193. Green, S. J. *et al.* Potential and pH Dependence of Photocurrent Transients for Boron-Doped Diamond Electrodes in Aqueous Electrolyte. *Electrochimica Acta* **107,** 111–119. ISSN: 0013-4686. doi:10.1016/j.electacta.2013.05.153 (Sept. 30, 2013).

194. Yeap, W. S. *et al.* Diamond Functionalization with Light-Harvesting Molecular Wires: Improved Surface Coverage by Optimized Suzuki Cross-Coupling Conditions. *RSC Adv.* **4,** 42044–42053. ISSN: 2046-2069. doi:10.1039/C4RA04740K (Sept. 8, 2014).

195. Zhong, Y. L. *et al.* Suzuki Coupling of Aryl Organics on Diamond. *Chem. Mater.* **20,** 3137–3144. ISSN: 0897-4756. doi:10.1021/cm703686w (May 1, 2008).

196. Zhong, Y. L. *et al.* Diamond-Based Molecular Platform for Photoelectrochemistry. *J. Am. Chem. Soc.* **130,** 17218–17219. ISSN: 0002-7863. doi:10.1021/ja805977f (Dec. 24, 2008).

197. Kovaříček, P. & Lehn, J.-M. Merging Constitutional and Motional Covalent Dynamics in Reversible Imine Formation and Exchange Processes. *J. Am. Chem. Soc.* **134,** 9446–9455. ISSN: 0002-7863. doi:10.1021/ja302793c (June 6, 2012).

198. Kovaříček, P. & Lehn, J.-M. Directional Dynamic Covalent Motion of a Carbonyl Walker on a Polyamine Track. *Chem. – Eur. J.* **21,** 9380–9384. ISSN: 1521-3765. doi:10.1002/chem.201500987 (2015).

199. Fu, C.-C. *et al.* Characterization and Application of Single Fluorescent Nanodiamonds as Cellular Biomarkers. *PNAS* **104,** 727–732. ISSN: 0027-8424, 1091-6490. doi:10.1073/pnas.0605409104. pmid: 17213326 (Jan. 16, 2007).

200. Funk, R. H. W., Monsees, T. & Özkucur, N. Electromagnetic Effects – From Cell Biology to Medicine. *Progress in Histochemistry and Cytochemistry* **43,** 177–264. ISSN: 0079-6336. doi:10.1016/j.proghi.2008.07.001 (Feb. 2009).

Appendices*

A) Efficiency and stability of spectral sensitization of boron-doped-diamond electrodes through covalent anchoring of a donor-acceptor organic chromophore (P1)

B) Diamond photocathodes sensitised with a bis(perylenemonoimide-dithiophene) donor-acceptor dye

C) Chemical Modification of Diamond Surface by a Donor-Acceptor Organic Chromophore (P1): Optimization of Surface Chemistry and Electronic Properties of Diamond

D) Proton-gradient-driven oriented motion of nanodiamonds grafted to graphene by dynamic covalent bonds

E) Nanoscale dynamic readout of a chemical redox process using radicals coupled with NV^-centers in nanodiamonds

*Appendices (published articles) for the digital version of the thesis are located in a separate file. Charles University requires compliance with archiving standard PDF/A 1a or 2u (Rector's Measure no. 72/2017). Unfortunately, the PDFs created by publishers do not meet (those) archiving standards. Published articles can be directly attached in the thesis only as a picture, which contradicts the requirement for full-text searchability of the document.